2006

An experimental investigation of runner based flow imbalances during injection molding processes in multicavity molds

Rhyu Kevin Takarada
Lehigh University

Takarada, Rhyu Kevin

An Experimental Investigation of Runner Based Flow Imbalances during Injection Molding...

May 2006

AN EXPERIMENTAL INVESTIGATION OF RUNNER BASED FLOW IMBALANCES DURING INJECTION MOLDING PROCESSES IN MULTICAVITY MOLDS

Rhyu Kevin Takarada

A Thesis

Presented to the Graduate and Research Committee

of

Lehigh University

In Candidacy for the Degree of

Master of Science

in

Mechanical Engineering and Mechanics

Lehigh University
Bethlehem, Pennsylvania

May, 2006

LEHIGH UNIVERSITY

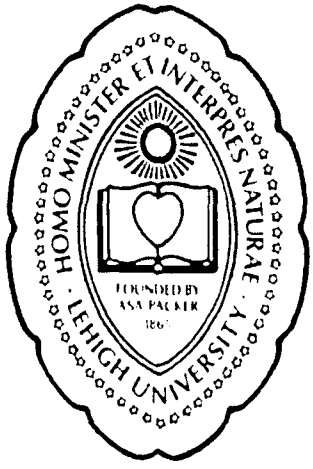

Bethlehem, Pennsylvania

This Thesis is accepted and approved in partial fulfillment of the requirements for the Master of Science

---

John P. Coulter, Ph.D.,
Thesis Advisor

Herman F. Nied, Ph.D., Chair,
Mechanical Engineering and Mechanics

4/24/06

Date

ACKNOWLEDGMENTS

I would like to take this opportunity to thank my immediate family for their kind support and patience they gave me during these 2 years I spent at Bethlehem, Pennsylvania. It has been quite a contrasting experience yet with their warm support, I was able to spend my time in a youthful manner.

Secondly, I would like to thank my advisor Dr. John P. Coulter, who ultimately led me through the path of pursuing a higher degree in mechanical engineering. His guidance, expertise, and flexibility allowed me to capture the raw essence of research in the field of injection molding, ultimately helping me to make a novel discovery. Guidance throughout the research project also came from the expert in the field of injection molding, John Beaumont. His valuable advice helped culminate the positive results of this project. A special thanks goes to Mason Myers, my teammate from Penn State University – Erie, who worked with me from the initial phases of the project all the way until the completion.

I would also like to thank Dr. Herman Nied and the department of mechanical engineering and mechanics for providing me with the necessary financial support during my stay at Lehigh University. I would like to recognize my colleagues at the Manufacturing Science Laboratory, Greg Layser, Alexander Angelov, Mike Casarrela, Alan Tom, and Rajesh Gomatam who contributed to the everyday chores of conducting research in the field of injection molding.

Finally I would like to thank Natasha Pchlintseva and her immediate family. Their continual support and welcome arms throughout my years here helped me to balance my lifestyle, social life, and ultimately maintain my happiness.

TABLE OF CONTENTS

LIST OF TABLES

LIST OF FIGURES

ABSTRACT

Utilization of family molds or multi-cavity polymer injection molds has proven itself to be economical to the manufacturing industry as it helps lower cycle time per individual part and ultimately drive profit increases. With the demand for higher output per cycle and utilization of multi-cavity molds, runner systems have evolved to better fill individual cavities. Studies have shown however, that an imbalance in fill characteristics between cavities exists based on their location with respect to the sprue. Current research has indicated that a polymer's shear thinning characteristic is a contributor to this manufacturing problem. The analysis is however not complete, and there are additional factors that have yet to be tested. The primary objective of the proposed research study was to identify key elements which contribute to this fill imbalance and more specifically study the effect primary runner length has towards the phenomenon. This study presents the brief history of multi-cavity runner systems, the problems associated with runner design, an in-depth discussion of known factors causing fill imbalance, and the methodology used to study the effects of primary runner length on this phenomenon. The results of the experimental study combined with a more in-depth material property observation will lead to a more complete understanding of what the causes are for this manufacturing problem.

1 INTRODUCTION

In today's polymer molding industry, manufacturers are pushed to develop capabilities for more parts per cycle by increasing the number of cavities within molds with the goal of lowering the total cost per part. In order to meet this demand, the design of runner systems has evolved. To date however, no perfect and standardized model runner system has been developed which evenly fills each individual cavity. The most recent and highly applied runner design, a geometrically balanced runner system, is also subject to these conditions with fill imbalance of up to 90% weight variation between part cavities being recorded in certain cases. Since this significantly impacts part quality, the industry seeks to find reasons behind this phenomenon in hopes to solving it.

1.1 PURPOSE OF THE STUDY

Currently the most popular runner design is the naturally balanced runner system with T-configuration runner intersections. Compared to its predecessors of the "Fish Bone" and "Tree" configurations, the balanced runner system is an improvement as the total melt travel distance between the sprue and cavity is guaranteed to be equal. Nonthe-less the quizzical fill imbalance, which was a rampant problem with the earlier runner designs, has also been observed through geometrically balanced runner systems. The most conclusive diagnosis points towards the polymer's non-Newtonian thinning characteristics as the cause, which will be discussed in more detail later. It is this author's belief that indeed shear rate does have an enormous impact on fill imbalances yet there is room to discover additional factors also impact this problem. The purpose of this study was to create an experimental apparatus that tests additional parameters involved in

injection molding and help better explain the phenomenon of fill imbalance in a geometrically balanced runner system.

This research project served to support and build upon the hypothesis of shear induced fill imbalance. Thereby instead of trying to tackle the plethora of parameters and aspects of injection molding that may affect the fill characteristics, this study focused on a particular aspect of the process that had yet to be tested; the length of the primary runner.

According to theory the melt's outer perimeter is subject to higher shear rates which reduce viscosity through thinning effects, as well as through shear heating. If shear heating directly relates to temperature increases of the outer perimeter, then it is expected that extended exposure to this heating will further exacerbate the viscosity differences between the core and outer perimeter. If the theory proves to be valid, fill imbalance characteristics will change if the primary runner length is altered.

1.2 TARGET PROBLEM DESCRIPTION

Multi-cavity molds are essential to companies for ensuring profitability at a time when manufacturing is under pressure from overseas competition. With various industries increasing the demand for higher quality output from injection molding processors, it is essential to evaluate the utilized runner system to see if product quality and future business can be assured. Although the industry standard runner design ensures even melt travel distance, it does not ensure even fill characteristics nor does it assure equal part quality. In fact in a standard 8 cavity mold, it has been observed that the inner most 4 cavities fill at different rates than the 4 outermost cavities. Illustrated in Figure

1-1, the phenomenon of fill imbalance in a geometrically balanced runner mold was first discovered by John Beaumont in late 1990's [1]. Beaumont theorized that the imbalance is caused by viscosity differences between the core and outer perimeter of the melt traveling down the primary runner length. As the melt enters the initial runner intersection, the high viscosity core shifts with respect to the fixated runner diameter, resulting in an asymmetric viscosity profile across the melt. When the melt reaches the tertiary runner, low and high viscosity materials then flow into opposite directions leading to differences in fill pattern between the inner and outer cavities.

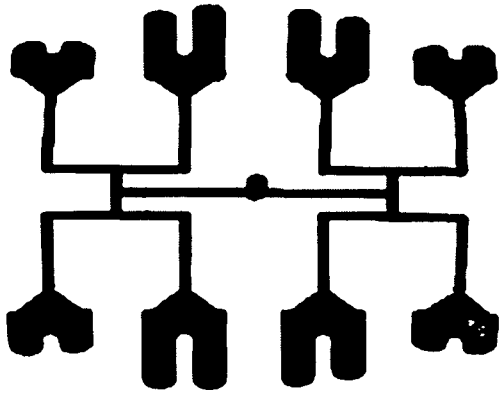

Figure 1-1: Fill Imbalance in Geometrically Symmetrical Runner Mold

Although parts may visually be identical after the packing process, inspection through part testing shows key material property differences.[2] Based on the quantity of cavities in the mold, a number of distinct material property groups can be extracted from a single shot. Based on specifications for the fabricated product, a certain percentage of the batch could be nothing more than scrap. Thereby, the phenomenon of fill imbalance

in a geometrically balanced mold poses serious risk within the injection molding industry.

1.3 OBJECTIVES OF THE PRESENT INVESTIGATION

While there is an abundance of factors that can influence and cause fill imbalance in molds with geometrically symmetrical runner systems, within this sea of factors there are only a few that play a major role on fill imbalance. The objective of this investigation was to clarify the major factors associated with this problem, and discover the true nature of the melt profile as it goes through the runner system. More specifically the goal was to map a relationship between primary runner length to fill imbalance characteristics. Based on the theory that viscous heating effects lower the viscosity of the melt's outer perimeter, how would the fill imbalance characteristics be affected by increasing the duration of the high shear? By answering this question, a correlation between fill characteristics and the viscous heating effects at the boundary layer can be made. Additionally, focusing on the boundary between the melt and the mold wall would help the industry better understand the thermodynamics and heat transfer that occurs.

An additional goal of this study was to discover the key components of a polymer's material rheological response that cause differences in results of fill profile. Previous experimentations have concluded that fill imbalance is very much dependant on the material. [1]

1.4 OUTLINE OF THE THESIS

This appears to be the first time that a thesis for a master of science degree is to be devoted to the topic of fill imbalances in geometrically balanced runner systems. Thus, a significant part of the thesis will focus on summarizing previously conducted research in the specific topic. The thesis will begin in Chapter 2 with a review of polymer injection molding and it's evolution from single cavity mold to the now widely popular multi-cavity molds. Runner design has played a large role in this evaluation. After categorizing the various designs of multi-cavity runner systems, the problems associated with each runner system will be discussed, with particular emphasis placed on the most popular design for a geometrically balanced runner system. Following this, published explanations of fill imbalance in geometrically balanced runner systems will be listed and discussed. Considering the splitting debate within the injection molding industry as to why the problem occurs. Chapter 2 will categorize the fundamental hypotheses and theories, and discuss research results generated by the separate groups. Finally the MeltFlipper^{TM}, which is the only current solution to the problem, will be detailed with respect to its design and supporting experimental results.

After completing the review of the general outline of multi-cavity runner systems, and detailing the theory of shear induced fill imbalance. Chapter 3 begins by bridging the theory of shear induced fill imbalance with the purpose of this particular experimentation, which parallels closely with the direction of previous studies on the theory of shear induced fill imbalance. Within this chapter, the design of the experimental apparatus is laid out which fully details the exact capabilities of the mold and how the user interfaces

with it during the experimental procedures. After the design has been discussed the chapter dives into the various stages involved in fabricating the experimental apparatus, starting from the list of tools and materials used and ending with quality confirmation of the mold assembly. A great amount of detail pertaining to the manufacturing stage is included, as methods needed to be employed to successfully fabricate a mold that was geometrically symmetric about the sprue within a tolerance of 0.001".

With the manufacturing process completed, actual experimentations could begin. In Chapter 4, the design and experimental procedure is explained beginning with the overall goal of the experiment. With the purpose highlighted, the polymers tested are then discussed from a material science perspective. Keen detailing and discussion of the chosen materials reveals how the material properties play a major role in the fill imbalance characteristics. After the materials and equipment are listed, the actual experimental procedure is laid out in full detail with explanations as to why certain processing parameters were selected as controlled variables.

The running of the experimentation was actually the easiest and quickest part of the research study. The coupled process of collecting the data and analyzing it, on the other hand involved considerable effort. Chapter 5 includes the results from the experimentation. For each of the three tested polymers, the results are displayed as fill imbalance with respect to the primary runner length, as well as with respect to the controlled processing condition (injection velocity). From these empirical data and graphs, novel relationships and characteristics are hypothesized and defended.

Finally as the experimentation concluded, novel discoveries were made that relate fill imbalance in geometrically balanced mold, to primary runner lengths and injection velocity. These as well as additional indirect relationships are presented in Chapter 6. Although a major part of the phenomenon is explained through this experimentation, the complexity of what really happens in the runner system allows room for further research to be conducted. Suggestions for future research directions are presented as the concluding remarks to this thesis.

2 BACKGROUND OF FILL IMBALANCE

In a competitive market it is only natural that a manufacturer improves its process efficiency in order to cut costs and maintain its share of the market. By increasing the number of parts produced per single injection molding cycle, a company could significantly lower costs through reduction of overall per product cycle time. Yet with this increase in economic competitiveness, a manufacturing problem arises as cavities do not evenly fill. The problem disrupts homogeneity, jeopardizes quality, and undercuts profits. With the earlier runner designs, fill imbalance problems were clearly evident and resulted in additional costs for continual modifications to the mold. Since the earliest design, the runner design has evolved yet quizzically the fill imbalance problem persisted. Now with quality and tolerances becoming ever more restrictive, both the academic and the industry commitments have focused on the runner system in hopes to finally understand the root cause of the problem.

This chapter presents the brief history of multi-cavity runner systems, the early and current designs, and problems associated with each design. Following this, details of a geometrically symmetrical runner system will be provided with an in-depth summarization on the theory and hypothesis surrounding it, the research work and results, as well as the MeltFlipper^{TM} solution.

2.1 MULTI-CAVITY RUNNER DESIGNS & THEIR PROBLEMS

Given the short history of multi-cavity molds, there are only a few runner designs including the geometrically balanced system that have been regularly applied by the

industry. This section will separate the designs to two categories, the early "FishBone" and "Tree" designs, and the currently popular "Geometrically Symmetrical" system.

2.1.1 "FishBone" and "Tree" Runner Configuration

Economic justification naturally evolved the industry of injection molding to develop molds with multi-cavities in order to increase productivity. These early multi-cavities had runner systems in configuration of the "fishbone" or "tree" style where cavities farther away from the mold had longer runner lengths than those towards the center, as illustrated in Figure 2-1.

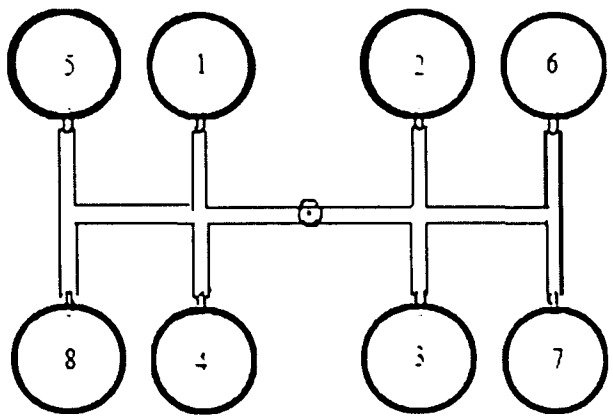

Figure 2-1: Early Design of Multi-Cavity Runner System

As was the case, parts closest to the sprue typically filled first and were heavier and larger than those parts farther away from the injection location. The cause of the fill imbalance was diagnosed as uneven length and pressure drop to each cavity. Polymer melt, like any other fluid, moves in the path of least resistance thereby cavities with lower

pressure drops fill faster than those of higher pressure drops. The following is a commonly applied equation to calculate pressure drop through a die,

$$\Delta P_{round} = \frac{8Q\eta l}{\pi r^4} \qquad (2\text{-}1)$$

$$\Delta P_{rectangle} = \frac{12Q\eta l}{wh^3} \qquad (2\text{-}2)$$

where P is pressure, Q is volumetric flow rate, l is length, r is radius, w is runner width, h is runner height, and η is viscosity. Calculations show that if the diameter of the runner system was consistent throughout, the pressure drop to the inner cavities would be far less than those on the outside.

Manufacturers corrected this problem by artificially balancing pressure drop to each cavity by altering individual runner and gate sizes. At a time when industry relied heavily on hand calculations and previous experiences, the runner system was machined numerous times until acceptable consistency was reached. The negative economic impact to correct this issue must have been significant to the industry at that time. From the 1980's, computer simulation began to play a role in helping to configure the design of the runner system by reducing time and effort necessary to prepare a multi-cavity mold. The simulation programs artificially balanced the runner system by using straightforward principals such as equations above. It is important to note that these software packages did not apply complex modeling of the runner.

2.1.2 Geometrically Balanced Runner Configuration

In the 1980's the geometrically balanced runner system was developed as an improved model as it guaranteed equal flow lengths to every single cavity. Until this day it is widely considered to be superior over the "fishbone" and "tree" configuration. Interestingly it was discovered while short shooting the mold that fill imbalance was still occurring in molds with more than 4 cavities. The observed fill characteristic was that the inner cavities, closest to the sprue hole, were filling faster in comparison to the outer cavities. Figure 2-2 illustrates the design of an 8-cavity geometrically balanced "H-configuration" runner mold.

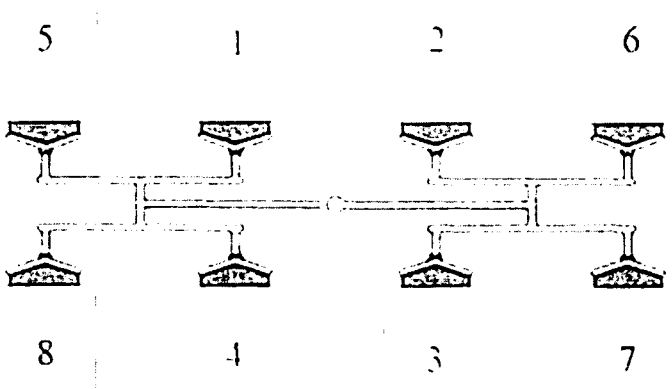

Figure 2-2: A Geometrically Symmetrical "H-Configuration" Runner System [1]

In the 8 cavity configuration shown above, which is the basic design for this experimental study; there are two distinct flow groups. Part cavities #1~4 are categorized as the "inner" cavities since they are physically closer to the sprue, while part cavities #5~8 are

classified as the "outer" cavities. By short shooting the mold, it has been recorded that the inner cavities fill faster compared to the outer cavities.

Many part defects can be attributed to this flow imbalance. Cavities that fill first are typically heavier than the remaining parts due to uneven packing pressure and duration, potentially sticking in the mold and causing damage. Uneven cavity filling leads to an imbalance in the packing stage where cavities experience different pressure values as well as packing duration. Other abnormalities such as flash, sink and short shots can arise from uneven cavity filling. [3] Dimensional variations between cavities also result due to uneven shrink rates and part weights.

2.2 VARIOUS DIAGNOSIS FOR FILL IMBALANCE

As indicated in chapter 1, the objective of this paper is to explore specific details related to John Beaumont and Beaumont Technologies Inc's theory of shear induced fill imbalance in geometrically balanced runner molds. Prior to detailing Beaumont's theory, this section will first discuss other various theories and ideas that have been presented by the injection molding industry in order to provide readers with a more complete background of this phenomenon.

2.2.1 Sharp Square Corners Cause Localized High Shearing

The conventional design of the intersection, where the primary runner branches into the secondary runner, is a straightforward "T" intersection with square corners as illustrated in Figure 2-2. When the fast melt front splits at the junction, a localized high shear occurs at each corner, causing the melt flow to continue to turn in the same

direction. As the initial flow front makes a left, it will continue to make another left when reaching the 2nd junction, causing the inner cavities to fill first.[4] Once back pressure builds within the inner cavities, the melt begins to flow into the outer cavities.

In order to reduce the high concentration of shearing at corners of the intersection, it was proposed that the turn to enter the secondary and tertiary runner be a gradual turn following a path of an arc. The proposed runner design is illustrated in Figure 2-3 .

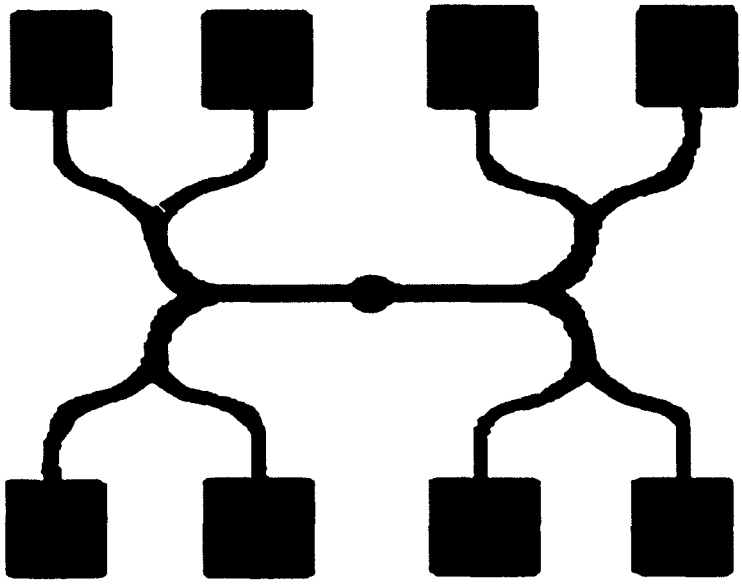

Figure 2-3: Proposed Design – Runner with Rounded Corners [4]

Following the proposal of the hypothesis and design, experiments with molds having rounded corners were tested to see if improvements in fill imbalance could be observed. Results illustrated in Figures 2-4 indicates the fill characteristics did not improve with the intersections rounded off. Although square corners may create localized shear imbalances, results indicate that magnitude of impact to the problem is negligible.

Non-the-less valuable clues were extracted from this particular experiment to better understand the nature of fill imbalances in naturally balanced runner systems.

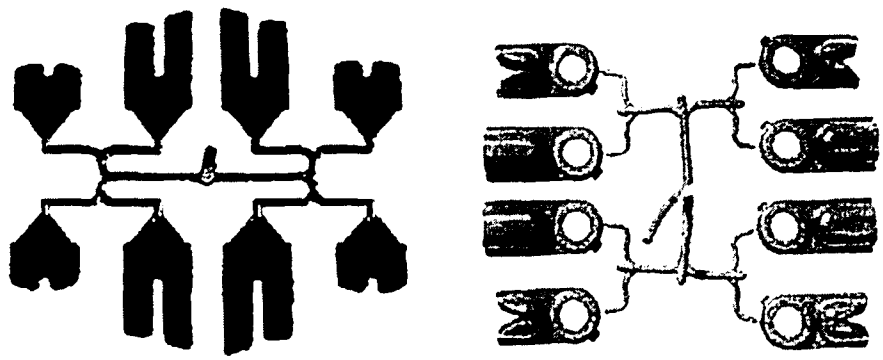

Figure 2-4: Results with Rounded Runner Intersections [5]

2.2.2 Mold Temperature Gradient

While the hot polymer melt flows through the runner system and enters the part cavity, it is continually losing heat to the cold metal mold. The material in contact with the mold loses heat at rates proportional to the temperature difference between the melt and the mold. With the hot injection nozzle continually in contact with mold at the sprue location, as well as the continually injection of new hot material through the sprue, it is expected then that the mold's temperature gradient will have the highest value at the sprue and decrease with radial distance. A hypothesis based on this principal was developed to explain fill imbalances.

If the mold temperature towards the center is hotter than the location of the cavities, then total heat transfer between melt and mold would be highest at the outer locations. Thereby the melt flowing towards the inner cavities would better retain their

temperatures and have a lower viscosity value allowing it to better flow into the inner cavities.

If mold temperature gradient were to be the cause of the fill imbalance then it is expected that the first shot would have the most balanced fill characteristic and as the cycle is repeated, the fill profile would become imbalanced. Results from this experiment, as well as those conducted by other members in the industry, shows that fill characteristic does not change and maintains consistency throughout the shot cycles. Non-the-less it is this paper's recommendation that maintaining consistent temperature gradient on the mold is an important practice towards developing consistency in parts.

2.3 CURRENT DIAGNOSIS OF FILL IMBALANCE

Now that other hypotheses have been discussed, this section will specifically focus on the theory of shear induced fill imbalance. As mentioned during the introduction, the objective of this thesis is to create, test, and yield experimental results that if appropriate, buttress the theory developed by John P. Beaumont in 1997. This section will dive into the theory of shear induced fill imbalance by first discussing established theories that constitute it, and then explain how the theories interact with one another to cause flow imbalance in a naturally balanced runner system. Furthermore this section will visit previous experiments conducted by Beaumont and his research team, and discuss the implications of their results.

2.3.1 Component Theories to Shear Induced Fill Imbalance

There are several main principals that serve as foundations for the theory of shear induced fill imbalance. It is important to discuss then the boundary condition of no-slip at a wall, which establishes the velocity profile across the polymer melt flow. Following this, a relationship between a polymer's viscosity and the shear rate will be established to help readers grasp the concept of shear thinning. Finally the concept of viscous heating will be discussed.

2.3.1.1 No Slip Condition at the Wall and Resultant Velocity Profile

A polymer melt is a viscous fluid with capabilities to flow and change shape due to its inability to support shear stresses. Using the typical assumption of a no-slip condition at the walls, when a viscous fluid flows over a solid surface there is no relative motion between the fluid and the surface. As a result, strong velocity gradients develop in the region near the surface. This region, called the boundary layer, has velocity gradients large enough to produce significant viscous stresses and shear rates. The region outside of the boundary layer is called the freestream where there are neither significant velocity gradients nor any significant viscous stresses. The resultant flow profile is classified as a Poiseuille flow, illustrated as Figures 2-5, it shows the velocity is fastest at the center and decays to zero in a parabolic manner.

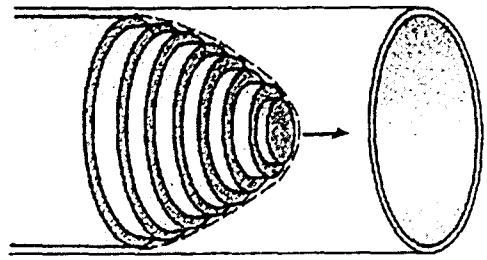

Figures 2-5: Fountain Flow of Polymer Traveling Through a Circular Runner [6]

An important factor to injection molding processes and polymers, the rate of shear strain, more commonly referred to as shear rate, is a function of the velocity gradient of the melt flow.

$$\dot{\gamma} = \frac{\partial v_z}{\partial r} \qquad \textbf{(2-3)}$$

As illustrates, the shear rate increases if the change in velocity increases with radial location. Having established the steady state velocity profile, it is then apparent that the shear rate profile across the runner cross-section is as shown in Figure 2-6.

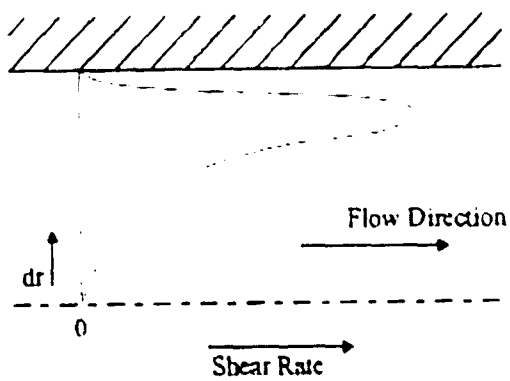

Figure 2-6: Shear Rate Profile in Circular Channel

2.3.1.2 Viscosity Relative to Temperature

Simply stated, viscosity is associated with the ability of a fluid to flow freely. As the viscosity decreases, it increases the polymers' ability to flow faster and fill smaller cavities with finer features. In common industrial terms, the polymer has become thinner. This section will focus on the one of the two most significant factors affecting viscosity: temperature. Section 2.3.1.3 will discuss viscosity relative to applied shear rates.

A volume of polymer at room temperature consists of tightly knitted and inter-twined molecular strands that can be uncrossed into a viscous liquid at sufficiently high temperatures. This transition from a hard solid to the liquid is not sharp; there is an intermediate rubbery stage in which the material begins to behave like a rubbery elastomer after the glass transition temperature, T_g, has been reached. Above the glass transition temperature, the polymer backbone flexes to create room for recoverable deformation. For ease of flow, a polymer molecule must have enough thermal energy to make it mobile or able to get away from its neighbors, and in addition, there must be enough space around it allow for it to move past other polymer molecules. The magnitude of viscosity is then dependant on the availability of free volume which is zero at 0 K and increases with rise in temperature [7]. It is apparent then that the viscosity will decrease with increases in temperature.

EQ 2-4 is known as the WLF equation (named after the founders Williams, Landel, and Ferry). Using the approximation that all polymer viscosities at their

corresponding T_g are 10^{12} PA-sec, the equation is applicable within the temperature ranges of $T_g \sim T_g + 100K$.

$$\log \frac{\eta_0(T)}{\eta_0(T_g)} = \frac{-17.44(T - T_g)}{51.6 + (T - T_g)} \quad \textbf{(2-4)}$$

It is clear that temperature has a major impact on the viscosity. In order to calculate viscosity at higher temperatures, it is appropriate to utilize the Arrhenius equation.

$$\eta_0 = K \cdot \exp(E / RT) \quad \textbf{(2-5)}$$

In this equation, K is representative of the constant characteristic of a polymer and its molecular weight, E is the activation energy for the flow process, R is the universal gas constant, and T is temperature in Kelvin. The equation indicates that temperature still significantly impacts viscosity at temperatures above $T_g + 100K$.

2.3.1.3 Viscosity Relative to Applied Shear Rates

Polymers are well known for their non-Newtonian shear-thinning behavior where their apparent viscosity decreases with increase of shear rate. This non-Newtonian trait serves tremendous practical importance to the injection molding industry as it allows increase in process-ability when filling small channels and features, and also helps reduce the required energy to operate large injection molding machines.

The phenomenon of shear-thinning occurs because of the disentanglements of polymer chains caused by high rates of shear. Application of high rates of deformation causes individual molecules to better orient themselves so they can slide past each other with more ease, hence lowering the bulk viscosity as illustrated in Figure 2-7. The bulk viscosity is really a factor of the material and composition of the polymer. With increase in molecular weight, number of branching chains, as well as the size and quantity of the attached side groups, the bulk viscosity is known to increase.

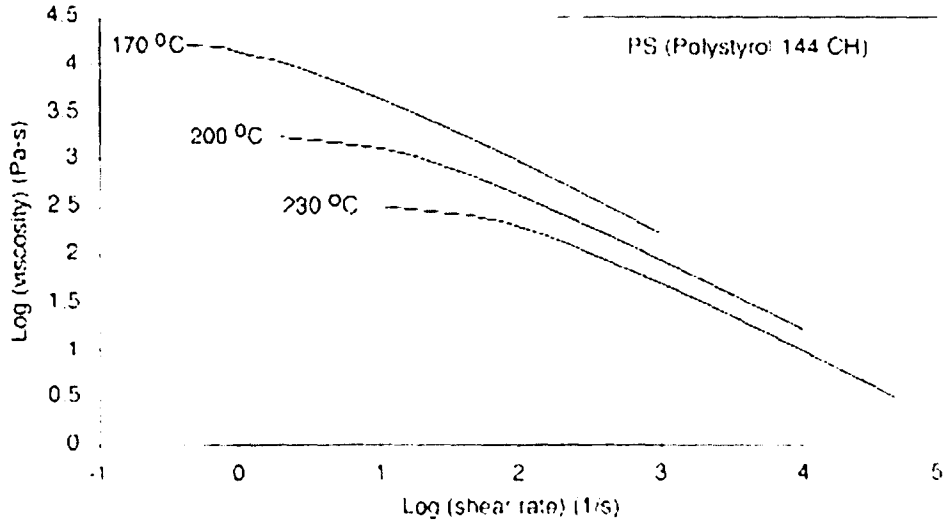

Figure 2-7: A Polymer Viscosity's Relationship to Shear Rates [8]

Several equations have been developed to calculate viscosity relative to shear rates. Due to its non-Newtonian characteristic, where viscosity is relatively steady at low shear rates, an accurate model utilizes multiple material dependant factors that are difficult to find and determine. There are several popular equations to model viscosity relative to shear rate, such as the power-law model, the Bird-Carreau-Yasuda model, and

the modified Cross model which fits the whole range of strain rates. The modified Cross model is shown by:

$$\eta = \frac{\eta_0}{\left[1 + \left(\frac{\eta_0 \dot{\gamma}}{\sigma^*}\right)\right]^{(1-n)}} \quad \textbf{(2-6)}$$

where η_0 is the viscosity at zero shear rate, n is the power law index, and σ^* is the shear stress at the transition between Newtonian and non-Newtonian behavior. In order to properly use accurate models such as EQ 2-6, measurements using rheometers must be performed to properly capture the values of transition shear stress and power law index.

2.3.1.4 Viscous Energy Dissipation

Polymers are viscous fluids and as they flow over a surface, the velocity at the solid surface interface is zero due to the no-slip condition. (Please refer back to 2.3.1.1). Having a general understanding of viscous fluids and a visualization of the velocity profile, then it is easily understood that the frictional forces exerted by the steady surface onto the fluid causes the relative velocity to be zero at the interface. These frictional stresses also cause viscous energy dissipation (VED) in the fluid, which appears as mechanical heat. The quantity of heat generated through friction is proportional to the polymer viscosity (η), and the square of the shear rate ($\dot{\gamma}$), as shown:

$$VED \propto \eta \dot{\gamma}^2 \qquad (2\text{-}7)$$

Now recalling that shear rate is highest at the wall and zero at the core of the flow, the viscous heating effect at the walls could have a significant impact on the material temperature within the outer flow layer, possibly causing the viscosity to drop even further.

2.3.2 Theory of Shear Induced Fill Imbalance

Now that well established principals of no-slip condition, viscosity characteristics with respect to both temperature and shear rates, and viscous heating effects have been explained, this section can proceed to explaining the theory of shear induced fill imbalance. The theory of shear induced fill imbalance, first published in 1997 by John Beaumont [1], is an amalgamation of all the principals cited in the previous section.

With the fully developed laminar velocity profile of a melt traveling through a circular runner being of parabolic shape, the resultant shear rate profile with respect to radial coordinates will be as follows in Figure 2-8

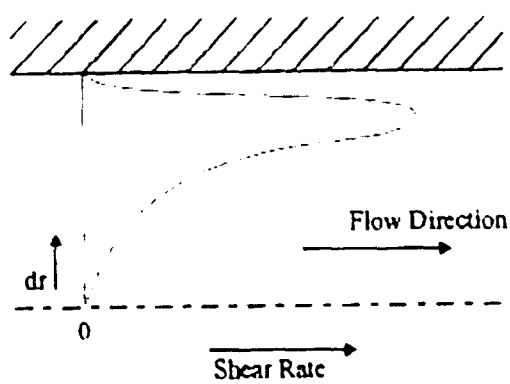

Figure 2-8: Shear Rate Profile Across a Circular Runner [1]

As a function of shear rate, the viscosity within the boundary layer will then be significantly lower than that of the core. An additional reduction of viscosity will also occur if the viscous heating overcomes the heat loss effects to the cool mold wall, which would cause temperatures to rise at the boundary. The resultant combination of both the shear rate and temperature gradient across the melt flow causes the viscosity to change relative to the radial distance from the core. In this case, the viscosity would be significantly higher in the core region than within the outer boundary layer.

During the development of the theory it was observed that fill imbalance occurs in naturally balanced molds when the quantity of cavities exceeds 4. For molds with only 1, 2, or 4 cavities, illustrate below in Figure 2-9, fill imbalance does not occur.

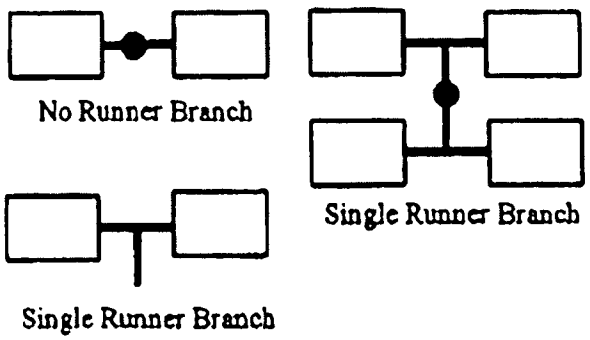

Figure 2-9: Naturally Balanced Molds with less than 8 Cavities

From this observation that fill imbalance is related to the number of cavities, and more importantly to the number of branches in the runner system. As the melt travels down the primary runner, the melt's viscosity will maintain a symmetrical profile, and when it

reaches the first junction the temperature, viscosity, and temperature distribution will become non-symmetrical from side to side [1]. This is illustrated in Figure 2-10.

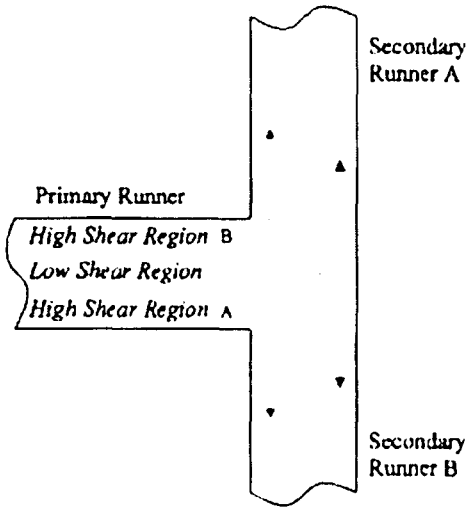

Figure 2-10: Initial Separation of Melt Laminates [1]

The change in direction causes the highly sheared and hotter polymer that was originally at the boundary along the perimeter to now flow along the left wall of the secondary runner illustrated in Figure 2-10, while the cool and thicker core ends up flowing along the wall on the right side. Figure 2-11 illustrates the imbalance of viscosity and temperature profile as the melt splits into the secondary runner.

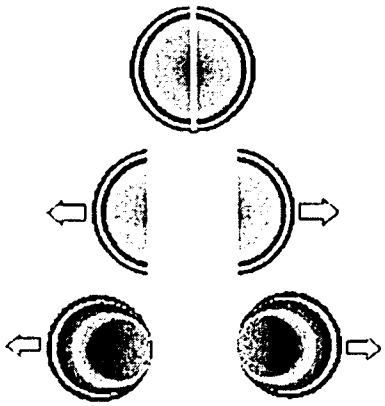

Figure 2-11: Imbalance of Viscosity / Temperature Profile [9]

Now as the radially asymmetrical melt reaches the tertiary runner junction, the cooler core is directed towards the runner entrance closer to it; the runner that leads to the outer cavities. Meanwhile the less viscous melt will be directed towards the inner cavities. With injection pressure evenly applied to both the inner and outer cavity-directions, the inner cavity fills at a faster rate as the material directed towards it is thinner, allowing it to flow through the thin channel more easily. While the inner cavities are filling, melt flows into the outer cavities at a slower velocity until back pressure builds up in the inner cavities. Figure 2-12 illustrates the complete representation of this theory.

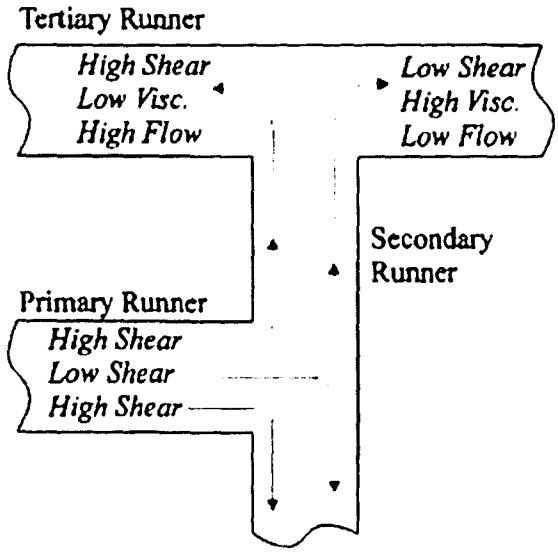

Figure 2-12: Second Separation of Melt Laminates [1]

2.3.3 Supporting Previous Research

Much experimentation has been conducted by Beaumont and his colleagues at BTI Corporation to better defend and provide corroborating results to their theory. Their research focused on various processing conditions as well as geometric dimensions that affect fill imbalances. Studies also include those that investigated the component theories such as temperature invariance and their corresponding relationship to certain processing conditions. This section will summarize this previous work and discuss the implications of their results to the theory of shear induced fill imbalance.

2.3.3.1 Fill Imbalance vs Injection Velocity

According to Beaumont's theory, fill imbalance occurs due to the development of distinct viscosity boundary layers that result from differences in both applied shear rates and temperature. With respect to the fundamental principals, increasing shear rate

will thin a melt and also increase temperature due viscous heating effects, which in turn further decreases viscosity. Thereby it is anticipated that increasing velocity, which increases shear rate gradient across the flow, would further exacerbate the fill volume differences between the inner and outer cavities.

Experimentation began in 1997 with initial results showing that indeed fill imbalance was occurring and was strongly related to injection velocity [1]. By observing results with LDPE and PP, it was clear that an increase in injection velocity increased the fill imbalance percentage, with the most severe case being ~64% fill difference. In 2001, Reifschneider [10] conducted a similar test using PA66 and PP with results illustrated in Figure 2-13. The results corroborate with the theory that fill imbalance is strongly related to injection velocity.

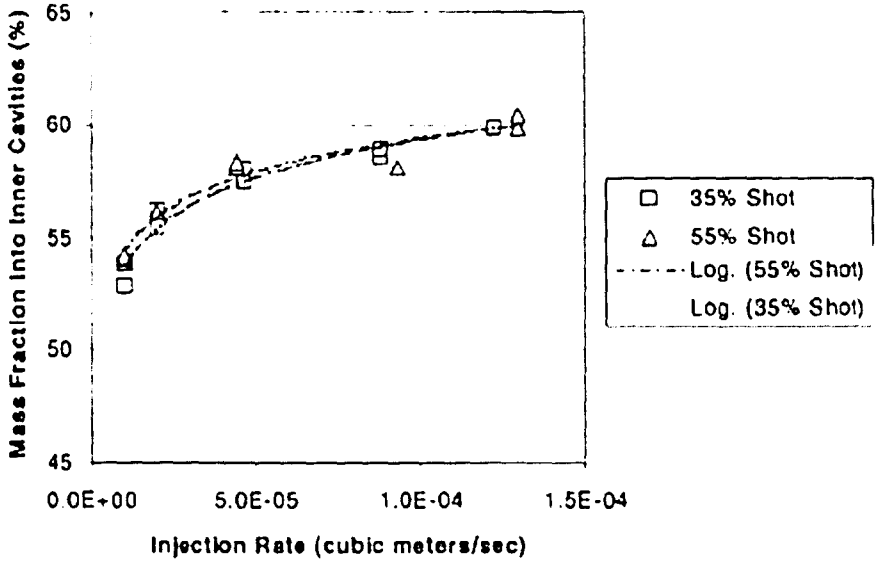

Figure 2-13: Fill Imbalance with respect to Injection Rate using PA-66 [10]

Although results of Figure 2-13 corroborate well with the theory that increase of injection velocity would further decrease the outer perimeter's viscosity, other test results showed that in some materials' case, fill imbalance decreases with increase in injection velocity [1]. These results imply that materials strongly affect the fill imbalance characteristics and are shown in Figure 2-19.

2.3.3.2 Temperature Increases within Runner System

In 2003, Cleveland conducted an experiment to quantify actual melt temperature increases due to accumulated viscous heating effects while it shoots through the runner system [11]. The method chosen was straightforward; a mold, proportionally similar to the runner system, was purged with melt at controlled process settings. The purge was collected into an isothermal container, and its temperature was measured using a thermocouple. This experiment also studied temperature changes due to pressure increases.

$$\Delta T = \Delta P / C_p \rho \qquad \textbf{(2-8)}$$

Equation (2-8), shown above, indicates that an increase in pressure, ΔP, would increase temperature, ΔT, given the constant, C_p, and density, ρ, are constant. It is prudent then to consider the effects of pressure when quantifying temperature increases. Tests results have indicated that pressure factors into increases in melt temperature. More importantly the overall bulk temperature rise to shear heating was considerably high. The results for ABS and PP are shown in Figure 2-14.

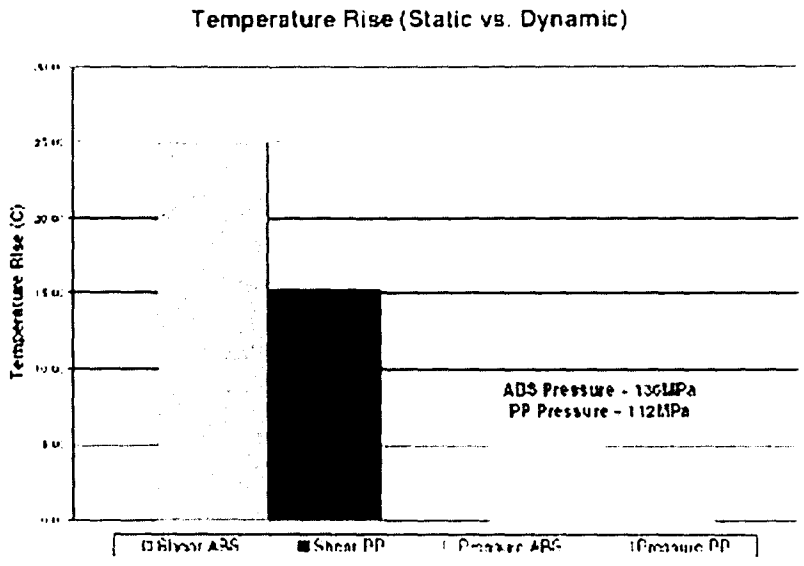

Figure 2-14: Temperature Increases due to Shear Rates and Pressure [11]

Of course the data would be more convincing if an array of tiny thermocouples had been somehow incorporated into a test mold, but due to the complexity of both the fluid dynamics and thermodynamics, no experiment has ever been successfully conducted in such a fashion. None-the-less Cleveland's study utilized an appropriate method as it proved that bulk temperature could increase while traveling from the injection nozzle to the part cavity.

2.3.3.3 Material Strength Difference

Polymers consist of chains that are inter-twined with each other, and at high enough temperatures and shear rates, the chains can slide past each other and orient themselves according to the direction of shear and elongation. Re-orientating and stretching of polymer chains results in property variations, which can be tested and observed using standard tests [8]. By the theory of shear induced fill imbalance, the inner

cavities experience far greater shear rates than the outer cavities. It can be expected then that parts ejected from the inner cavities will differ in test results compared to the outer cavities. Richard Bishop [2] tested material property strength of glass-filled nylon 6/6 using a dart impact test (Dynatup 8250). Parts were created with the standard 8-cavity mold, previously illustrated in Figure 2-2.

The dart impact test method consists of a standardized weight dropped from a certain height perpendicularly straight above the thin specimen [8]. Using the standard equation that calculates potential energy, this test method can be used to observe differences in impact strength between the inner and outer parts made in a geometrically balanced runner mold.

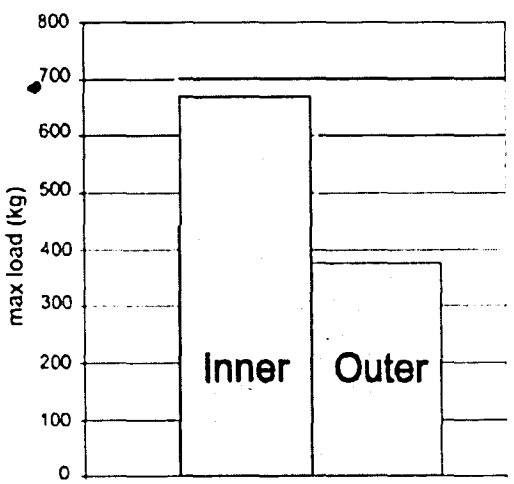

Figure 2-15: Dart Impact Test Result Comparison [4]

The test results of Figure 2-15 illustrates that inner cavity parts were able to withstand more impact load in comparison to the outer cavities. It is important to note that this does not indicate an overall strength increase or decrease, but instead a ductile

strength variation in a single direction. It indicates that material property strength variation of around 50% will occur between the inner and outer cavities when molded using the standard geometrically symmetrical mold. Given the current trend for higher quality control, this research experiment proved there to be a need for additional research in the area of multi-cavity molds in order to produce parts that are homogenous, both from a visual perspective and a mechanical performance perspective.

2.3.3.4 Computer Simulation Programs

Injection molding simulation programs such as MoldFlow have added fuel to the confusion of trying to properly understand the phenomenon of fill imbalance. The actual program designated for the runner has been over-simplified, modeling it as an array of 1-dimensional nodes that calculates a single value for temperature and pressure. These values are at the center of the runner channel and calculated using the standard equations cited earlier. The runner system modeled in MoldFlow thereby lacks the detailed programming necessary to model temperature, viscosity, and velocity profiles across the melt flow while traveling through the runner system. As the melt splits into the secondary and tertiary runner, temperature, pressure, and velocity is evenly directed in both directions, causing actual simulations to show even fill patterns in the standard 8-cavity mold as shown in Figure 2-16.

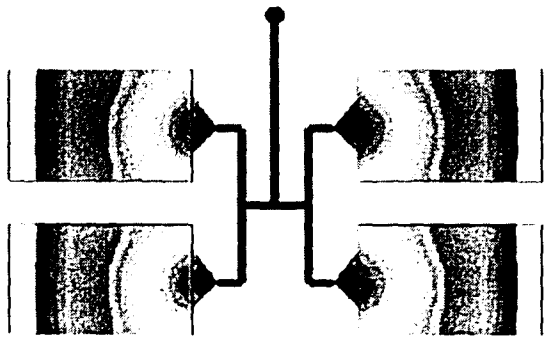

Figure 2-16: MoldFlow Simulation Using Standard 2.5D Mid-Plane Nodes [9]

What truly occurs within the runner system is indeed very complex and difficult to simulate and model. The extreme shear rates changes temperature and viscosity which are also functions of time and location (radially and length wise). Additionally heat transfer effects between the cool mold walls and the melt affect melt conditions. These factors, as well as the complex nature of fountain flow, make successful simulation of the flow front at the local intersection more than difficult. None-the-less, Beaumont and Hayllet has, with some success, modeled the runner system using a 3D extrusion based software package to show the shear effects within the runner [12].

Using Altair Engineering's HyperExtrude, a 3D extrusion software, the runner model was meshed with a standard meshing program called Altair Engineering's HyperMesh. The compilation of the two systems led to simulation results which illustrated the theory of shear induced fill imbalance. Figures 2-17 (a) and (b) show the melt with higher temperature enters the inner cavity at a higher bulk velocity compared to the outer cavities.

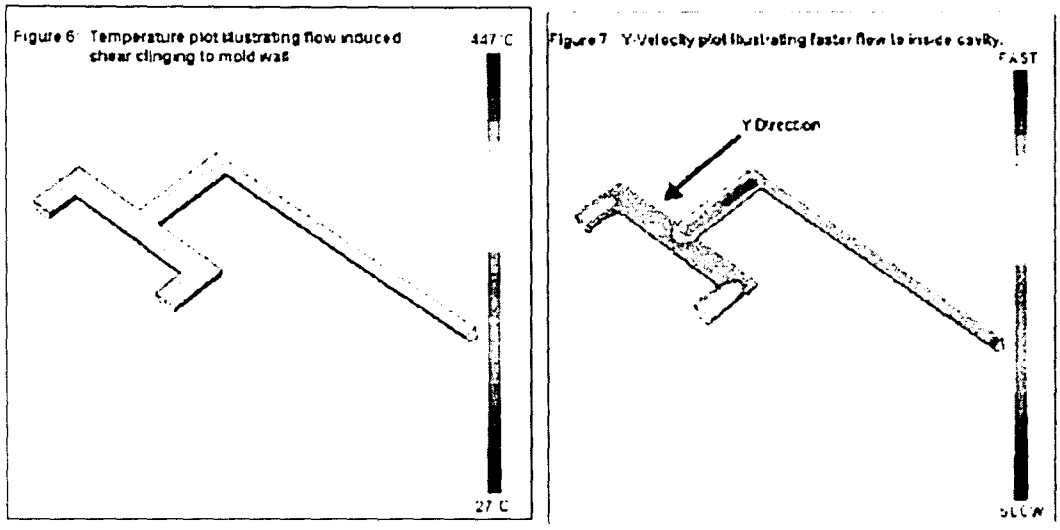

(a) (b)

Figures 2-17 (a) & (b): Shear Induced Fill Imbalance using Extrusion Software [12]

Although the simulation succeeded in simulating the theory of shear induced fill imbalance, the results are not accurate with comparison to actual test results. Figure 2-18 shows that the simulated fill imbalance becomes worse with increase in flow rate, while actual tests show the problem being improved. It has been concluded that the discrepancies occurred because the program had not been optimized for conductive heat losses.[9] Regardless of the accuracy, the program succeeded in simulating fill imbalance in geometrically balanced molds.

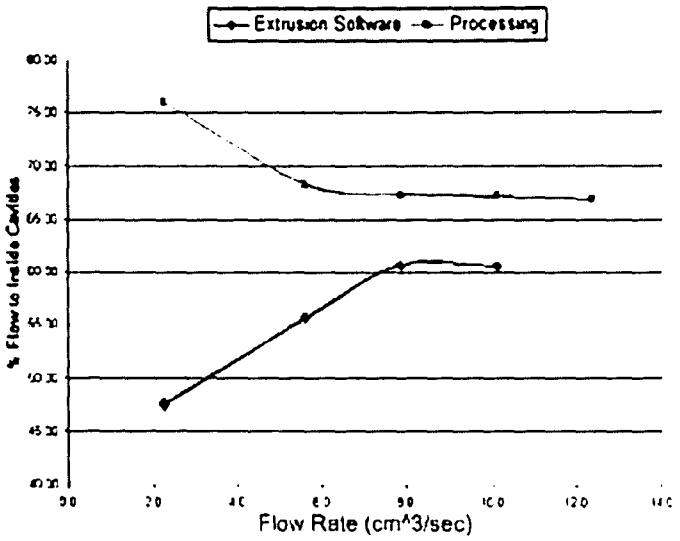

Figure 2-18: Simulation vs Actual Results [12]

2.3.3.5 Material Dependence

From the moment the theory of shear induced fill imbalance was developed, it was known that the fill behaviors were heavily dependant on the selected material. Repetition of the standard test procedure with different polymers yielded results that were considerably different from one another. Overlaying charts that graphed fill imbalance with-respect-to injection rate showed, in some cases, totally different relationship a specific polymer has to fill imbalance and injection rate. In other cases, reverse fill imbalances occurred where the outer cavities fill faster than the inner cavities. These results, shown in Figure 2-19, accentuated the need to investigate the various rheological properties of polymers in order to better understand the key properties that distinguish the fill imbalance characteristics between polymers.

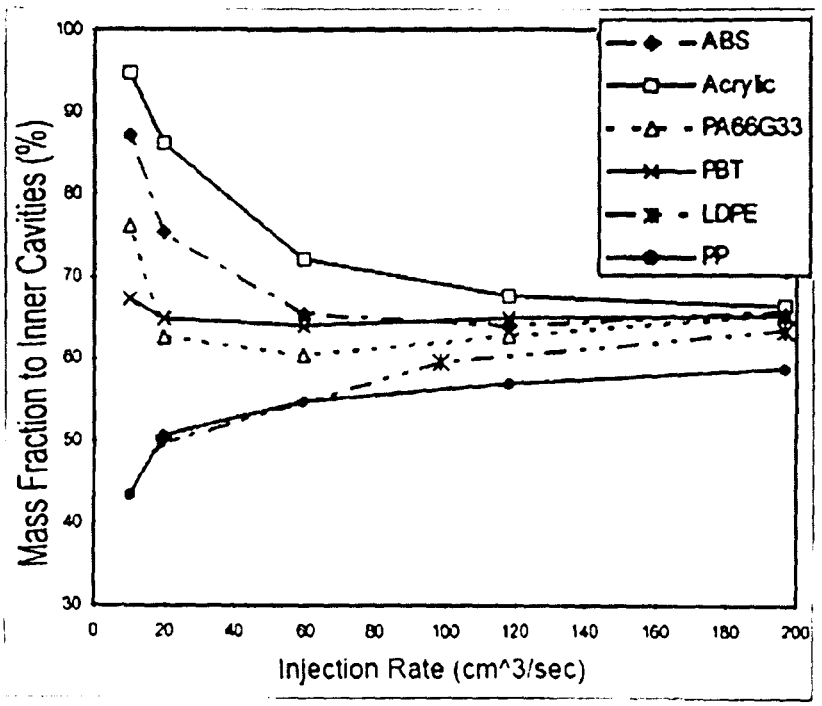

Figure 2-19: Fill Imbalance Dependence to Polymer Material [1]

It has been hypothesized that differences in flow imbalance may be attributed to the melt-viscosity's sensitivity towards temperature changes. This sensitivity can be quantified using equations and is more formally known as the temperature sensitivity factor, T_b, which can be calculated using the modified WLF equation.

$$T_b = \frac{A_1(A_2 + D_1)T^2}{[A_2 + (T - D_2)]^2} \qquad \textbf{(2-9)}$$

In this equation, T is the processing temperature, A_1 and A_2 are WLF shift factors, D_1 is the viscosity scale factor, and D_2 is the glass transition temperature at zero gauge pressure. If the constituent factors are not readily available, then T_b can be determined by

evaluating the tangent on the natural log of viscosity versus the inverse of temperature at the process temperature [10]. The temperature sensitivity parameter is then used to calculate viscosity using the Arrhenius equation:

$$\eta(T) = A\exp\left(\frac{T_b}{T}\right) \qquad \textbf{(2-10)}$$

By observation it is evident that the viscosity of a material with a larger T_b(units of Kelvin), would be much more sensitive to temperature changes when compared to a material with a lower T_b. With identical shear processing, an educated assumption would be that the more temperature sensitive material would have the higher fill imbalance value. Actual test results do parallel this correlation as shown in Figure 2-20.

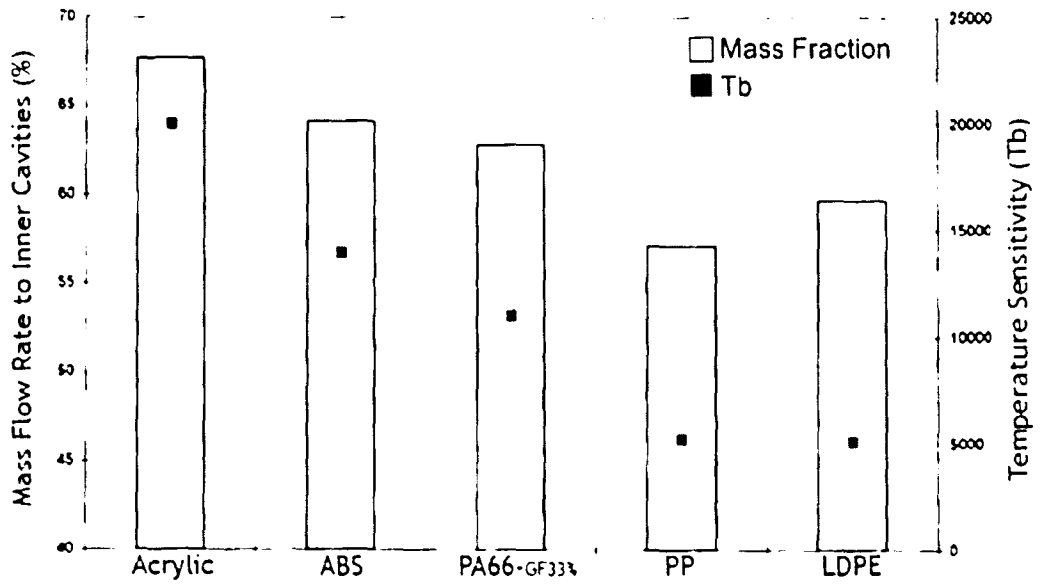

Figure 2-20: Viscosity Temperature Sensitivity factor versus Fill Imbalance [1]

Additional to the temperature sensitivity parameter, T_b, the viscosity constant has also been hypothesized to be a key material property that has correlations to fill imbalance. The power law model, another variation to calculating viscosity:

$$\eta = A * \left(\dot{\gamma}\right)^{B} * \exp(C * T) \qquad \textbf{(2-11)}$$

consists of the viscosity constant A, shear constant B, and temperature constant C. The viscosity constant signifies the initial magnitude of the viscosity at zero shear rate, thereby a large value will allow larger viscosity fluctuation to occur between the inner and outer boundary layers. A research project tested 5 polymers using the standard 8-cavity mold with an adjustable heater band on the injection nozzle head and measured side-to-side fill imbalance. The results illustrated in Figure 2-21 indicate that indeed both the temperature constant and viscosity constant variations do appear to correlated with the observed side-to-side fill imbalances.

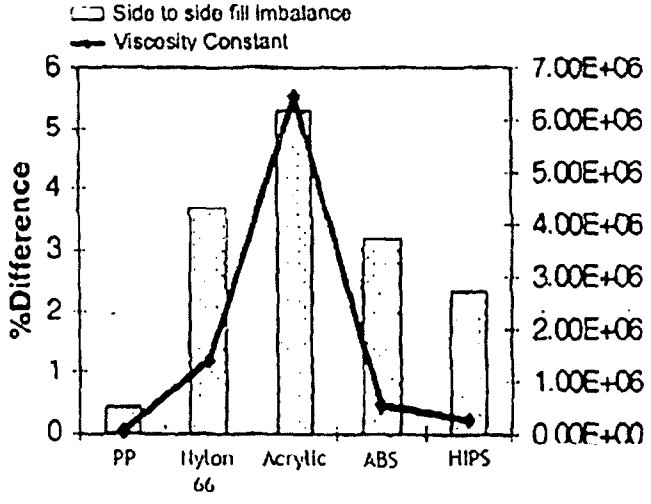

Figure 2-21: Side-to-Side Fill Imbalance Correlates with Viscosity Constant [13]

2.3.3.6 Other Significant Discoveries

During a study unrelated to those of Beaumont, Salamon at Dow Chemical Corporation [14] also made a connection between shear heating and fill imbalances. In this particular case though, the mold consisted of only a single wide and flat cavity with a gate fanned across the entrance. Unlike the CAD simulation which showed a uniform parabolic flow front, actual test results showed a development of a secondary flow at the sides of the cavity that outpaced the bulk flow rate.

Salamon theorized that excessive shear heating and thinning effects that occur in the runner leads to the development of a melt profile that consists of a low viscosity and hotter material on the outer perimeter. Once at the gates, the melt stream expands in the plane of cavity and the lower viscous material is concentrated at the sides of the part creating a "secondary" flow. Due to its lower viscosity, the secondary flow can flow more readily, allowing it to advance at a faster pace than the central flow.

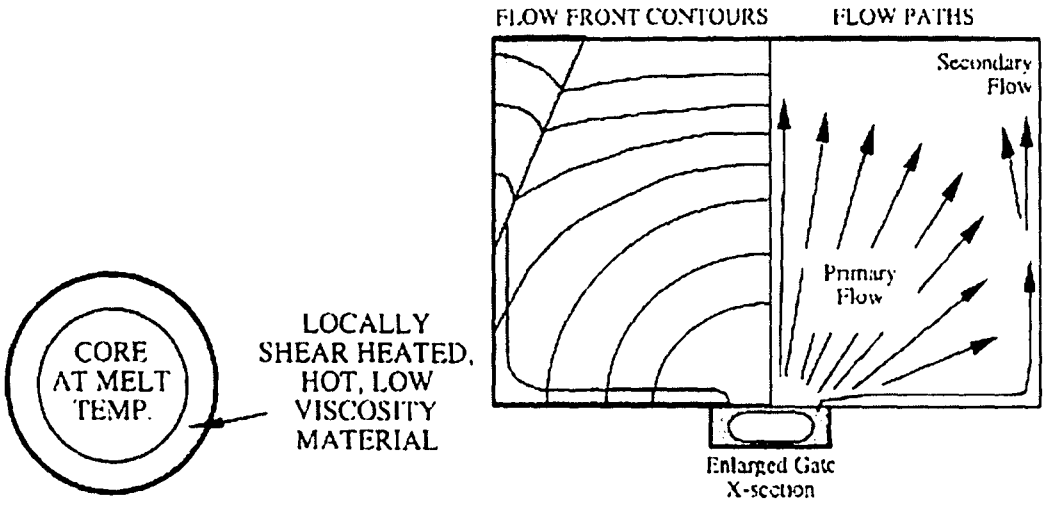

Figure 2-22: Shearing in Runner Causes Development of Secondary Flow [14]

The two research studies cross paths again as Salamon describes the ability to control secondary flow by manipulating the concentricity of the cool core with respect to runner. By utilizing valves located along the runner, the path of the melt could be slightly detoured creating a visco-elastic effect on the melt profile that shifts the core location, ultimately changing the fill pattern in the part cavity.

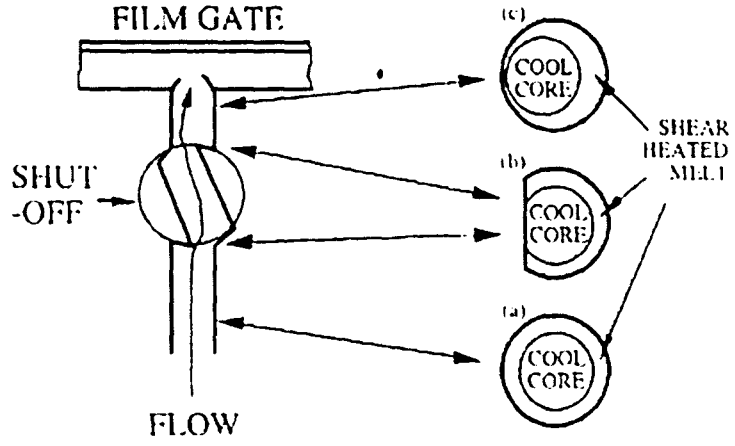

Figure 2-23: Effect of Runner Geometry Changes on Melt Domains [14]

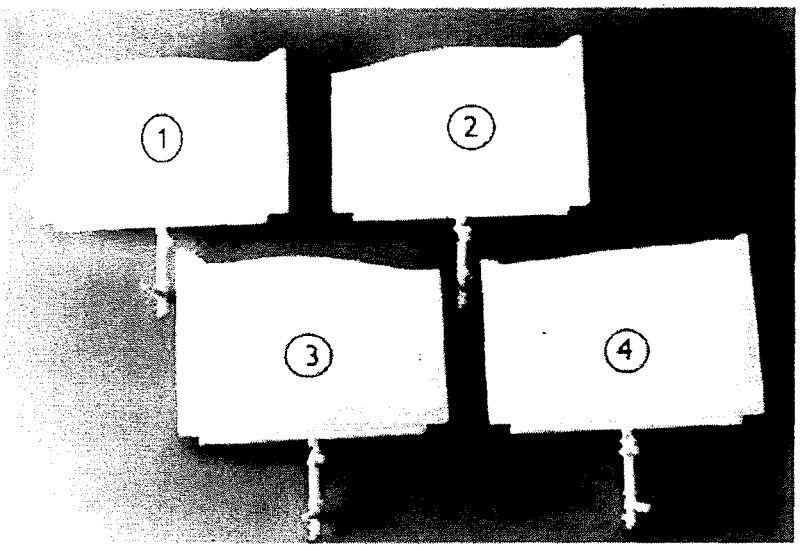

Figure 2-24: The Effect of Valve Position. 1-Full Pass 2-Rotated Counter Clockwise 3-Rotated Clockwise 4-Counter-Rotated [14]

What is important with Salamon's results is that it proves the existence of a localized high sheared material on the perimeter of the melt stream, which flows into the cavity at a faster rate than cooler core. Additionally the discovery of controlling the cross-sectional flow profile through changes to the runner geometry parallels Beaumont's patented technology which balances fill patterns in multi-cavity molds.

2.4 CURRENT SOLUTION – THE MELT FLIPPER

Salamon's theory that a melt's core can be shifted based on runner geometry parallels Beaumont's shear induced fill imbalance theory. According to Beaumont, the cooler core is thrust towards the outer walls when intersecting the secondary runner while the outer material clings to the inner walls (Refer to Figure 2-11). Shifting of the melt

core causes uneven flow rates between the inner and outer cavities when the secondary runner splits to become the tertiary runner.

If geometry of the runner system were to be the cause of viscosity profile shift, which according to both Beaumont and Salamon is the case, then the runner could be geometrically altered to re-balance the melt. John Beaumont has developed the design and has patented it as the MeltFlipper^{TM}.

2.4.1 Design of the MeltFlipper^{TM}

The purpose of MeltFlipper^{TM} is to rotate the orientation of the melt profile by altering the geometry of the runner intersections. Considering the intersections are the cause to losing axial symmetry, the MeltFlipper^{TM} design is installed at selected intersections. The patent operates by machining deeper and shallower runners on both the A and B plate at the particular points. This causes the melt to travel through additional bends, ultimately readjusting the location of the cool core with respect to only the vertical axis. After flowing through the primary-to-secondary MeltFlipper^{TM}, the melt profile maintains symmetry about the vertical axis, allowing equal amount of both high and low viscous materials to flow into the inner and outer cavities. Please refer to the illustrated models of Figure 2-25.

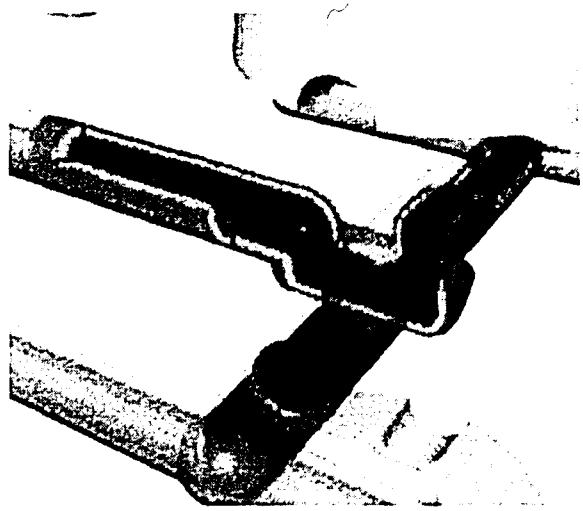

Figure 2-25: Design of the MeltFlipper™

2.4.2 Results with the MeltFlipper™

Results using the melt rotation technology have been very promising, with most cases having perfect fill balance occurring between the inner and outer cavities. In some cases the fill may not be 100% balanced, yet comparison to results without the technology indicates that this technology is a major step towards perfection for the industry as a whole.

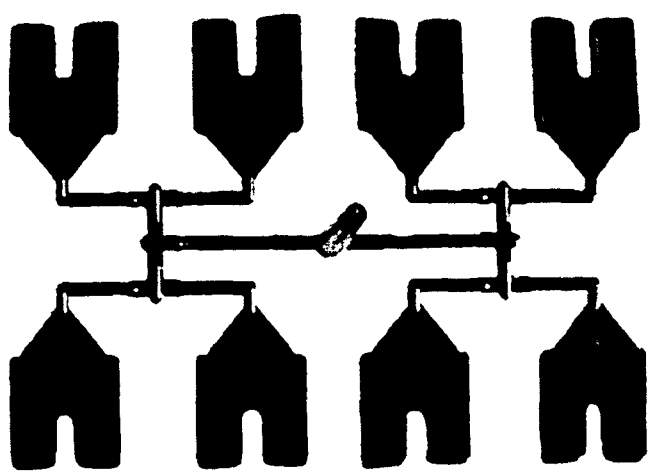

Figure 2-26: Results with MeltFlipper™ Technology

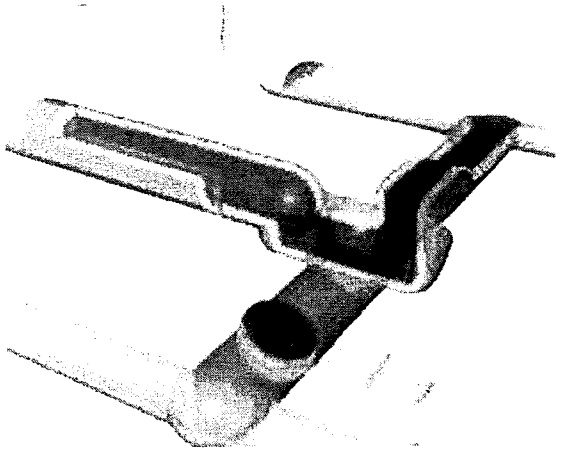

Figure 2-25: Design of the MeltFlipper™

2.4.2 Results with the MeltFlipper™

Results using the melt rotation technology have been very promising, with most cases having perfect fill balance occurring between the inner and outer cavities. In some cases the fill may not be 100% balanced, yet comparison to results without the technology indicates that this technology is a major step towards perfection for the industry as a whole.

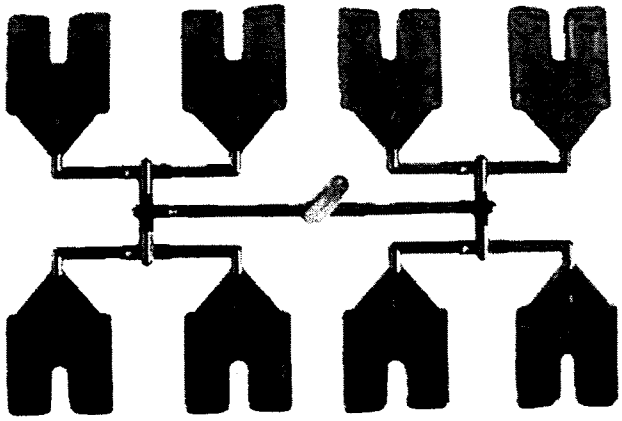

Figure 2-26: Results with MeltFlipper™ Technology

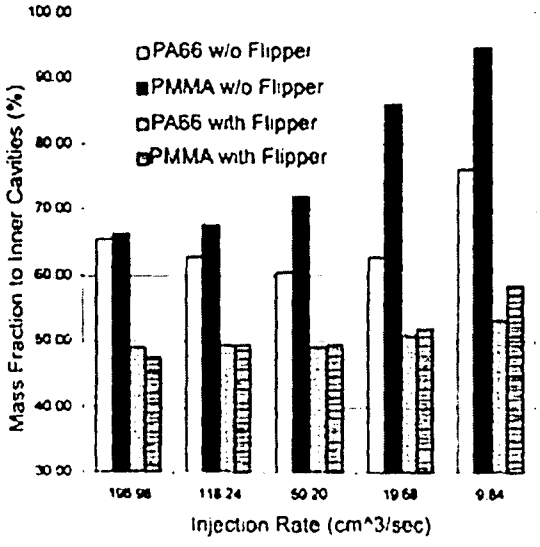

Figure 2-27: Comparison of Fill Imbalance with and without MeltFlipper™ [1]

2.5 NEED FOR FURTHER SCIENTIFIC CLARIFICATION

Indeed the MeltFlipper proves to be a viable countermeasure to fill imbalance problems, yet there are still so many unknowns that surround the dynamics within the runner system that further scientific investigation into this matter is necessary. So far numerous relationships have been established between fill imbalance and various processing conditions yet as Figure 2-27 illustrates, perfect fill balance has yet to be achieved under all processed conditions. The current research project aimed to develop further relationships and characteristics of fill imbalance, hoping to contribute towards the effort of revealing the entire scope of the phenomenon.

3 EXPERIMENTAL TOOLING DEVELOPMENT

With the previous chapter detailing the background of fill imbalance and the relationships with processing conditions and material properties, Chapter 3 will present the design and manufacture of a test mold that would yield results to establish a novel relationship. Chapter 3 begins by further clarifying the purpose of the experimentation and what it is required in the design of an experimental mold. With the objectives for the test mold stated, the chapter will detail the specific nature of the resultant mold design. Finally the fabrication methods and procedures will be presented in step-by-step fashion with the resulting parts pictured at the end.

3.1 PURPOSE OF EXPERIMENTATION

The purpose of the experiment conducted during the present investigation was to establish a novel relationship between molding parameters to fill imbalance. For this project, the focus was on the primary runner where volumetric flow rates are at their highest. If the runner diameter is homogenous throughout the system, then the volumetric flow rate will be halved after each intersection, thereby in the standard 8 cavity mold, the flow rate going to each individual cavity would be $1/4^{th}$ of the original flow rate through each primary runner, and $1/8^{th}$ of the total flow rate. Directly related to the shear rate, the high volumetric flow rate in the primary runner causes the development of the localized viscosity gradient.

The project focuses on the primary runner in order to understand how it affects the fill imbalance characteristics, more specifically how the length would affect it. If

viscous heating effects truly cause temperature imbalances, then increasing exposure duration through length adjustments would show a difference in fill characteristics. Additional to just observing a relationship, this experiment hopes to better understand the balance between shear thinning and shear heating. The industry has not quite agreed on the relative magnitude each factor has towards total fill imbalance. Some say the magnitude of the shear thinning alone creates the problem, while others state that temperature changes are the bulk cause. By controlling only the length of the primary runner, the shear rates would remain constant while the viscous heating duration is changed, helping to segregate the 2 closely related effects. The results would be able to chart the relationship and help industry better understand the effects of the primary runner. Results would also serve to answer questions from the industry such as, "if the primary runner was infinitely long, will there still be fill imbalances?"

3.2 ELEMENTS OF THE DESIGN

With the purpose of the experimentation stated, this section will continue by discussing how the objective and numerous criteria finalized the design of the mold. There are several restrictive criteria to developing the mold such as cost, ergonomics, etc. Each will be separately listed and discussed.

3.2.1 Criteria – General

First and foremost the purpose of this project was to follow Beaumont's past and current research work, and in order to maintain consistency the general design chosen is similar. The chosen geometry was the standard 8-cavity mold with the naturally balanced runner system which has the "H" pattern intersections. Gates connecting the tertiary

runner to the part cavity were designed to be standard fan gates used in previous tests, and the runner diameter was designed to be consistent throughout the system. With an intended use of measuring intra-cavity fill imbalances, the part cavity was designed to be U-shaped. Based on these general criteria, the base design selected was as shown in Figure 3-1.

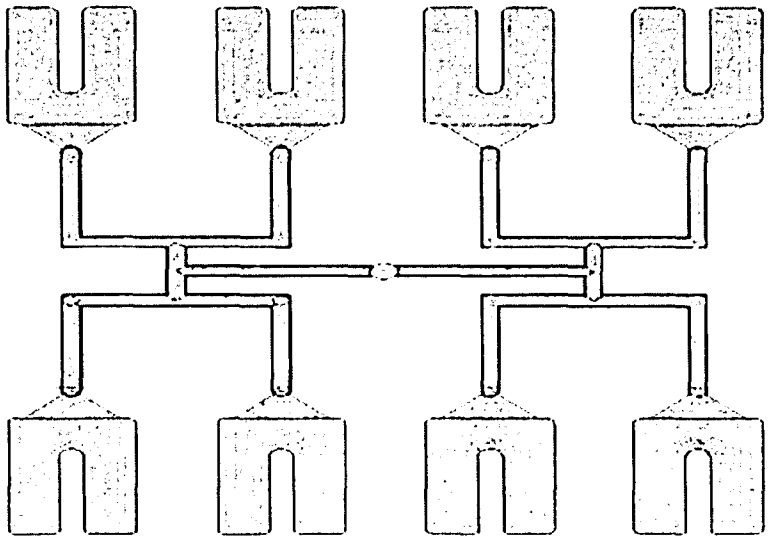

Figure 3-1: Base Design of Multi-Cavity Mold

Although the objective of the experiment has been cited several times thoughout this thesis, it is still important to review this again as it is the heart of the design. The mold had to be designed so that one could adjust the length of the two primary runners while assuring that they remained equal to one another. This is important as uneven lengths would change the volumetric flow rate going to each side of the cavity, in effect voiding the credibility of the data.

In order to assure the validity of the resulting data, proper cooling lines were incorporated into the mold, in order to maintain an even temperature distribution

throughout the mold. Due to size of the chosen mold, which will be discussed later, the machining of the cooling channel holes were outsourced to a separate machine job shop.

3.2.2 Criteria – Mold Size and Other Tools

It would be nice to be able to conduct the investigation with a mold of colossal size on an injection molding machine that could operate such a large unit, as this would have allowed greater flexibility in the choice of runner lengths. Realistically speaking though, such an effort was cost prohibitive. Instead, a mold base of reasonable size readily carried by manufacturers was chosen. The mold base was manufactured by D-M-E and has an overall dimension of 9-7/8" x 20". The mold's overall length to width ratio enabled the study of runner lengths that were considered to be abnormally long. The blank mold's schematic is shown in Figure 3-2, and its complete drawings are cited in Appendix A.

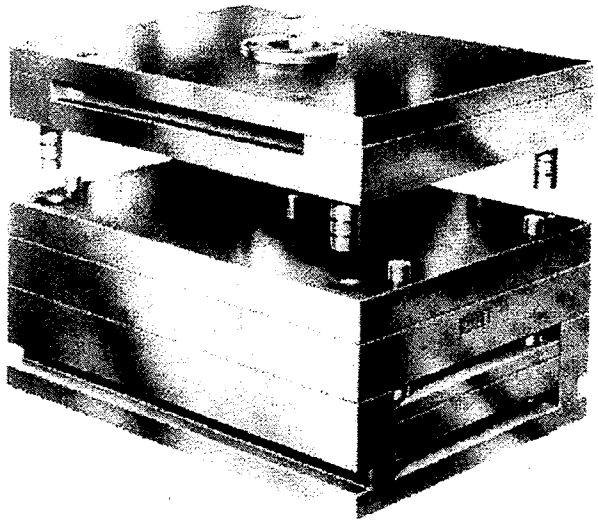

Figure 3-2: Standard DME A-Series 9-7/8" x 20" Mold Base

Based on the overall geometry of the mold, 3 lengths were chosen for the adjustable primary runner. For graphing purposes, the primary runner lengths were non-dimensionalized by dividing length by runner diameter, resulting in units of length-over-diameter ratio (L/D). The final dimensions are presented in Table 3-1.

Runner Setup	Length (inches)	L/D Ratio
- Short	1.625	13
- Medium	3.250	26
- Long	4.875	39

Table 3-1: Variable Lengths of Primary Runner

3.2.3 Criteria – Geometric Tolerances

Given the overall objective guidelines, it was obviously imperative that the mold be completely symmetrical about the sprue. This would guarantee the mold to be as geometrically balanced as possible. With this in mind, all dimensions including nominal and non-crucial dimensions were given tolerances of +/- 0.001". Such tight tolerances required the usage of a CNC milling machine, and in this case a properly calibrated 3-axis HAAS VF-2 vertical machining center was used. The milling unit's immense capability allowed for the confirmation of quality, by subsequently operating the machine as a CMM machine. An image of the utilized machine is shown in Figure 3-3.

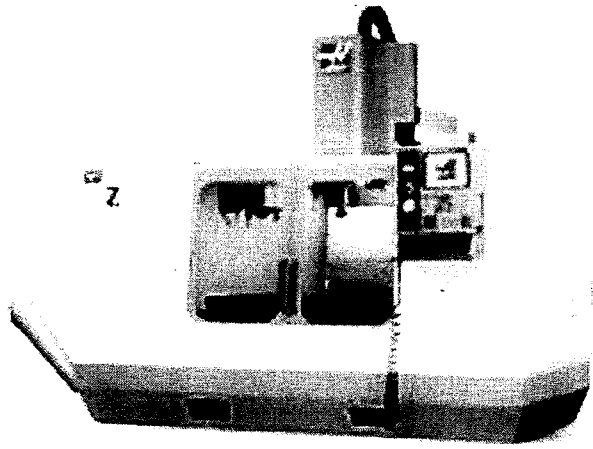

Figure 3-3: HAAS CNC Milling Machine

3.2.4 Criteria – Ergonomics and Ease of Manufacturing

When making design considerations, it was important to consider that actual people are going to be interfacing with the product. Physical operations such as assembling, lifting, and turning, should incorporate ergonomic elements so work can be conducted in safety and with ease. Accordingly, several ergonomic and safety factors were implemented into the design and will be discussed in detail in the next section, which discusses the final design.

Seeking to further improve the design for ease of manufacturing, created opportunities to save both time and money. With restrictive geometries, such as small radii at the corners of cavities, it requires the usage of a small diameter end mill, which costs more and requires a operation at lower machining speeds so the tool doesn't chip.

This becomes a burden as considerable time is wasted in order to finish a single corner. By increasing the radius, it negates the requirement of a small end mill, which in turn saves money and time, thereby the usage of small radii was kept to a minimum. Additional considerations also taken into account will be discussed in the next section.

3.3 THE FINAL DESIGN

With the criteria set, the final design allows users to alter the primary runner length to the three settings of short, medium and long. This is accomplished by inter-changing appropriate inserts which in turn creates a new runner configuration. The design incorporates all of the criteria listed earlier. Considering the quantity of parts and assemblies, this section will separately discuss the B-plate assembly, A-plate assembly, and the guide / ejector plate.

3.3.1 The B-Plate and its Inserts

The B-plate is the heart and soul of the test mold. It houses all the important interchangeable inserts that create the runner configurations. There are two main inserts that assemble into the B-plate, the multi part-cavity inserts, and the runner bar. First and foremost this discussion will begin with the actual B-plate itself. It comprises of a single cavity with a large footprint machined into it. The ejector pin system that is machined into the plate is able to eject parts regardless of the configuration within the plate cavity, thereby the B-plate has a total of 72 holes machined into it, as shown in Figure 3-4.

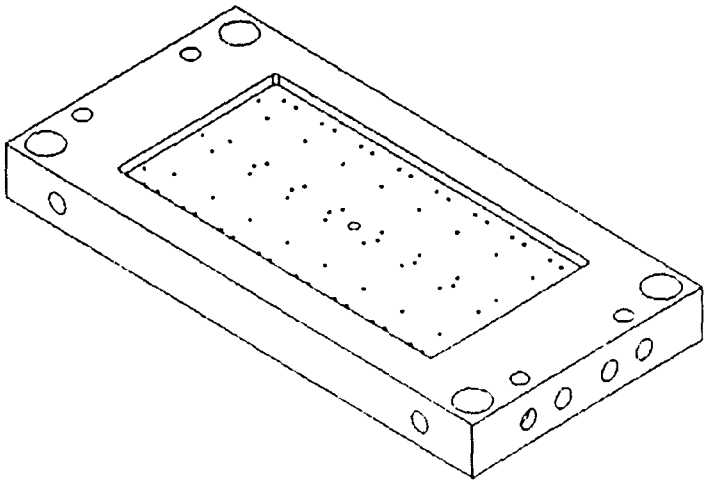

Figure 3-4: B-Plate Design

As mentioned in the earlier section, ease of manufacturing and ergonomics have been incorporated into the every part and especially the B-plate. With 72 holes to drill through a 2" slab of 1030 steel, making all the holes with only 1/8" drills would take a very long time as manufacturing speeds are slow. At the same time the maximum allowable drill depth for an 1/8"drill is less than 2", requiring duplication of the slow drilling pass on the other side. In order to boost productivity the holes consist of two diameters, the back side is a 1/4" diameter, which allows drilling with a generous operating speed compared to the 1/8" drill. Guiding chamfers at the hole entrance were incorporated to improve assemble-ability while trying to align 72 ejector pins. Figure 3-5 details the cross-sectional view of a local configuration.

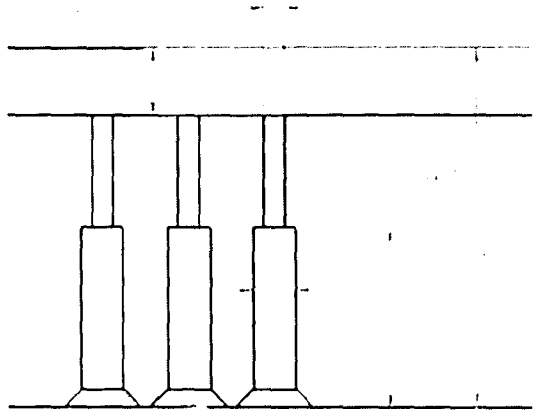

Figure 3-5: Incorporation of Ease of Manufacturing (B-Plate)

The part cavities and individual fan gates were machined into inserts separate from the other tooling components. Four cavities were machined into each insert, and two pairs of cavity insert variants were manufactured. Each insert has two threaded holes through which small machine screws can be used to clamp down the part to the B-plate. The threading of the holes served the dual purpose of enabling jack screws for lifting the inserts out during disassembly. Counter-sinks were also included on the back side so ejector pins could be better guided into the holes. A resultant cavity insert pair is shown in Figures 3-6.

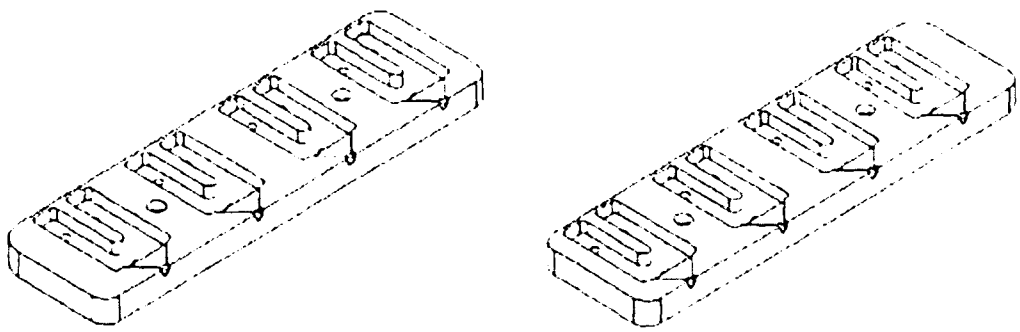

Figures 3-6: 4-Cavity Runner Bars

With the cavity bars lining the sides of the B-plate, a runner bar with the corresponding L/D ratio can be inserted between. The insert that houses the runner configuration is called the runner bar and has cavities machined at both primary-to-secondary intersection locations. These cavities are intended to house inserts which could incorporate the melt rotation technology, but for this particular study, the MeltFlipper was never used.

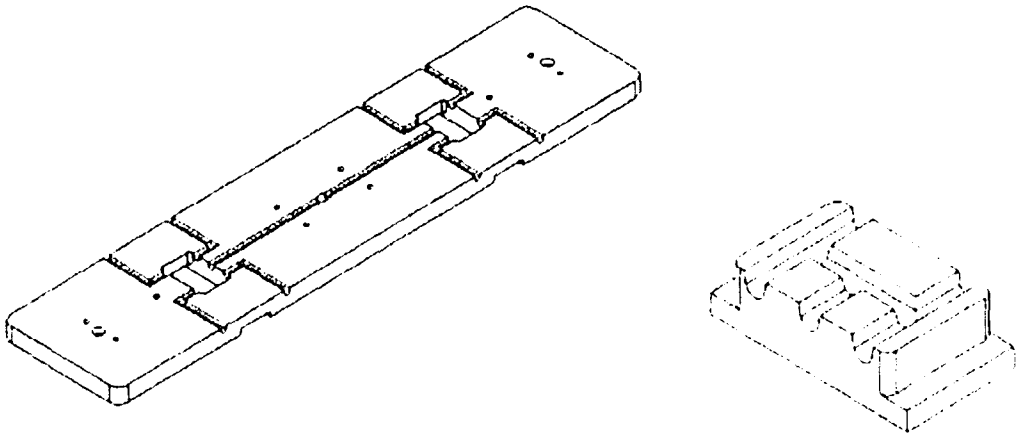

Figures 3-7: Medium Runner Bar & Runner Intersection Insert

As Figures 3-7 illustrates, two runner intersection inserts are fitted into the runner bar cavity. The entire runner bar sub-assembly can then be inserted in between the array of part cavities, finalizing the assembly of the B-Plate. With regards to ergonomics, all the holes were counter-sunk to better guide the pins into the holes. Additionally, the corners of the runner bars were rounded so assembly would not require tight fitting of sharp corners. The three final configurations of the B-plate assembly are shown in Figure 3-8.

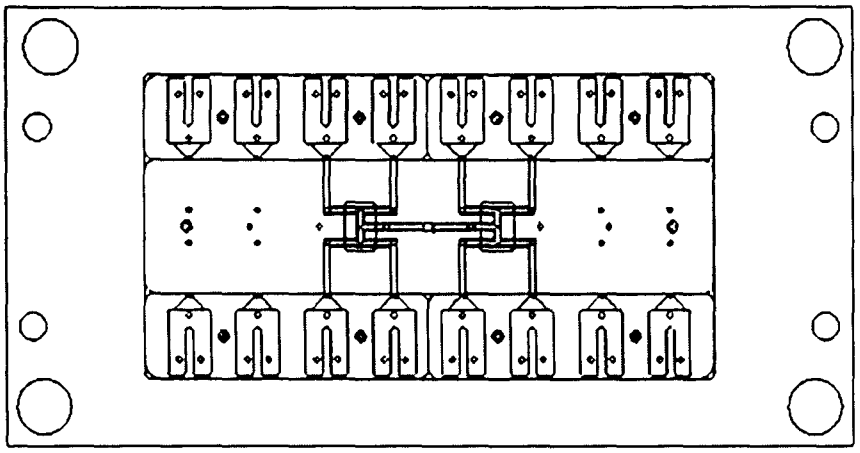

(a)

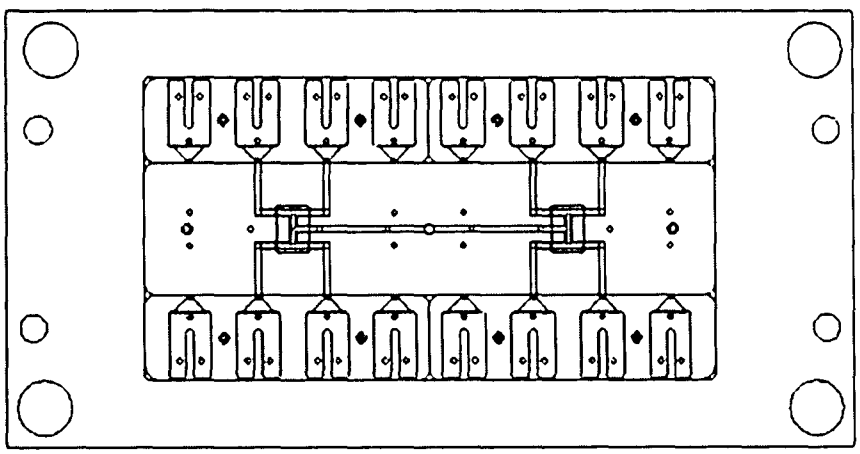

(b)

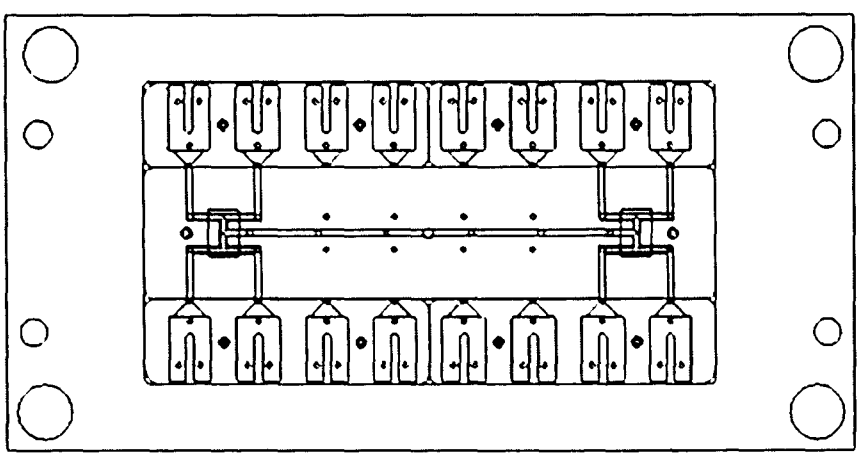

(c)

Figure 3-8: Configuration of B-Plate Assembly. (a) Short, (b) Medium, (c) Long

3.3.2 The A-Plate and its Inserts

The A-plate is the part that interfaces with the B-plate assembly. By hydraulically compressing the two plates together, it assures that the melt injected through the sprue hole, which is centrally located on the A-plate, does not leak and flash from its intended course of travel. In some cases though, partial runner paths are machined onto the A-plate surface as the joining of the two machined surfaces creates an intended geometric shape, in most cases a perfect circular runner profile. Due to the complexity of the mold, the chosen runner for the current study was parabolic in shape and houses a full 1/8" diameter circle within it as shown in Figure 3-9.

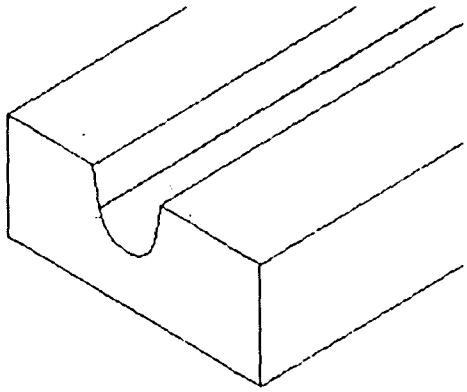

Figure 3-9: Runner Shape and Dimensions

The parabolic shape eliminates the need to machine runner paths onto the A-plate, which simplifies disassembly and assembly procedures during testing.

As mentioned before, there are future intentions of applying melt rotation technology into this mold. Thereby, the A-plate needed to have the ability to house

inserts that complete the technology. Compared to the B-Plate, the A-Plate was relatively simple, as it consists of a single long cavity where an insert retainer plate can be fitted into. At both ends of the cavity, there are threaded holes to help hold the retainer bar into place. Prefabricated into the plate is a circular hole, centrally located on the plate, for a sprue bushing. Thus, the resulted A-plate is shown as Figure 3-10.

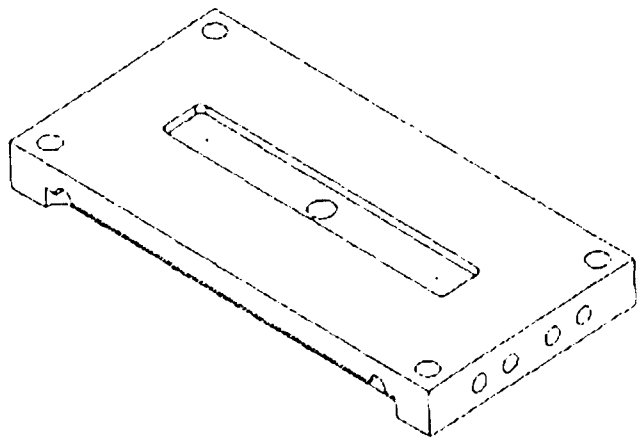

Figure 3-10: A-Plate

Within the cavity, a retainer called the A-half retainer plate can be fitted. The A-half retainer plate has cavities and slots placed according to the location of the primary-to-secondary intersections, which will be filled with six blank inserts, as shown in Figure 3-11

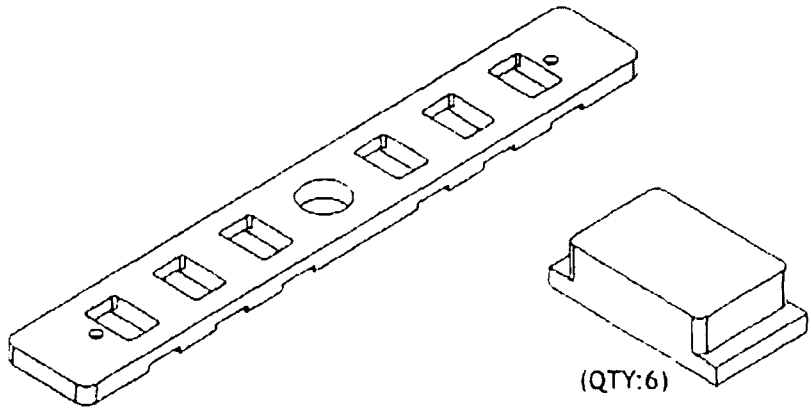

Figure 3-11: A-Half Retainer Plate & Blank Insert

When all the parts are assembled together, the A-plate becomes a solid flat surface with a hole in the middle for the sprue bushing as shown in Figure 3-12.

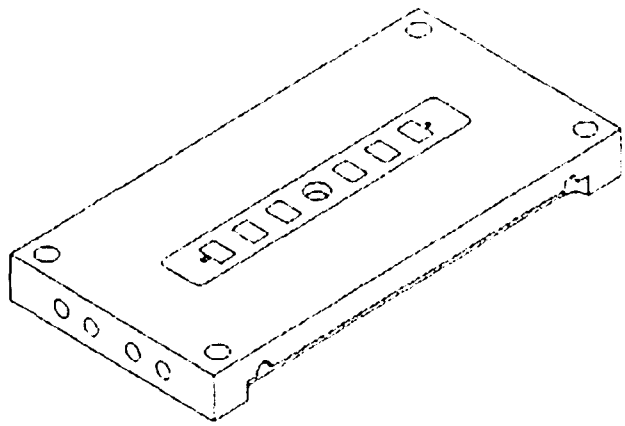

Figure 3-12: Configuration of A-Half Plate after Assembly

3.3.3 The Support and Ejector Retainer Plates

As the title itself explains, the purpose of the support plate is to support the B-plate and the ejector housing. These functions are done through the standard pre-

fabricated features, and do not require any additional manufacturing. In order for the ejector pins to be properly installed through both the support and ejector retainer plates, holes with appropriated dimensions were machined through them. Much like the situation with the B-plate, the holes of the support plate have 2 different dimensions for ease of manufacturing. Additional chamfers were designed into the holes to enable ease of assembly. The holes of the ejector retainer plate consisted of two diameters so that ejector pins would be secured. These two plates are shown in Figures 3-13.

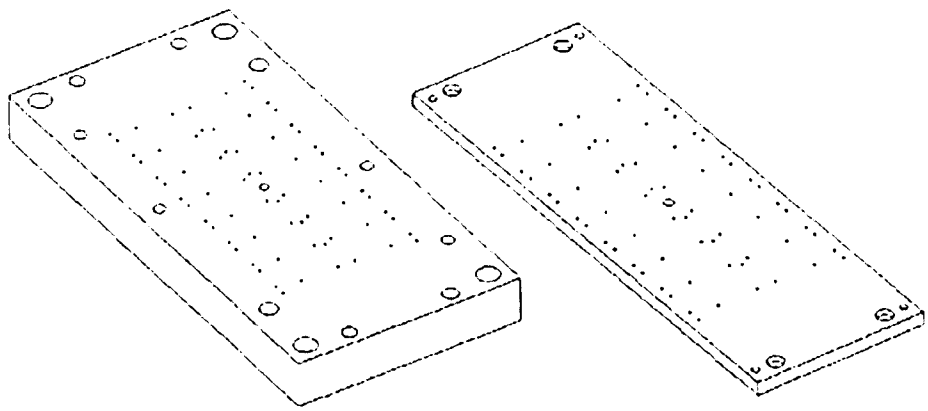

Figures 3-13: The Support and Ejector Retainer Plates

3.4 MANUFACTURING OF THE MOLD

With the design of the experimental mold complete, the project moved forward into the fabrication process. The intention of this section is to layout the methodology used to construct the experimental mold, and ultimately serve as a resource for future research groups that may fabricate a similar mold. Prior to actual machining, preparations such as purchasing of the raw material will be discussed. Additionally a list of utilized

tools and machineries will be itemized followed finally by a step-by-step description of the machining procedure.

3.4.1 Preparation: Raw Material, Tools, and CNC Programming

Aside from ordering the standard mold base consisting, the raw material for the inserts and bars had to be purchased. To maintain consistency with the injection molding industry, the chosen material was P20 steel, which is considerably harder to work with compared to the 1040 steel mold due to its harder composition. The choice of working with P20 steel not only made machining difficult, but it also limited the availability for purchasing. Major vendors did not readily stock the material and would charge enormous monetary figures for the requested rough sizes. Through aggressive web searching a small vendor called Express Steel was chosen for their affordability [15]. In order to save time and money, the stock material received were rough cuts, which were immediately outsourced to a local machine shop to be precision ground and milled to the according size and tolerance.

When taking into consideration both the parts' size and desired dimensional accuracy, it became obvious that automated machining was a necessity for successful fabrication. The entire machining process was conducted on the 3-axis HAAS CNC (computer numerical control) milling machine, pictured in Figure 3-3. The machine has the ability to accomplish all the desired milling and drilling processes and can also function as a coordinate measuring machine (CMM) to confirming feature dimensions. For the CNC milling machine an entire cache of drill bits and end mills were prepared as listed in Table 3-2.

#	Function	Description	Diameter	Features	Quantity
1	Drill	#31	Ø 0.1201"		6
2		#29	Ø 0.1360"		12
3		3/16"	Ø 0.1875"		12
4		Center / Spot	Ø 0.250"		1
5		Reamer	Ø 0.1265"		3
6		3/8" - Chamfer	Ø 0.375"		1
7		1/2"	Ø 0.500"		1
8		3/32"	Ø 0.09375"		1
9	End Mills	1/8" - Square	Ø 0.125"	No Radius	4
10		1/8" - Tapered Ball	Ø 0.125"	20° Taper	4
11		1/4" - Square	Ø 0.250"	No Radius	12
12		1/2" - Square	Ø 0.500"	No Radius	1
13		1/2" - Square (Insert)	Ø 0.500"	0.030" Radius	4
14		1/2" - Square (Insert)	Ø 0.500"	No Radius	2

Table 3-2: List of Tools for CNC Machining

With the material and tools prepared, numerical codes for the operation were generated using a computer assisted manufacturing (CAM) program called I-DEAS. The machining was first simulated on the screen, and G-codes that command the CNC machine were then generated in a text file. For quality control purposes, each of the major milling and drilling operations that constituted the entire operation were separated and individually checked prior to manufacturing. With the codes prepared, a trial run using wax blocks was conducted in order to reduce room for error in machining.

3.4.2 Machining: B-Plate and A-Plate

The two A and B-plates are very similar to one another as they both consist of a square cavity with holes for securing inserts as well as for ejector pins, thereby this section will address them together. To assure that the runner would be 100% geometrically balanced about the sprue, all numerical travel distances were called from the center of each plate.

In order to complete the holes, it was necessary to flip the B-plate. Each time the plate is flipped, time is wasted as the plate needs to be recalibrated onto the table, and thereby it is important to properly sequence the steps. First the larger holes on the back were drilled, then the plate was flipped, re-calibrated, and the cavity was machined followed by the drilling and reaming operation. When machining 72 holes at depths of up to 10 times the diameter of the hole, the drill tips wear and have to be replaced, each time requiring the need to recalibrate to the surface of the plate. To reduce the number of these occurrences, spindle speed, feed rates, and pecking depths were chosen according to the machinist's right hand rule. When machining the cavity, three ½" end mill types were used, each designated for a specific task. While the bulk is hogged out with a 0.030" radius end mill, the finishing cuts on the bottom and sides were performed with ½" end mill with no radius. The sharp corners are prone to wear, thereby exposure to additional machining was limited. The resultant procedure for the A and B plates are listed below in Table 3-3 and 3-4.

Process #	Feature	Process	Process Description	Tool#	Time (mins)
1	Back Holes	Drill	Center Drill (72 Locations)	4	12
2		Drill	Drill counter bore	3	69
3		Drill	Chamfer on hole	6	15
4	Cavity	Drill	Enlarge central hole diameter to 0.500"	7	1
5		Mill	Volume clear the bulk of the cavity	13	60
6		Mill	Machine bottom surface of cavity	14	15
7		Profile Mill	Machine side walls of cavity	12	5
8	Front Holes	Drill	Center Drill (72 Locations)	4	12
9		Drill	Drill holes	1	30
10		Ream	Ream holes to 0.1265" diameter	5	18

Table 3-3: Fabrication Steps for B-Plate

Process #	Feature	Process	Process Description	Tool#	Time (mins)
1	Cavity	Mill	Volume clear the bulk of the cavity	13	17
2		Mill	Machine bottom surface of cavity	14	5
3		Profile Mill	Machine side walls of cavity	12	5
4	Side Holes	Drill	Center Drill (2 Locations)	4	2
5		Drill	Drill secure holes	8	2

Table 3-4: Fabrication Steps for A-Plate

3.4.3 Machining: Support and Ejector Retainer Plates

The machining procedure for the support and ejector retainer plates were very similar and quite simple compared to other parts as it only required repetitive hole making processes. Tables 3-5 and 3-6 below list the steps and process times for both plates.

Process #	Feature	Process	Process Description	Tool#	Time (mins)
1	Back Holes	Drill	Center Drill (72)	4	12
2		Drill	Drill counter-bore (72)	3	69
3		Drill	Chamfer on hole (72)	6	15
4	Front Holes	Drill	Center Drill (72)	4	12
5		Drill	Drill through-holes (72)	2	42

Table 3-5: Fabrication Steps for Support Plate

Process #	Feature	Process	Process Description	Tool#	Time (mins)
1	Holes	Drill	Center Drill (72)	4	12
2		Drill	Drill Through-Holes (72)	2	18
3		Drill	Square Shoulder (72)	11	4

Table 3-6: Fabrication Steps for Ejector Retainer Plate

3.4.4 Machining: A-Plate Insert Bar and Runner Bars

The two parts were designed to be similar to one another as both have geometrically identical cavities and slots, as well as the same rounding on the outer edges. The only major difference between the parts from a machinist's perspective was the milling of the runner paths onto the runner bar as well as the additional drilling and reaming for the ejector pin holes.

For the runner bars, after the central hole was made, the CNC's coordinate system was recalibrated to the center of the hole. Once the slots and rough holes were complete on the back, the bar was flipped over, recalibrated, and the cavities were machined. It is important to remember that as material is removed from either surface, an imbalance of stress and strain causes the bar to slightly bow; thereby it is crucial that flatness of the working surface is confirmed prior to continue machining the cavities and runner paths. Once the parts were properly secured into the vice and cavities are complete, the runner paths were milled. Reaming the ejector pin holes was the last step as it assured that no chips or burrs are left in the holes. The overall process sequence is presented in Table 3-7.

Process #	Feature	Process	Process Description	Tool#	Time (mins)
1	Blank	Ground	Precision ground to proper thickness	- outsourced	
2		Mill	Mill to proper length and width	- outsourced	
3	Holes	Drill	Center drill (27)	4	4
4		Mill	Mill central hole (1)	1	6
5		Drill	Drill ejector pin holes (24)	1	10
6		Drill	Square shoulder holes (2)	11	2
7	Slots	Mill	Volume clear slots (2)	13	7
8		Mill	Machine bottom surface of slots (2)	14	3
9		Profile Mill	Machine side walls of slot (2)	12	4
10	Cavity	Mill	Volume clear cavities (2)	11	8
11		Profile Mill	Machine side walls of cavity (2)	9	12
12	Sides	Profile Mill	Round outer corners (left)	12	8
13		Profile Mill	Round outer corners (right)	12	8
14	Runners	Mill	Machine runner paths	10	40
14	Holes	Ream	Ream ejector pin holes	5	3

Table 3-7: Fabrication Steps for Individual Runner Bars

One of the differences between the A-plate insert bar and the runner bar is that the central hole is bigger on the insert bar and requires profile milling to get the correct diameter. Aside from the central hole, the quantity of cavities and slots to mill is six as opposed to just two, which adds additional wear to the ¼" end mill (process #9), creating the need to switch to a new tool at mid-process. When profile milling the sides of the cavity (process #10), the small 1/8" end mill tended to flex a little causing the walls to taper in slightly. By repeating the process several times, the cavity width finally fell into specification. Table 3-8 summarizes the associated process sequences.

Process #	Feature	Process	Process Description	Tool#	Time (mins)
1	Blank	Ground	Precision ground to proper thickness	- outsourced	
2		Mill	Mill to proper length and width	- outsourced	
3	Holes	Drill	Center drill (3)	4	4
4		Drill	Drill Center Hole	7	2
5		Profile Mill	Open Central Hole	11	6
6	Slots	Mill	Volume clear slots (6)	13	21
7		Mill	Machine bottom surface of slots (6)	14	9
8		Profile Mill	Machine side walls of slot (6)	12	12
9	Cavity	Mill	Volume clear cavities (6)	11	24
10		Profile Mill	Machine side walls of cavity (6)	9	36
11	Sides	Profile Mill	Round outer corners (left)	12	8
12		Profile Mill	Round outer corners (right)	12	8
13	Holes	Drill	Drill clamping holes (2)	1	2
14		Mill	Square Shoulder holes (2)	11	2

Table 3-8: Fabrication Steps for A-Plate Insert Bar

3.4.5 Machining: 4-Part Cavity Bar

After the stock bars were ground and milled to the initial dimensions, the ejector holes were drilled from the top surface followed by milling of the part cavity. Once the walls of the cavity were profile milled, the triangular gates were milled. The entrance of the gate was made using the 1/8" tapered ball end mill. Finally the runner bars' sides were profile milled and the ejector holes were reamed. The entire process was then repeated three more times.

Manufacturing the part cavity bar was probably the most difficult. With the highest toll on the tools, more specifically the process of milling out the part cavity, creating a single part required a lot of time. With so much volume to clear out, and the material being composed of hard P20 steel, the flanks on the ¼" end mills were dull and useless after finishing only two to three cavities. Non-the-less with plenty of end mills the

parts was successfully made. The part cavity bar fabrication process is listed in Table 3-9.

Process #	Feature	Process	Process Description	Tool#	Time (mins)
1	Blank	Ground	Precision ground to proper thickness	- outsourced	
2		Mill	Mill to proper length and width	- outsourced	
3	Holes	Drill	Center Drill (16)	4	4
4		Drill	Drill ejector pin holes (12)	1	6
5		Drill	Drill clamping holes (2)	1	2
6		Mill	Square shoulder holes (2)	11	2
7	Cavity	Mill	Volume clear part cavity (4)	11	40
8		Mill	Machine bottom surface of cavity (4)	11	14
9		Profile Mill	Machine side walls of cavity (4)	9	40
10	Gate	Mill	Machine triangular gate (4)	11	3
11	Runner	Mill	Runner to gate entrance (4)	10	8
12	Sides	Profile Mill	Round outer corners (left)	12	8
13		Profile Mill	Round outer corners (right)	12	8
14	Holes	Ream	Ream ejector pin holes	5	4

Table 3-9: Fabrication Steps for 4-Part Cavity Bar

3.4.6 Machining: Runner-Intersection and Blank Inserts

The runner-intersection is the blank insert with the runner paths milled into it. Thereby it makes sense to first build all the blank inserts plus a few extra, then check dimensions and proceed with milling the runners into two of the blank inserts. Initially the long stock material was received with the proper thickness and width. The stock bar was sectioned using a band saw, and then clamped into milling machine and cut to the proper length. The next and final step into making the blank insert was the profile milling of the sides. In order to make the runner-intersection insert, the blank insert was modified

by milling runner paths into it using the tapered ball end mill. The process is summarized in Table 3-10.

Process #	Feature	Process	Process Description	Tool#	Time (mins)
1	Blank	Ground	Precision ground to proper thickness	- outsourced	
2		Cut	Bandsaw to oversized length	Band Saw	
3		Mill	Mill to proper length and width	12	5
4	Shoulder	Profile Mill	Round shoulder (right)	12	8
5		Profile Mill	Round shoulder (left)	12	8
6	Runner	Mill	Machine runner paths	10	6

Table 3-10: Fabrication Steps for Runner-Intersection Inserts

3.5 QUALITY CHECK

With geometric tolerances set to 0.001", the ability to check dimensions using standard gauges and calipers become arduous. By fitting the CNC machine with a probe, the milling unit was converted into a CMM machine. With dimensional accuracy of 0.0001", the machine was better able to confirm the dimensions to be within specification. Other dimensions such as the width of cavities on the runner bars and part cavity were confirmed using pin and block gauges, as well as calipers. Additionally the clearance of all the ejector holes were confirmed by assembling the plates and inserts together, and passing an 1/8" ejector pin through every hole. With all the critical dimensions measured to be within tolerance, the total assembly was confirmed to be completely geometrically balanced about the sprue hole. Figure 3-14 and 3-15 present examples of the fabricated test mold product.

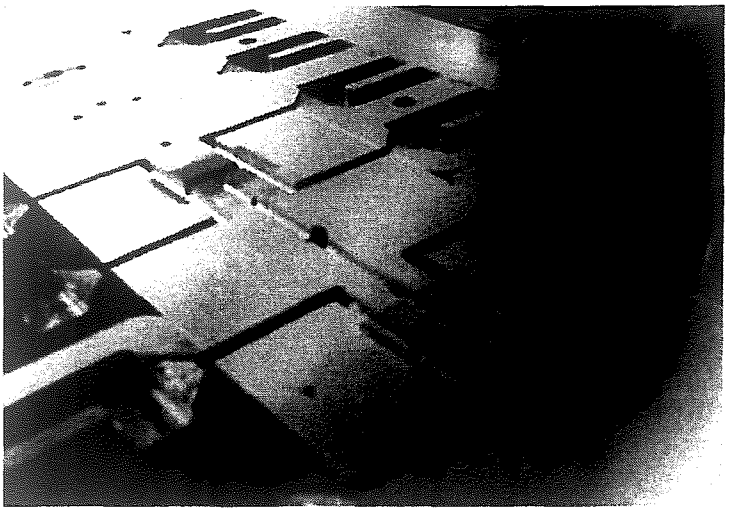

Figure 3-14: B-Plate Assembled (Short)

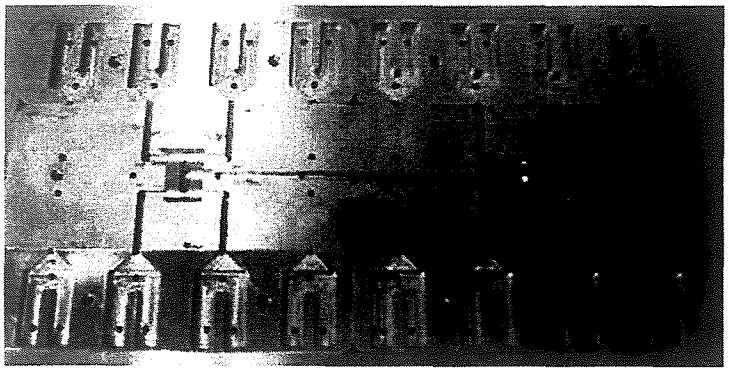

Figure 3-15: B-Plate Assembled (Medium)

4 IMBALANCE INVESTIGATION: DESIGN & PROCEDURES

With cooling lines machined into the mold, the experimental tool was now complete and ready for actual testing. Chapter 4 begins with the objective of the experiment that serves as a guideline for preparation and procedure. Preparation starts with a list of the required machines and equipment necessary to complete the objectives. The groundwork also incorporates selection of the proper material and its preparation prior to injection molding. The controlled process settings also had to be chosen based on the needs of the test. With the preparation complete, a step-by-step procedure, illustrating the followed methodology during the entire experiment, will be laid out.

4.1 EXPERIMENTAL OBJECTIVE

Considering the mold allows for three primary runner settings, it is evident that part of the objective is to analyze a material's fill imbalance data with respect to the other runner lengths. By switching the runner setting, the duration to shear heating would change, possibly having an impact on fill characteristics. Additional to the runner length, injection velocity, which has been proven to be a great factor towards fill imbalance, is to be tested. Recalling that viscous energy dissipation is a function of shear rate squared, by increasing injection velocity the total heat generation should increase causing the outer perimeter to be even less viscous. Additional to the processing conditions, it is important to test more than a single polymer as it has been cited numerous times that the selected material greatly impacts the results. By testing a multitude of polymers, additional material properties could be compared with respect to the results. The objective was then

to compare fill imbalance measurements for different materials, injection velocities, and primary runner lengths.

4.2 EXPERIMENTAL SETUP

Prior to making short shot parts, proper preparation had been completed to smoothly operate the experiment. First and foremost, an injection molding machine capable of operating the large mold had to be selected, as well as other tools and equipment necessary to create data.

4.2.1 Equipment and Tools

It is important to note prior to diving into this chapter that this project was conducted jointly between Lehigh University's Manufacturing Science Laboratory (MSL), and Pennsylvania State University Erie's Plastics Engineering Technologies department. Manufacturing of the test mold was completed at Lehigh University, while actual testing and data gathering were done at PSU's Plastic Processing Laboratory in Erie. The decision of where to machine and operate was based on comparison of capabilities between the two institutions. Lehigh University's MSL group specializes in manufacturing molds but does not have an injection molding machine that could house such an immense mold. PSU's Plastic Processing Laboratory on the other hand, has more than a few large scale molding machines available for use.

The chosen injection molding machine within the laboratory was the Husky 90-ton Hylectric injection molding machine. Easily capable of operating the large test mold, its processing abilities, limits, and features are impressive as pictured below.

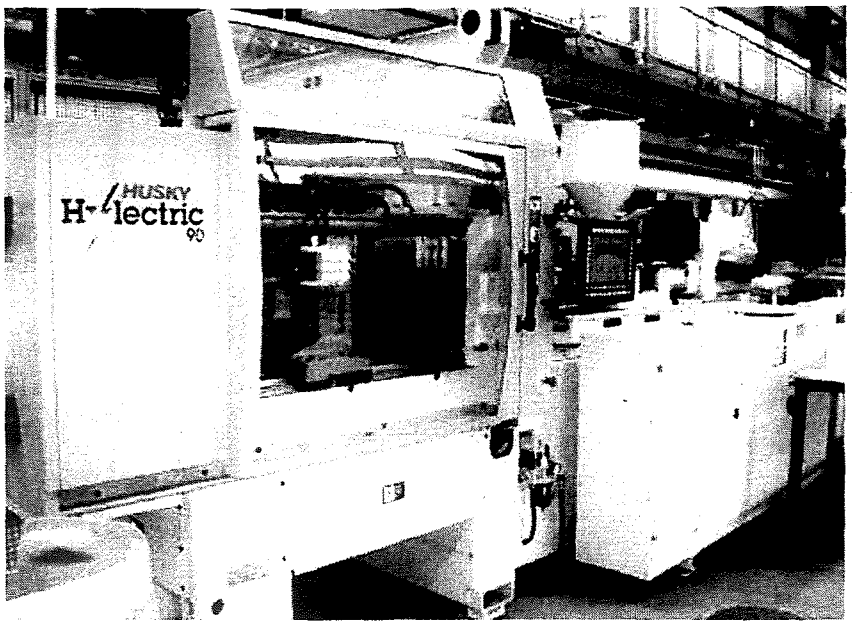

Figure 4-1: Husky Hylectric 90-ton Injection Molding Machine at PSU-Erie

In order to measure fill imbalance characteristics, individual parts had to be weighed and recorded and compared to one another. In order to obtain precise data, parts had to be measured using scales that have sensitivity of at least $1/100^{th}$ of a gram, and have a digitized readout for ergonomic purposes.

4.2.2 Material Selection and Preparation

With the injection molding unit ready and the proper tools necessary to record data on hand, the material to be tested had to be chosen. As specified in previous sections, fill imbalance characteristics heavily fluctuate based on the selected material. Within the sea of properties that distinguishes a polymer, there are certain unknown factors that are the cause of variation in fill imbalance with respect to tested material. It

was this research project's secondary objective to identify one of these factors; thereby it was important to pick materials that were from different families with distinguishing material characteristics. Considering time and budget constraints, in the end the testing of three materials was decided upon.

The tested materials were chosen based on both previous experimental results and material availability. ABS or *acrylonitrile butadiene styrene* was the first material chosen as it had been extensively tested in the past. The material is an amorphous polymer with good impact strength and excellent physical appearance. Industries such as the housing, small appliances, and automotive regularly use this material due to its ease of process ability. More specific material properties will be listed and discussed in chapter 5 when test results will be correlated to fill imbalance characteristics.

The second material chosen was HIPS or *high impact polystyrene*. It is a vinyl copolymer and has a molecular structure of a styrene backbone with polybutadiene branching off the main chain. These rubbery polybutadienes act to absorb energy when the material is hit, thereby making it stronger and more capable of handling larger impacts, hence the name "high impact". From previous experiments, HIPS has shown a clear trend of increasing fill imbalance with increase of injection velocity.

The third material chose was HDPE, or *high density polyethylene*. It is in essence a semi-crystalline polymer comprised of only ethylene monomers chained together with low amounts of branching. The lack of branching allows HDPE to occupy a lower volume per weight, hence the name "high density", which contributes to stronger intermolecular forces and tensile strength. During previous experiments, HDPE has

shown unique trademarks where a "reverse" fill imbalance occurs in which the outer cavities fill at faster rates than the inner cavities. These results strengthened the theory that fill imbalance is indeed material dependant, and polyethylene is a unique material that needed to be studied.

After the selection of polymers was reduced to the three families, it was necessary to choose the particular grade and manufacturer of each material. It is widely known that there are an abundant amount of choices when searching within a particular family. Numerous companies produce the material and offer varying grades that yield differences in material property and other features. Manufacturers change the grade in order to meet a particular customer need by altering the manufacturing process and mixing additives such as color, glass, and other fillers. In order to provide clarity between data and material property, the particular grades chosen are considered basic with no fillers or additional additives. The three particular materials chosen are as of such:

- Dow Chemicals Magnum 1040-7, ABS
- Paxon LA068E, HDPE
- Nova 9100 782H2, HIPS

4.2.3 Controlled Processes and Settings

Aside from the injection velocity, there are numerous settings of the injection molding process that can be controlled during a shot cycle. Parameters such as mold temperature, velocity-to-pressure (V P) switchover, and hold pressure are part of the

larger processing window and each will have an impact towards fill imbalance results. In order to reduce complications, these settings were fixed throughout the experiment.

The V/P switchover point for the Husky 90-ton is designated as a fraction of the incremental unit length in inches prior to the screw coming in contact with injection nozzle. The length signifies that the screw will move at the chosen injection velocity until reaching the mark, at which point the screw's velocity changes so the back pressure equals the packing pressure chosen by the operator. Considering the experiment focuses on fill imbalance with respect to shear heating, it would be optimal to set the switch-over point to the maximum value so the molded parts would mostly consist of material sheared at the chosen injection velocity. The maximum allowable V/P switchover value was determined to be 0.05" as anything higher than that would cause the screw to ram into the inner walls of the injection nozzle at high injection velocities. Since all parts that are to be produced are going to be short shots, there is no need to apply packing pressure, thereby an arbitrarily low value of 75 Psi was chosen for the packing pressure.

Mold temperature and cooling time for each material were manually determined based ease of part ejection. These values were held consistent for each of the three polymers along with the melt temperature, which was set according to manufacturers' suggested temperatures. Additionally, the injection volume was chosen by manually adjusting the value until the highest filled cavities visually looked to be 80% full. With change in runner length, the injection volume had to be changed as the longer runner settings constitute to a higher runner volume.

Finally the focused injection velocities were chosen based on several factors such as the capabilities of the injection molding machine and the ability to fill the mold. The highest value is ultimately driven by what the Husky 90-ton can accomplish, 13 inches/sec, while the lowest speed is slightly higher than the setting of when an undesired short shot due to runner freeze occurs. It would be optimal if numerous injection speeds could be tested in between the upper and lower values, yet due to the constraint of time, only two arbitrary values were chosen as the intermediate speeds. The tables below illustrate the final process settings for all three materials and runner lengths.

ABS	Runner Lengths		
	Short	Medium	Long
Injection Velocity	1, 2, 8, 13 ("/sec)		
Fill Volume (inch^3)	1.68	1.68	1.75
VP switchover	0.05"		
Cooling time	25 sec		
Mold Temp	100 F		
Melt Temp	490 F		
Hold	75 Psi		

Table 4-1: Test Settings for ABS

HIPS	Runner Lengths		
	Short	Medium	Long
Injection Velocity	1.5, 3, 8, 13 ("/sec)		
Fill Volume (inch^3)	1.87	1.93	2.00
VP switchover	0.05"		
Cooling time	18 sec		
Mold Temp	100 F		
Melt Temp	470 F		
Hold	75 Psi		

Table 4-2: Test Settings for HIPS

HDPE	Runner Lengths		
	Short	Medium	Long
Injection Velocity	0.5, 3, 7, 13 ("/sec)		
Fill Volume (inch^3)	2.31	2.37	2.37
VP switchover	0.05"		
Cooling time	25 sec		
Mold Temp	85 F		
Melt Temp	490 F		
Hold	75 Psi		

Table 4-3: Test Settings for HDPE

4.3 EXPERIMENTAL PROCEDURE

In any scientific field, it is important to produce clean data that can support a proposed theory or relationship. This experiment's goals were no different, and the method chosen to legitimize the data was by means of quantity. For every experimental

setting, at least ten consecutive parts were collected after the new setup had been stabilized by running it 3~4 times.

The repetitive process began with the shortest runner length at the slowest injection velocity, and ABS as the melt. The mold was first stabilized by running it 3~4 times at the chosen process settings, then ten parts were produced and collected. Additional information of injection pressure and fill time were recorded after every single run and each part was properly numbered in order to have the ability to track individual data with respect to these processing results. Additionally to the numbers, the parts were labeled with the injection velocity values in order to avoid confusion as well as to establish orientation to the mold. After the ten parts were collected and labeled, the injection velocity and the fill volume were changed, the setup was re-stabilized, and the process of collecting and labeling parts was repeated. Once all the injection velocities were completed, the runner bar was switched to the next runner length, and the entire procedure was repeated until all three runner settings were tested. The injection molding machine was then purged with the next material, and the entire process was repeated until all three materials had been tested. Table 4-4 below illustrates the 36 settings that were tested.

	ABS			HIPS			HDPE		
Runner / Inj Vel	Short	Med	Long	Short	Med	Long	Short	Med	Long
Very Low	X	X	X	X	X	X	X	X	X
Low	X	X	X	X	X	X	X	X	X
Medium	X	X	X	X	X	X	X	X	X
Fast	X	X	X	X	X	X	X	X	X

Table 4-4: Experimental Test Layout

4.4 EXPERIMENTATION COMPLETED

With all test settings complete, data was gathered by weighing each of the individual eight parts per short shot using a digital scale with accuracy of one-hundredth of a gram. The parts were de-gated from the runners, placed onto the scale for weighing, and recorded into a spreadsheet. The individual part weights were categorized as numbers 1 through 8, according to the format of Figure 2-2. In order to save time, out of the ten manufactured parts for each test setting, only six were measured and recorded as the weight fluctuation between consecutive shots were found to be minor. After completing measurements, individual cavity numbers were averaged and non-dimensionalized using the total average weight of all 48 parts (eight cavities, quantity of six) according to the equations 4-1 and 4-2.

$$W'_{avg} = \sum_{i=1}^{8}\sum_{j=1}^{6} W'_{ij} \qquad (4\text{-}1)$$

$$W(ND)_i = \frac{\sum_{j=1}^{6} W_{ij}}{W_{avg}} \qquad \text{for i=1:8} \qquad (4\text{-}2)$$

Where W represents the weight by grams, W(ND) represents the non-dimensionalized weight, i represents cavity number, and j represents trial number. The resulting values illustrate the volumetric fill percentage difference between individual cavities.

To be consistent with the work of Beaumont and other previous researchers experiments, values that symbolize inner and outer flow groups were created by averaging the non-dimensional fill results for cavities one through four, and cavities five through eight. These two values were then used and graphed with relation to both runner length and injection flow rate to serve as the foundation for analyzing the collective experiment. Table 4-5 below visually illustrates the methodology used to calculate fill imbalance for a particular runner length, injection velocity, and material. Please refer to Appendices B, C, and D for results of all the test settings.

	Inner Cavities				*Outer Cavities*				
HIGH	1	2	3	4	5	6	7	8	
(1)	2.64	3.14	2.88	2.72	1.38	1.72	1.52	1.60	
(2)	2.78	3.05	2.85	2.72	1.45	1.76	1.45	1.57	
(3)	2.62	3.12	2.78	2.70	1.35	1.77	1.52	1.57	
(4)	2.74	3.02	2.80	2.72	1.50	1.79	1.43	1.53	
(5)	2.70	3.03	2.62	2.57	1.43	1.71	1.54	1.66	
(6)	2.78	3.01	2.79	2.77	1.50	1.78	1.47	1.52	Total Avg.
Average (g)	2.71	3.03	2.79	2.73	1.43	1.75	1.49	1.57	2.196
ND Value	1.23	1.41	1.27	1.24	0.65	0.80	0.68	0.72	
	1.288				0.712				

Table 4-5: Fill Imbalance Calculation Method for ABS with Medium Runner Length, and Injection Velocity of 13 inches/sec.

With fill imbalance data calculated for all test settings, graphs were made to correlate the results to the tested settings of injection velocity and primary runner lengths. The visual plot illustrates relationship fill imbalance has to these settings, and Chapter 5 will discuss these plots for all three materials.

5 RESULTS AND DISCUSSION

With all the parts measured and tabulated, this chapter will focus on displaying the final results, and discussing the relationship fill imbalance has to primary runner length and injection velocity. As mentioned previously, fill imbalance is heavily related to melt material and results from this experiment were not an exception to this case. The resulting plots illustrated strikingly different characteristics; thereby this chapter will be sectioned according to the three tested materials. Each section will display fill imbalance with respect to injection velocity and then to primary runner's length-to-diameter ratio.

5.1 RESULTS FOR HIPS

Unlike other materials such as ABS, PE, and PMMA, previous work by Beaumont and his research group never really focused on high impact polystyrene. One experiment conducted by Shuttleworth [13] though did include HIPS and noted that its viscosity is more thermally sensitive than polypropylene's. Other than this piece of information, all the results yielded from this experiment will serve to chart a new profile for HIPS, and will be added to the cache of existing data that will eventually help shape the complex relationship material properties have to fill imbalance. During this experiment, fill imbalance to the inner cavities ranged anywhere from 1.004 to 1.155. The data for all the testing for HIPS is presented in Appendix B.

5.1.1 Fill Imbalance With Respect to Injection Velocity

Grouping data by runner setting and plotting it with respect to injection velocity resulted in three distinct curves. The corresponding data and plot are illustrated in Table 5-1 and Figure 5-1.

HIPS	Runner Lengths					
	Short		Medium		Long	
Injection Vel	Outer	Inner	Outer	Inner	Outer	Inner
1.5	0.996	1.004	0.912	1.088	0.856	1.144
3	0.968	1.032	0.897	1.103	0.853	1.147
8	0.930	1.070	0.884	1.116	0.856	1.144
13	0.912	1.088	0.878	1.122	0.845	1.155

Table 5-1: Fill Imbalance with respect to Injection Velocity (HIPS)

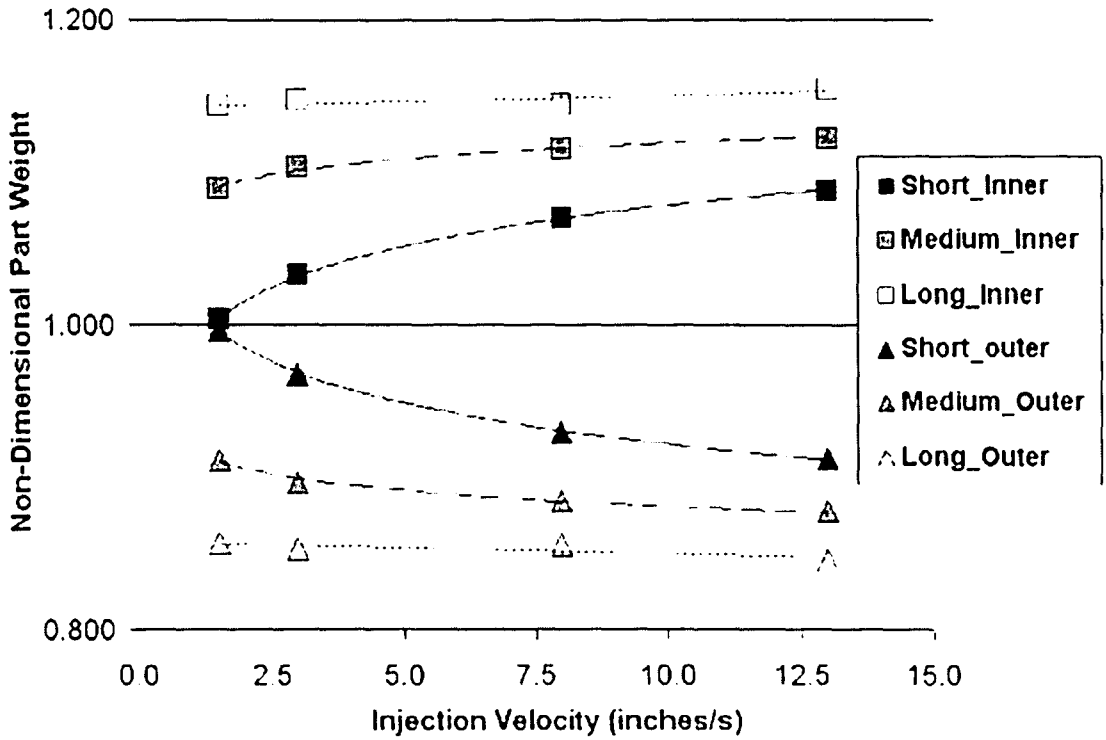

Figure 5-1: Fill Imbalance with respect to Injection Velocity (HIPS)

At the shortest runner length, the characteristic curve is a clean trend of fill imbalance increasing with injection velocity. As the runner lengths are increased though, the trend becomes less pronounced with the curve for the longest runner length setting resembling a rather flat line. If the plots were to be extended, the curves would perhaps reach an asymptote where change in fill imbalance becomes negligible with respect to injection velocity. This existence of a limitation parallel results of previous experimentation which also studied fill imbalance with respect to injection velocity. [1, 10, 16]

Close observation of Figure 5-1 shows that at low injection velocity, fill imbalance results significantly fluctuate between the three runner settings, and as injection rates are increased, the range narrows. Additionally, comparison of the extreme values between very low injection velocity (@ L/D of 39) to high injection velocity (@ L/D of 13) suggests that temperature may have a larger impact on HIPS's viscosity then shear rate. Regardless of judging which factor has more impact, the two processing conditions contribute in unison towards increasing fill imbalance. The largest weight difference occurred when both the injection rate and runner length were at their maximum settings.

A distinguishing feature for HIPS is that fill imbalance does not occur when both the runner length and injection velocity are at their lowest. Using the fill imbalance vs L/D plot below, a better assertion can be made about the nature of thermodynamics and heat transfer that occurs at this specific setting.

5.1.2 Fill Imbalance With Respect to L/D Ratio

Reorganizing the data in Table 5-1 so it's grouped according to primary runner length, and plotting it with respect to L/D ratio generates Figure 5-2 which illustrates an additional relationship HIPS has to the controlled settings.

HIPS	Injection Velocity							
	1.5"/sec		3.0"/sec		8"/sec		13"/sec	
L/D Ratio	Outer	Inner	Outer	Inner	Outer	Inner	Outer	Inner
13	1.00	1.00	1.03	0.97	1.07	0.93	1.09	0.91
26	1.09	0.91	1.10	0.90	1.12	0.88	1.12	0.88
39	1.14	0.86	1.15	0.85	1.14	0.86	1.15	0.85

Table 5-2: Fill Imbalance with respect to L/D Ratio (HIPS)

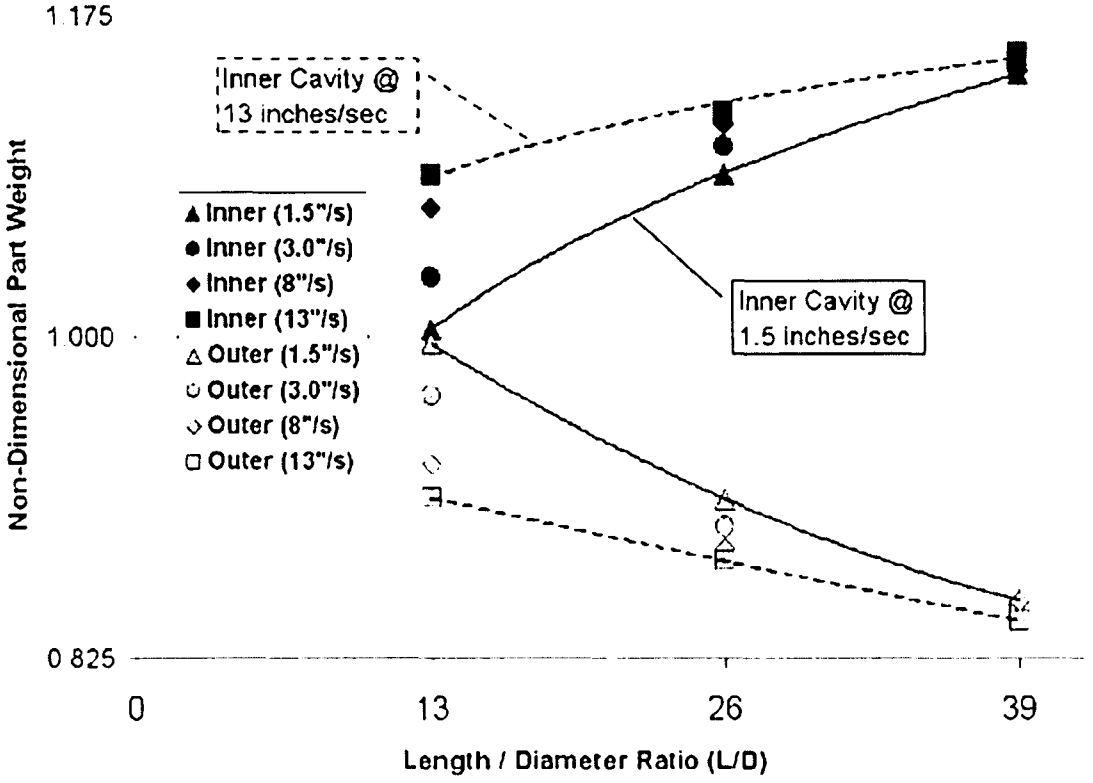

Figure 5-2: Fill Imbalance with respect to L/D Ratio (HIPS)

In the previous section the existence of an asymptote, a limit injection velocity has towards total fill imbalance, was discussed. Figure 5-2 helps to support this case as the data of the higher injection rates, 8"/sec and 13"/sec, are very close to one another at every L/D setting, resembling a low ceiling. On the other hand the limitation of L/D towards fill imbalance does not seem to have been reached yet during this experiment. Room exists for higher imbalances to occur at longer runner settings, but the parabolic curvature implies that extension of both curves would perhaps result in an eventual asymptote at around 1.2.

Changing the runner length does not alter applied shear rate but only the exposure to viscous heating which causes a change in temperature profile. Thereby each consecutive point on the same trend line for Figure 5-2 illustrates how additional exposure to heating could cause the temperature difference between the perimeter and core to occur, ultimately controlling fill imbalance. Analyzing the figure from a heat transfer perspective would give an assertion that indeed viscous heating effect plays a significant role in developing the melt viscosity profile.

$$\dot{Q}_{generated} = \dot{Q}_{VED} - \dot{Q}_{Loss} \qquad \textbf{(5-1)}$$

As long as the rate of heat generation through viscous energy dissipation rate, VED, is larger than the rate of heat loss through the cold mold walls, extending the duration would result in a higher temperature of the outer perimeter as it reaches the secondary runner. Thereby parts made at a longest runner setting would be the most imbalanced as the viscosity differences between perimeter and core would be even higher. Considering rate of heat generation through viscous heating as a function of both time and shear rate squared, differences in injection velocity would yield individual trend lines. Figure 5-2 proves that indeed these factors create slopes of different value for every injection rate. For HIPS, the fill imbalance increases with respect to L/D, is high for the slowest injection velocity and decreases as the injection rates are increased.

With regards to the condition where a near perfect filling pattern occurs, it occurred when settings would produce the lowest viscous energy dissipation rate, give the shortest exposure to any heating, and shear rates at the outer boundary would be

lowest. This can only add up to minimal viscosity differences between the outer perimeter and core of the flow, causing only a slight fill imbalance variation. Results for HDPE which will be discussed later, sheds more light to why this perfect fill characteristic occurred for HIPS.

5.2 RESULTS FOR ABS

ABS has been tested in the past on several occasions and the resulting correlation to injection rate has conflicted with the original theory that the problem should be exacerbated by increasing injection rate. Earlier experiments by Beaumont (GE Cycolac GPM 5500 ABS), showed that fill imbalance actually improved with increase in volumetric flow rate [1]. This characteristic has also been observed during Reifschneider's experiment while utilizing a similar ABS (GE Cycolac 4700) [10]. This primary runner length experiment on the other hand, utilized a different grade of ABS, and results did not parallel previous findings. Additionally the novel comparison to runner length illustrated that runner length does indeed have an impact on fill imbalance.

5.2.1 Fill Imbalance With Respect to Injection Velocity

Summaries of the results generated with ABS are presented in Table 5-3 and Figure 5-3. When comparing results generated with HIPS, it is immediately apparent that ABS has a much larger problem with fill imbalance. With the maximum non-dimensional flow imbalance value of 1.15 for HIPS being shy of the minimum value of 1.18 for ABS, the materials can be categorized according to their sensitivity towards shearing. Although this superficial description may have grounds, it is necessary to compare more in depth

trends and relationship the polymers have to injection velocity and L/D ratio. It is also important to review and compare material property differences between the three polymers and identify any characteristic that causes the difference in fill pattern. These issues will be discussed in a later section.

ABS	Runner Lengths					
	Short		Medium		Long	
Injection Vel	Outer	Inner	Outer	Inner	Outer	Inner
1.0 "/sec	0.802	1.198	0.717	1.283	0.651	1.349
2.0 "/sec	0.82	1.18	0.737	1.263	0.676	1.324
8.0 "/sec	0.775	1.225	0.733	1.267	0.711	1.289
13.0 "/sec	0.732	1.268	0.712	1.288	0.716	1.284

Table 5-3: Fill Imbalance with respect to Injection Velocity (ABS)

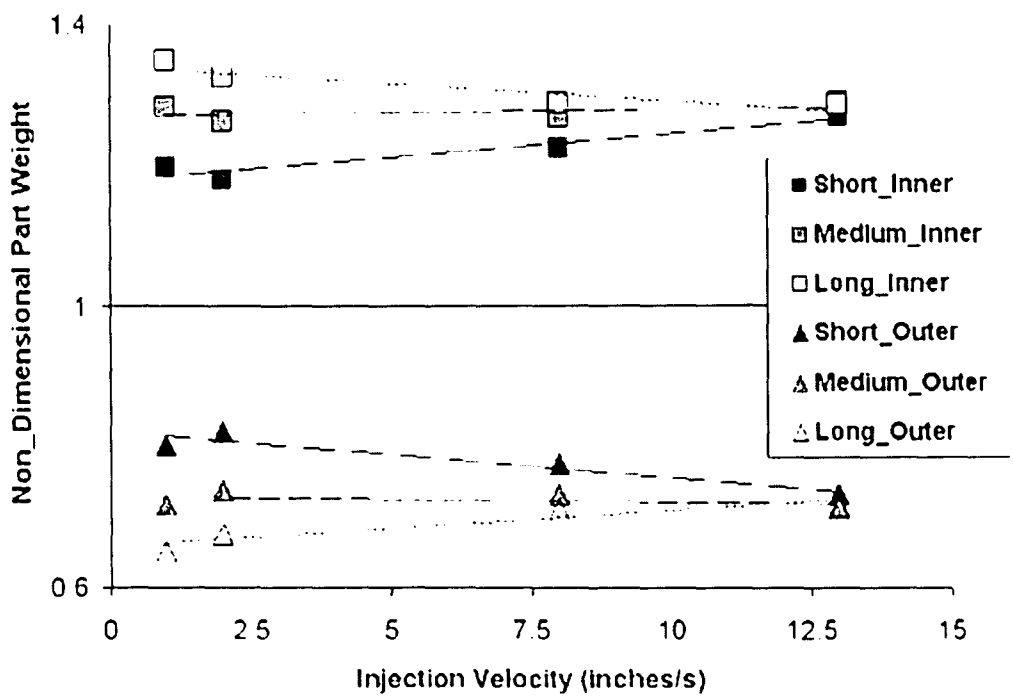

Figure 5-3: Fill Imbalance with respect to Injection Velocity (ABS)

For the setting which most closely resembles that of a conventional 8-cavity mold, the shortest runner length setting, fill imbalance increased with increase in injection velocity. With runner length extended to the medium setting, the results showed stability throughout the tested spectrum. Results for the longest runner length actually paralleled previous experiments where filling slightly improved with increase of injection rate. A possible explanation for this reverse trend is that radial heat exchange alters the temperature profile so the boundary layer of the hotter material creeps towards the center, causing more thin material to enter the outer cavities. This hypothesis will be discussed in more detail during the discussion of results with respect to L/D ratio.

Figure 5-3 shows that at low injection velocities, fill imbalance results significantly differs for the three runner settings. When injection velocity is at its maximum though, these differences are minor and the results are almost identical to one another. The joining of the trend line implies there to be a limitation injection velocity has towards fill imbalance, reaching an asymptote where the data clusters close together at the fastest injection rate.

5.2.2 Fill Imbalance With Respect to L/D Ratio

Reorganizing the data of Table 5-3 so results are compared to the L/D ratio, paints a different picture of how fill imbalance is related to primary runner length. The result is presented in Table 5-4, with the corresponding graph given in Figure 5-4.

ABS	Injection Velocity							
	1.0"/sec		2.0"/sec		8"/sec		13"/sec	
L/D Ratio	Inner	Outer	Inner	Outer	Inner	Outer	Inner	Outer
13	0.802	1.198	0.82	1.18	0.775	1.225	0.732	1.268
26	0.717	1.283	0.737	1.263	0.733	1.267	0.712	1.288
39	0.651	1.349	0.676	1.324	0.711	1.289	0.716	1.284

Table 5-4: Fill Imbalance with respect to L/D Ratio (ABS)

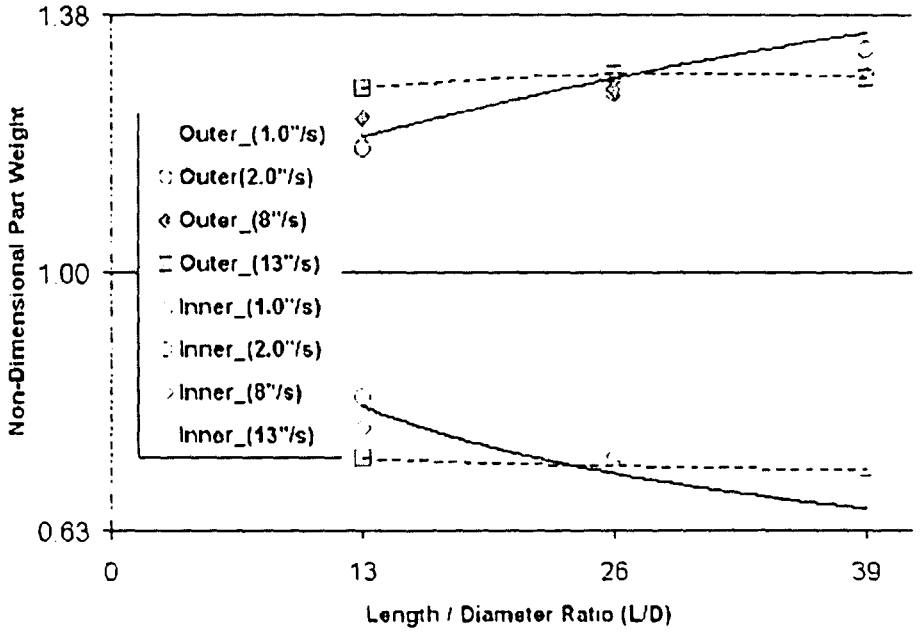

Figure 5-4: Fill Imbalance with respect to L/D Ratio (ABS)

Figure 5-4 supports the component theory of shear heating having an impact on fill imbalance. With viscous heating duration increased, it was originally hypothesized that the outer perimeter would become even less viscous, causing the imbalance between the two flow groups to be further exacerbated. The hypothesis holds well for the slower

injection rates, but as speed reaches the maximum, a more stable flat line develops where fill imbalance is not affected by L/D ratio.

Analyzing the stable trend from a heat transfer perspective, it is possible that another limit exists where the radial distance between the cooler and hotter material shifts towards the core as duration continues to increase. With viscous heating proportional to shear rate squared, the fastest injection velocity would generate immense heat which accumulates over the course of the long runner length. As the melt travels down the primary runner, heat exchange between adjacent materials cause the temperature gradient to morph and the radial boundary location of the hot and cool melt interface shift towards the core, as illustrated below in Figure 5-5.

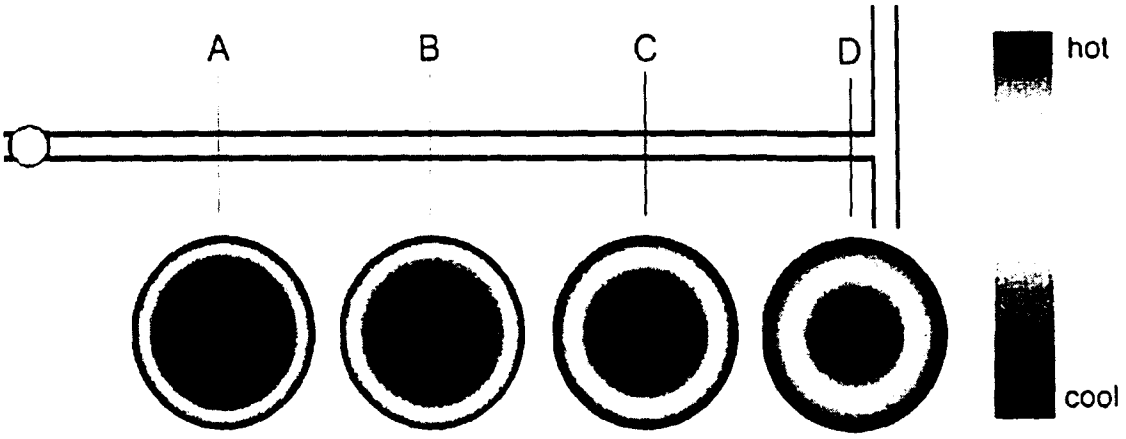

Figure 5-5: Shift of Temperature Profile with Increase of Runner Length

As the melt with the hotter temperature profile splits into the secondary layer, the cooler core constitutes a smaller volumetric flow rate, hence more material of lower viscosity can be directed towards the outer cavities causing the difference in fill rates to shrink. This theory helps to explain why Figure 5-3 shows a reverse trend when L/D is 39, and

also why the trend line becomes flat when injection rates are their highest. Explanation as to why ABS is susceptible to this reverse trend, and not HIPS, requires a more in depth review and comparison of material property differences between the two.

5.3 RESULTS FOR HDPE

Previous experiments yielded curiosity to further study polyethylene groups as it is one of the few materials that show a "reverse" fill imbalance, where the outer cavities fill at faster rates then the inner cavities. The contrasting phenomenon always occurs at very low injection rates, but returns to the normal fill imbalance as the velocity is increased. Interestingly enough, the reverse imbalance was also observed during this experiment, and a comparison with respect to certain material properties must be made to better explain why this occurs..

5.3.1 Fill Imbalance With Respect to Injection Velocity

Results for HDPE are presented in Table 5-5 and Figure 5-6. With reverse filling imbalance occurring at the lowest injection rate, there are more than a few differences HDPE has with the other two materials. Aside from this phenomenon, there are still distinct similarities between all three materials fill imbalance graphs. Listed below are the data and resulting graph comparing fill imbalance to injection velocity.

HDPE	Runner Lengths					
	Short		Medium		Long	
Injection Vel	Inner	Outer	Inner	Outer	Inner	Outer
0.5	0.89	1.11	0.84	1.16	0.85	1.15
3.0	1.04	0.96	1.05	0.94	1.07	0.93
7.0	1.07	0.93	1.08	0.92	1.09	0.91
13.0	1.07	0.93	1.08	0.92	1.10	0.90

Table 5-5: Fill Imbalance with respect to Injection Velocity (HDPE)

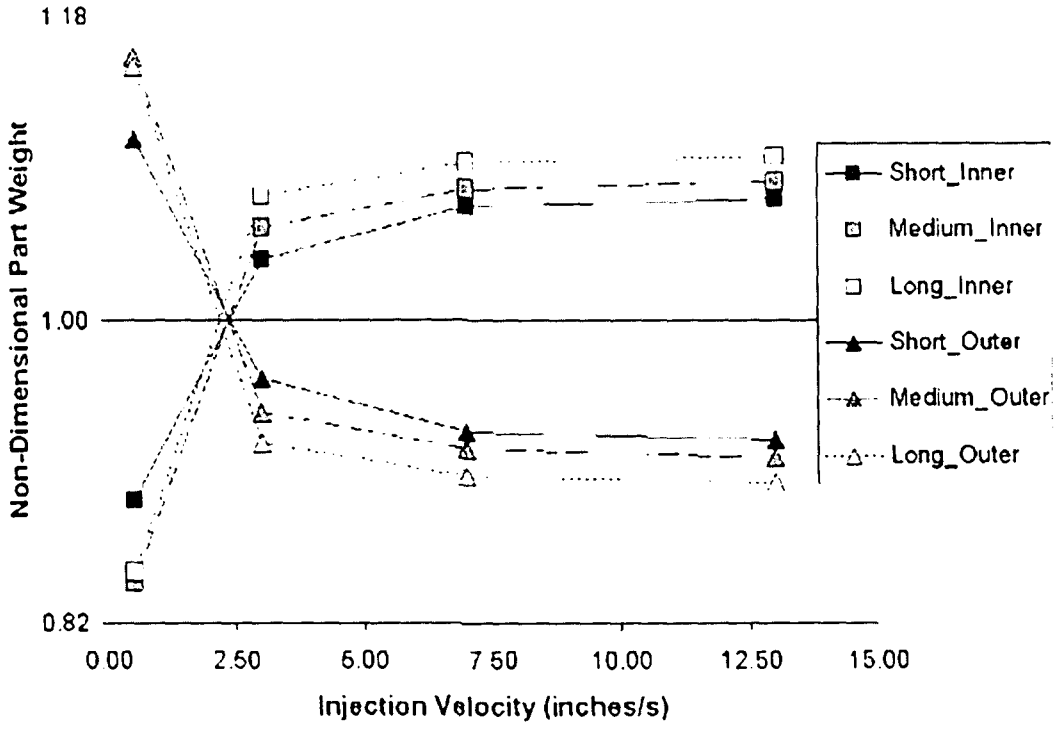

Figure 5-6: Fill Imbalance with respect to Injection Velocity (HDPE)

The figure and table above shows that maximum "normal" fill imbalance once again occurs at the highest injection rate and runner length, with the value being 1.10. This value is lower than HIPS's 1.15 and significantly smaller than ABS's maximum of

1.28. These values can be used to categorize HDPE as being the least shear sensitive material out of the group, but it falls short of explaining the differences in other characteristics. More notably the recovery from reverse to normal fill imbalance at a rather low injection rates indicates that HDPE can also experience perfect filling without the use of melt rotation technology. Additionally the similarity and trend implies that HIPS is also prone to reverse fill imbalance if injection rates are slow enough.

HDPE's fill imbalance with respect to injection velocity shares numerous similarities with ABS and HIPS. First, fill imbalance increase is proportional to injection velocity, and an asymptote exists where rate increases appear to no longer impact to the results. For HDPE's case, the limitation is reached rather quickly as results for injection rate of 7"/sec and 13"/sec are identical. A third similarity with the other polymers is how fill imbalance increases with increase in L/D ratio. It should be noted though that in the case of reverse fill imbalance, it is the outer cavities that fill more with increase in runner length.

The obvious difference between HDPE and the previous two materials is that an actual reversal of fill imbalance occurs at the slowest injection velocity. In order to better explain a possible reason for this reverse fill imbalance, it is pertinent to first relate fill imbalance to L/D and review the process from a thermodynamic perspective.

5.3.2 Fill Imbalance With Respect to L/D Ratio

Results for HDPE focusing on runner length effects are presented in Table 5-6 and Figure 5-7. With the data grouped according to injection rate and compared to the L/D ratio, a plot that is very extra-ordinary looking develops.

HDPE	Injection Velocity							
	0.5"/sec		3.0"/sec		7"/sec		13"/sec	
L / D Ratio	Inner	Outer	Inner	Outer	Inner	Outer	Inner	Outer
13	0.893	1.107	1.035	0.965	1.067	0.933	1.071	0.929
26	0.844	1.156	1.054	0.945	1.077	0.923	1.082	0.918
39	0.850	1.150	1.073	0.927	1.093	0.907	1.097	0.903

Table 5-6: Fill Imbalance with respect to L/D Ratio (HDPE)

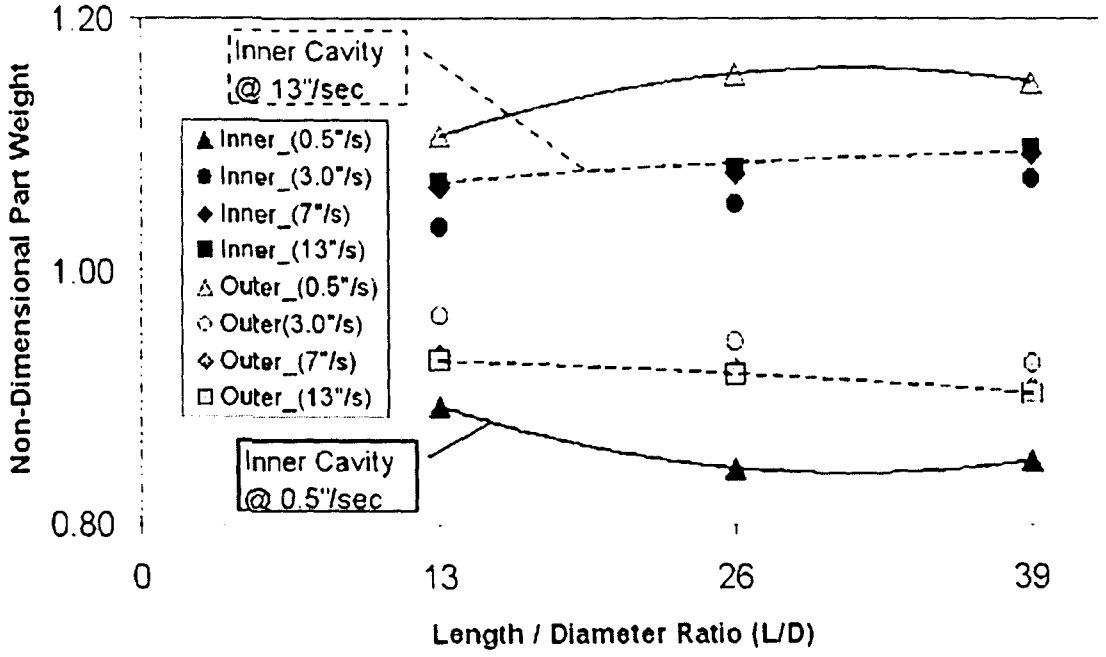

Figure 5-7: Fill Imbalance with respect to L/D Ratio (HDPE)

The graph's uniqueness is due to the reversal phenomenon where the outer cavities fill faster than the inner cavities at low injection velocities. This causes the plot to look rather confusing, but putting the results for lowest injection rate aside, the remaining results parallel those of ABS and HIPS. As the L/D ratio is increased, additional duration to

viscous heating causes the normal fill imbalance to worsen. With increase of injection velocity though, the degree of impact L/D has towards fill imbalance is reduced, much like the previous case studies. What sets HDPE apart from ABS and HIPS is how L/D has a minor impact towards fill imbalance as the trend lines are rather flat. It was stated earlier that HDPE can be carelessly classified to be the most shear-insensitive, but could it also be the more insensitive towards viscous heating? The following section will better explain how certain material property differences could be the key to the observed fluctuations based on material.

The phenomenon of reverse fill imbalance is a very important finding for this project as if it were to be misunderstood, it could be potentially be used to undermine the theory of shear induced fill imbalance. This author believes the theory holds grounds even for HDPE at the tested injection rates, but believes that the dynamics of heat transfer between the cool mold walls and melt are the additional factors that cause the reversal. Numerical programs tend to make assumptions that the walls are adiabatic, where heat transfer is negligible considering the short time lapse, yet this is assumed only to simplify codes and associated calculations. If in fact injection rates were slow enough, premature freezing would occur within the runner system and no material would ever reach the part cavity. Thereby if rates are slow enough and heat generated through viscous heating is over powered by heat loss through the mold walls, the bulk temperature of the outer material will drop causing the viscosity of the outer perimeter to rise above the core's viscosity. This will inevitably lead to thicker material being directed towards the inner cavities while the less viscous core is directed toward the outer cavities. At a certain

injection velocity, about 2.5 inches/sec for HDPE, the total heat loss counterbalances viscosity decrease due to shear rate, creating a rather flat viscosity profile across the melt flow. The theory is illustrated in Figure 5-8.

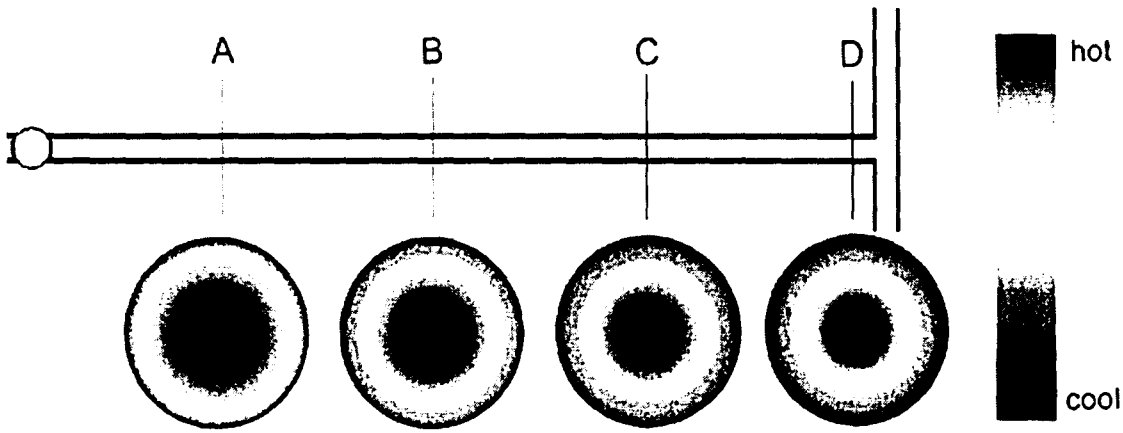

Figure 5-8: Shift of Temperature Profile with Distance for Reverse Fill Imbalance

5.4 COMPARISON OF RESULTS TO MATERIAL PROPERTIES

This experiment has shown that fill imbalance is highly dependant on the selection of material. The reason why though has not been really clarified thus far. Previous concluding remarks were rather broad with some pointing to certain factors such as temperature sensitivity, viscosity constant, and shear rate constant as related to the phenomenon. These general conclusions should be considered acceptable as research revolving around fill imbalance in naturally balanced runners is still in its early stages. Readers should also take into account that non-Newtonian polymers carry a plethora of properties that each could potentially have implications towards the result. With little

background work and guidelines to refer back to, early researchers experienced some difficulty in making connections between material and the phenomenon of fill imbalance. Additionally every polymer tends to be specialized according to a number of manufacturers, thereby the material properties change and are also not readily accessible to outside researchers.

This thesis will try to discover a correlation between an untested property to fill imbalance in hopes that future researchers will use it as a guideline. More specifically, attention would be placed on rheological properties and how the material's viscosity to shear rate characteristic relates to the observed experimental results.

5.4.1 Correlating Results to Viscosity vs Shear Rate Plot

Analyzing rheological properties requires the usage of complicated tools and procedures. A capillary rheometer would be the most applicable tool for this situation, as its range of shear rates are wide enough to match the high shear rate values experienced within the runner system. With proper testing conducted, plots such as the one below in Figure 5-9 can be developed, where viscosity is measured against both shear rate and temperature.

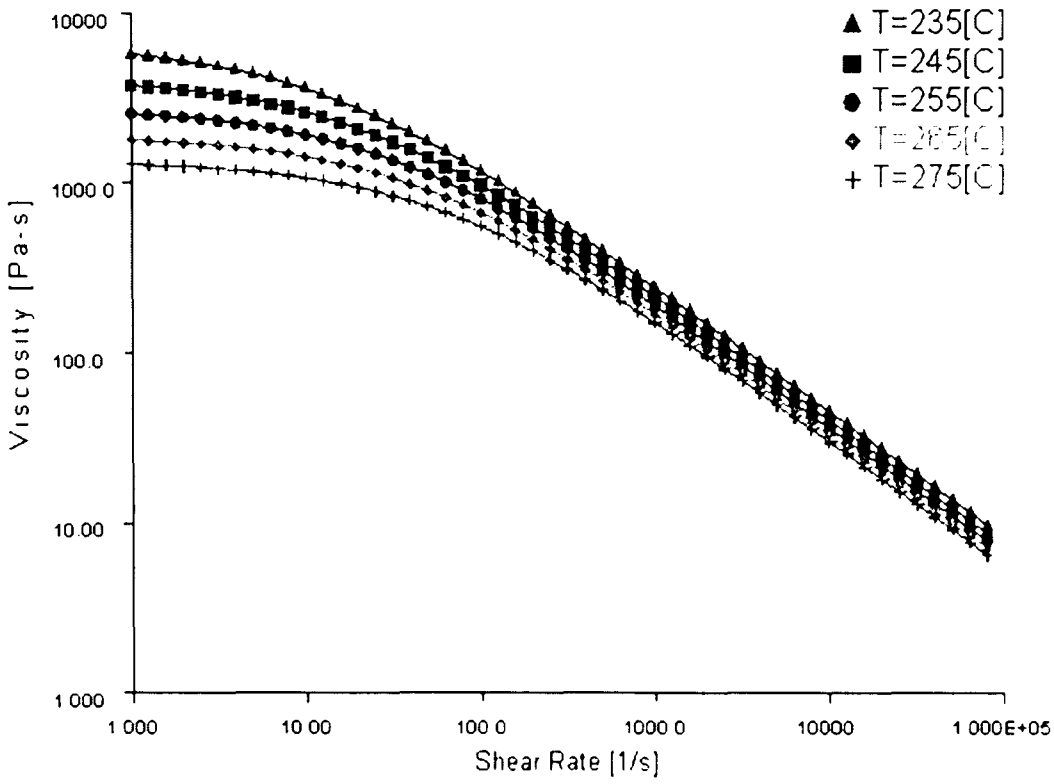

Figure 5-9: Viscosity vs Shear Rate Plot for DOW 1040 ABS

Manufacturers of polymers usually conduct these tests and are able to yield constants that can be later plugged into viscosity models to develop plots like Figure 5-9. The most comprehensive model is the Cross-WLF model which is well known to have the ability to accurately calculate viscosity across a very wide shear rate spectrum. The modified WLF equation [17] is listed below and is considered as the standard by both the industry and MoldFlow.

$$\eta(\dot{\gamma},T) = \frac{\eta_0(T)}{1+\left(\frac{\eta_0 \dot{\gamma}}{\tau^*}\right)^{1-n}} \qquad \textbf{(5-2)}$$

where

$$\eta_0(T) = D_1 \exp\left[-\frac{A_1(T-D_2)}{A_2+(T-D_2)}\right] \qquad \textbf{(5-3)}$$

Given the constants n, A_1, A_2, D_1, D_2, and τ^*, the viscosity of the polymer at a specified shear rate and temperature can be easily calculated. These values are very material grade specific, thereby exact values provided by the manufacturers should be used when trying to determine the viscosity. Fortunately both Dow Chemicals and Nova Chemicals cooperated by releasing these values for the tested materials in this study. A similar set of data for the Exxon Mobil HDPE was unfortunately not provided by the company. Thereby this section can only compare results for ABS and HIPS which are listed in Table 5-7. The complete material data sheets for the two material are provide in Appendix E.

Manufacturer	Dow Chemicals	Nova Chemicals
Trade Name	Magnum 1040 ABS	9100 - 782 HIPS
n	0.2535	0.3275
τ^* (Pa)	8.60E+04	2.17E+04
D1 (Pa-s)	9.44E+13	1.69E+12
D2 (K)	373.16	373
A1	32.34	28.77
A2 (K)	51.6	51.6

Table 5-7: Rheological Properties for the Tested ABS and HIPS

With the constants on hand, the only other required information is shear rate and temperature. Temperature will simply be the value at which the entire test was processed at, while the shear rate will have to be calculated using the apparent wall shear rate equation [5] listed below. As the name implies, the equation calculates the shear rate at the outer perimeter of the wall.

$$\dot{\gamma} = \frac{4Q}{\Pi r^3} \qquad \textbf{(5-4)}$$

Knowing the inner diameter of the injection molding machine's barrel, volumetric flow through the primary runner can be calculated by multiplying the barrel's cross-sectional area with the injection velocity. Since the melt splits into the left and right primary runner, the total volumetric flow rate must be divided by 2. The shear rate can now be calculated for the range of tested shear rates. The test setting is shown in Table 5-8 with temperatures in Celsius.

	ABS		HIPS	
Temperature	255 C		245 C	
Barrel Diameter	1.26 "			
	Min	*Max*	*Min*	*Max*
Injection Velocity (inches/sec)	1.5	13	1	13
Volumetric Flow Rate (inch^3/sec)	0.935	8.1	0.623	8.1
Shear Rate (1/sec)	4877	42268	3251	42268

Table 5-8: Testing Settings for ABS and HIPS

With all the necessary data on hand, data for viscosity curves was generated using a functional tool of MoldFlow. The data such as that presented in Table 5-9 was then exported into Excel and plots were created according to the experimented wall shear rates. Comparing the results and curves for HIPS and ABS at shear rate range of 3000 ~ 50000, an understanding of how rheological property plays a role in fill imbalance begins to develop.

Shear Rate	255 C - ABS	245 C - HIPS
2511.9	100.2	39.7
3162.3	84.9	34.2
3981.1	71.8	29.4
5011.9	60.7	25.3
6309.6	51.3	21.8
7943.3	43.3	18.7
10000.0	36.6	16.1
12589.3	30.9	13.8
15848.9	26.0	11.8
19952.6	22.0	10.1
25118.9	18.5	8.7
31622.8	15.6	7.5
39810.7	13.2	6.4
50118.7	11.1	5.5

Table 5-9: Viscosity vs Shear Rate Data for HIPS and ABS

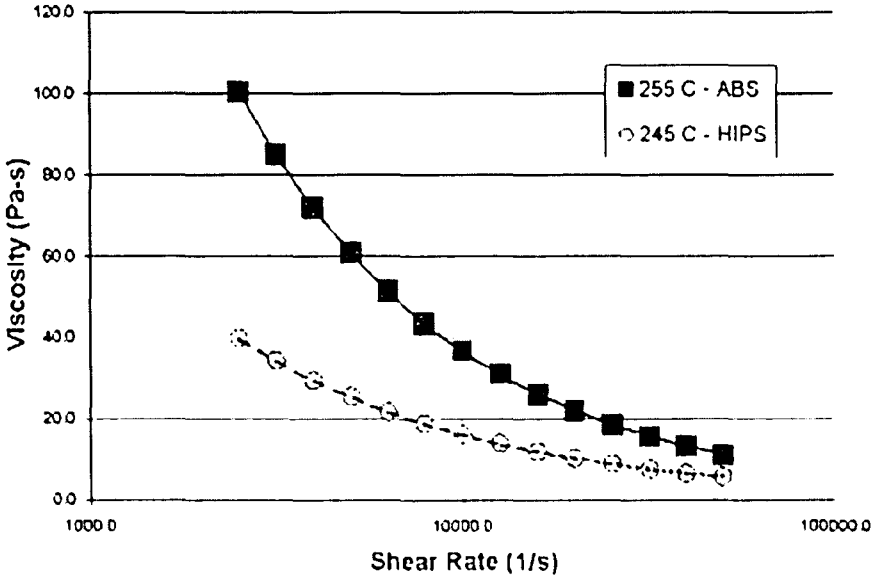

Figure 5-10: Viscosity Plot for ABS and HIPS at Operating Temperature

In the earlier sections of chapter 5, a simple observation was made where ABS was considered to be more shear sensitive than HIPS due larger fill imbalance.

Interestingly Figure 5-10 supports this superficial categorization as the slope of the curvature indicates that viscosity change due to shear rate is far higher for ABS than HIPS. With shear rates far higher at the outer perimeter, the magnitude of viscosity difference between the two layers is going to be larger for ABS, resulting in larger fill imbalance occurrence for ABS. When making an assessment between rheological properties and L/D ratio, additional calculations must be made to study the effect temperature has on the viscosity curve. MoldFlow was used again to generate viscosity relative to shear rate at additional temperatures. The data was exported to a spreadsheet, grouped according to shear rates, and plotted with respect to temperature as shown in Table 5-10 and Figure 5-11.

	ABS				HIPS			
Temp	5,000 1/s	10,000 1/s	25,000 1/s	50,000 1/s	5,000 1/s	10,000 1/s	25,000 1/s	50,000 1/s
235	76 4	45 9	23 1	13 8	29 1	18 4	10 0	6 3
245	67 8	40 8	20 6	12 3	25 3	16 1	8 7	5 5
255	60 7	36 6	18 5	11 1	22 3	14 2	7 7	4 9
265	54 9	33 1	16 8	10 1	19 9	12 7	6 9	4 4

Table 5-10: Viscosity Relative to Temperature and Shear Rate

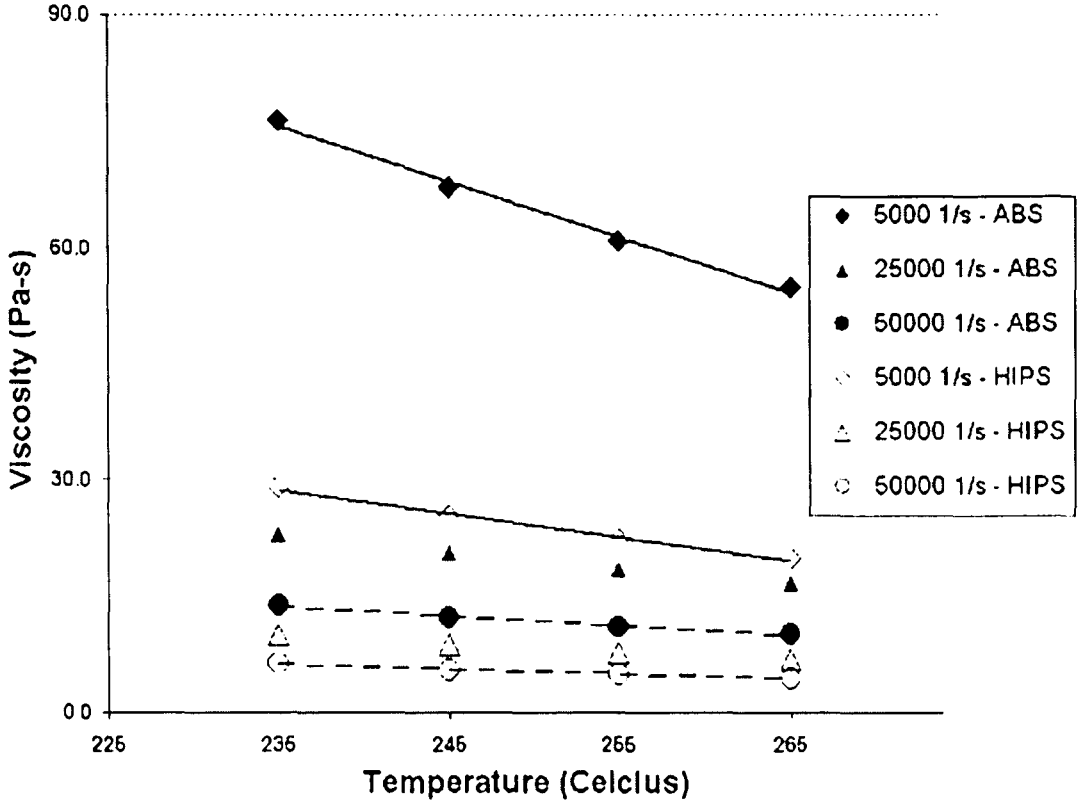

Figure 5-11: Viscosity Relative to Temperature and Shear Rate

Figure 5-11 illustrates that the viscosity's sensitivity to temperature is highly dependant on the original magnitude of viscosity. In fact the relationship is quite linear where viscosity decreases proportionally with increase in temperature, with the largest changes occurring when shear rates are relatively low. In other words viscosity change with respect to temperature is most evident when the magnitude of the viscosity is high. This correlates well with previous Figure 5-2 and 5-4where the largest change with respect to L/D ratio occurred when injection velocities were at their minimums.

5.4.2 Correlating Results to Thermal Properties

As theorized in the previous sections, conservation of energy results in a complicated heat transfer effect between the cool mold wall and the adjacent melt that is generating mechanical heat through viscous energy dissipation. In certain cases perfect fill balance occurs while other cases result in reverse fill imbalance, where the heat loss through mold walls causes the temperature to drop at the outer perimeter and ultimately increase the viscosity. As to why HDPE and HIPS experiences this while ABS is immune to this effect requires the study of the materials' thermal properties. Since specific properties were not provided by the manufacturer for HDPE, general data listed in a materials science handbook [8] will be substituted. Such data is presented in Table 5-11.

	HIPS	ABS	HDPE
k - Thermal Conductivity [W/m-K]	0.1827	0.15	0.63
Cp - Specific Heat [kJ/kg-K]	1866	2000	2300
ρ - Density [kg/m^3]	938	1000	1050

Table 5-11: Thermal Properties of Tested Material

When trying to make numerical simulation codes, industry tends to make several boundary condition assumptions such as the wall acting as an adiabatic surface, making heat transfer between the melt and the mold negligible. Through the development of reverse fill imbalance it has been proven that this is not the case, heat is being lost to the mold walls even though velocities through the runner system is fast. By reviewing the

data listed above, a link can be made between thermal properties and fill imbalance. The focused injection molding setting is at the slowest injection rates for HDPE and HIPS.

Thermal conductivity measures the ability to pass heat through its mass, and the higher the value, the more readily heat can transfer via conduction. At the same time heat conduction through the mold walls will be a function of the material's conductivity constant, and the higher the value, the more easily heat escapes through the cool mold walls. Comparing the three materials' thermal conductivity, it is apparent that HDPE will lose the most heat via the mold walls, and thereby should be susceptible to reverse fill imbalance.

Through studying the results from a material science perspective, certain novel connection seems to have been made between material properties and fill imbalance. The hope is that the analysis of this section and chapter will serve as guidelines for future researchers that hope to unveil the truly complexity of fill imbalance in geometrically balanced molds.

6 CONCLUSIONS AND RECOMMENDATIONS

6.1 CONCLUSION

This is the first time Lehigh University has conducted research on the topic of fill imbalance in geometrically symmetrical molds. Without knowing the existence of the theory of shear induced fill imbalance, previous guesses as to what would occur in the 8-cavity mold would have simply been that they all fill evenly. Even after reviewing papers by Beaumont and his research group, it was hard to imagine this phenomenon truly occurring thereby it was vital that this experiment first produce results of fill imbalance. Indeed fill imbalance occurred during this experiment and to such a significant degree that it validated Beaumont's previous work.

Other previous findings also surfaced during this project such as injection rate and materials having an impact on the phenomenon. With regards to injection rate, increasing the parameter exacerbated the problem in most situations. In some cases though, it had little effect. Additionally it has been declared within this thesis that a fill rate limitation exists where fill volume difference plateaus after a certain injection rate has been reached. The asymptotic limit varies based on both the material used and the length of the primary runner.

Besides confirming the phenomenon and observed previous findings, the main objective was to test if primary runner length has any impact towards the phenomenon. Changing the primary runner length would not affect shear rates as it is strictly a function of flow rate and runner diameter, but changing length would have an impact on the amount of heat generated through viscous heating. Considering viscosity is a function of

shear rate and temperature, results from this experiment would be able to segregate and quantify the magnitude of impact both parameters have on fill imbalance. The results supported this hypothesis as L/D had a significant effect on fill imbalance for all three tested materials.

Characteristic differences in the plotted results were explained from a heat and mass transfer perspective where the conservation of energy rule requires the outer perimeter to increase in temperature as long as heat generated through viscous energy dissipation overpowers heat loss through the mold. The empirical equation was valid for every situation as fill imbalance proportionally increased with L/D even when the reverse fill imbalance occurred while testing HDPE. Additionally, much like injection rate's relationship to the problem, it was discovered that L/D's impact on fill imbalance had a limitation. The rate of fill imbalance with respect to L/D, or simply put the slope of the resulting curve, decreased with increase in length. Combining the two asymptotic behaviors, it is this author's belief that 100% fill imbalance can never be reached even with an infinitely long primary runner and an unimaginably fast injection rate.

Besides mapping out relationships with mold geometry and processing conditions, this project had the objective to add clarifications as to why materials play a role in fill imbalance and what properties cause this fluctuation. Experiments conducted prior to this project tested a wide variety of materials and each published paper generally concluded that fill imbalance was heavily material dependant, with some adding correlations to temperature sensitivity and viscosity constants. With theory of shear induced fill imbalance focused on pinning the root cause to viscosity profile across the melt profile, it

was only natural that this project focused on polymers' rheological properties. With Cross-WLF constants provided by the manufacturers, viscosity curves for ABS and HIPS were produced and compared within the tested shear rate zone. The results showed that ABS's viscosity was far more sensitive to shear rate and temperature than for HIPS's. From an applied sense this indicates that the percentage of viscosity difference between the outer perimeter and the core for ABS would be higher than HIPS, resulting in higher fill imbalance for the former.

Rheological properties were also applied to help explain how L/D affects fill imbalance. Comparing viscosity at varying temperatures, the thermal sensitivity of a material can be yielded. The resulting plots illustrated that thermal sensitivity is based on the original layer thickness. As the material became thinner, the rate of viscosity decrease with increase in temperature declined. This finding proves that L/D would have the largest impact on fill imbalance when shear rates are lower, or when injection velocities are slow.

Finally in order to explain results for HDPE, thermal properties for all three materials were compared. With temperature of the outer boundary layer being a function of rate of viscous heating, heat loss through the cold mold walls, and heat transfer to adjacent material, thermal properties such as conductivity were considered pertinent factors towards total heat balance. Material data showed that HDPE had the largest thermal conductivity value out of the group, helping to explain why reverse fill imbalance occurred. With the highest rate of heat loss, the outer perimeter's temperature actually

decreased causing the viscosity to increase beyond the initial core value and ultimately leading to the outer cavities filling at a faster rate.

6.2 DIRECTIONS FOR FUTURE WORK

Although this research project made considerable progress in relating fill imbalance to runner length, processing parameters, and material property, the test was conducted on a limited scale and has left room for more research. Considering the complexity of the situation where a polymers temperature, viscosity, and possibly velocity profile continually change with travel distance and processing conditions, there are still numerous uncertainties revolving around what really causes the fill rates to fluctuate.

With regards to the primary runner's L/D ratio, fill imbalance seemed to have reached an asymptote. With HIPS and ABS though, there remained room for further imbalance while injection rates were at low speeds. Although this author firmly believes that 100% fill imbalance cannot be achieved in an infinitely long primary runner, it is still important to test if indeed these limits can be reached at L/D ratios a little bit larger than 39. To confirm the limitation of injection velocity, the test mold should be mounted onto larger machines capable of injection polymer at higher volumetric flow rate than the Husky 90-ton. Additionally it may be of interest to test the effect of secondary runner lengths to see if elongating it would have an effect on slowly rebalancing the temperature and viscosity profile across the melt.

In terms of a material's relationship to fill imbalance, there are still plenty of unknowns. With this project limited to three materials, with only two of them known for

their complete properties, it is difficult to defend the hypothesis that fill imbalance is highly related to both the sensitivity to shear rate and temperature. It is strongly recommended then to repeat the test with more materials for which the specific WLF and thermal properties are known before hand. Since most of these values need to be formally requested from the manufacturers, it is politely suggested to work with manufacturers that concentrate on polymers such as Nova and Dow, as their correspondence are more personal than larger companies that branch out too far. In terms of choosing the material, it would be best not to just randomly choose a number of materials, but perhaps materials that are of the same family yet have slightly different properties and sensitivity towards shear rate and temperature. By testing these similar materials from the same family, a process of elimination can be implemented to discover the true properties that control fill imbalance in naturally balance runner systems.

The reason why these projects must occur is because the industry lacks a proper program that can successfully simulate melt traveling through the runner system. It is strongly recommended to the entire industry that heavy investment of time and money be spent to develop codes that can accurately simulate fill imbalance. Results from this project can be used as an insight towards improving the numerical codes. It has been shown that reverse fill imbalance is a direct cause of heat loss through the cold mold walls. If the programs and codes still rely on the assumption of adiabatic surfaces, then accurate results can never be obtained. Additionally the code to simulate the runner should be multi-dimensional and incorporate a lot more nodes than just one. With the nodal structure in place, viscous heating effects and shear thinning effects need to be

incorporated into calculating the viscosity profile across the runner. Additionally it may be of interest to develop a code to calculate velocity profile across the melt instead of making the assumption that it will always be a fountain flow. If viscosity continually shifts with time and distance, perhaps the velocity profile would as well.

The author of this thesis hopes that the effort placed into studying primary runner length's and material properties' relationships with fill imbalance, will serve to help the industry better understand fill imbalances in naturally balanced runner molds. It is hoped that one day a complete analysis, which the entire industry agrees upon, will be provided by individuals who utilized this work as a guideline during their research process. Although the phenomenon is complex, complete detailed explanation can be achieved with additional future work.

REFERENCES

1. Beaumont, J., Young, J., and Jaworski, M., Solving Mold Filling Imabalances in Multi-Cavity Injection Molds: Journal o Injection Molding Technology. 1998. 2(2): p.47-58.
2. Bishop, R., Shearing of Plastic Runner Causes Property Differences in Parts: ANTEC, 2000
3. Hoffman, D., and Beaumont, J., Thermoset Filling Imbalances in Geometrically Balanced Runner Systems: ANTEC 2001.
4. Mold Making Technology, http://moldmakingtechnology.com/articles/050510.html
5. Beaumont, J.P., Runner and Gating Design Handbook: Tools for Successful Injection Molding, Hanser Publishers Inc: Munich, Germany
6. Smits, A.J., A Physcial Introduction to Fluid Mechanics, Factor, R., Editor, John Wiley & Sons, Inc: New York.
7. Gupta, Rakesh, Polymer and Composite Rheology, Hudgen, D.E., Editor, Marcel Dekker, Inc: New York
8. Osswald, T.A. and Menges, G., Material Science of Polymers for Engineers, Hanser Publishers, Munich, Germany
9. Beaumont Technologies, Inc. E-News Letter, http://www.beaumontinc.com/news/newsletters/News@BTI_August_2005.pdf
10. Reifschneider, L., Documenting and Simulating Flow Segregation in Geometrically Balanced Runners: Journal of Injection Molding Technology, 2001, 5(4) p. 208-223.
11. Cleveland, S.R., Jackson A., and Magnenau, D., Isolating and Quantifying the Development of Shear vs. Pressure Generated Heat in the Plastic Melt During Injection Molding: ANTEC 2004.
12. Haylett, R., Rhoades, D., True 3D Flow Analysis for Designing Hot and Cold Runners in Injection Molds: ANTEC 2001.
13. Shuttleworth, A., and Haylett, R., Effect of Heater Band Orientation on Cavity to Cavity Variations: ANTEC 2000.
14. Salamon, B., and Donal, R., Characterizing and Controlling Secondary Flows in Injection Molds, Journal of Injection Molding Technology, 1997, 1(1): p. 36-43.
15. Express Steel Inc., Supplier of P20 Steel, http://www.expresssteel.com
16. Casaldi, H., and Michel, T., Process Window as Effected by Shear Induced Flow Imbalance in Multicavity Molds: ANTEC 2001.
17. Reifschneider, L., Kostic, M.M., Vaddiraju, S.R., Computational Design of a U-Profile Die and Calibrator: ANTEC 2004
18. Boell, K., Beaumont, J., and Young, B., Artificially Balancing Geometrically Balanced Runner Systems: ANTEC, 2003
19. Cleveland, S., and Latchaw, J., Runner Diameter and Length Effects on Molded-in Stresses on Injection Molded Parts: ANTEC 2004.
20. Beaumont, J.P., Nagel, R., Sherman, R., Successful Injection Molding - Pocess, Design, and Simulation, Hanser Publishers: Munich, Germany

21. Harper, C.A., Handbook of Plastics, Elastomers, and Composites, Harper, C.A., Editor, McGraw-Hill, Inc: New York
22. Incropera, F.P., DeWitt, D.P, Fundamentals of Heat and Mass Transfer, Prinz, N., Editor, John Wiley & Sons: New York
23. Irani, R.K., Kodiyalam, S., Kazmer, D.O, Runner System Balancing for Injection Molds using Approximation Concepts and Numerical Optimization. ASME Design Automation Conference, 1992.

APPENDICES

APPENDIX A. DRAWINGS AND SPECIFICATION FOR TOOL MOLD

9⅞ x 20"
D-M-E Standard
A-Series
Mold Bases

GENERAL DIMENSIONS

D = DIAMETER OF LOCATING RING
Cat. No. 6501 (D = 3.990) Standard
Cat. No. 6504 (D = 3.990) Clamp Type
(For other rings, see pages K16-18)

E = LENGTH OF EJECTOR BAR
20", 23½ or 29½

O = SMALL DIA. OF SPRUE BUSHING ORIFICE
5/32, 7/32, 9/32 or 11/32

R = SPHERICAL RADIUS OF SPRUE BUSHING
½ or ¾

EJECTOR STROKE DATA					
C	2½	3"	3½	4"	4½
S	13/16	1 5/16	1 13/16	2 5/16	2 13/16

C = Height of Riser
S = Maximum Stroke of Ejector Bar

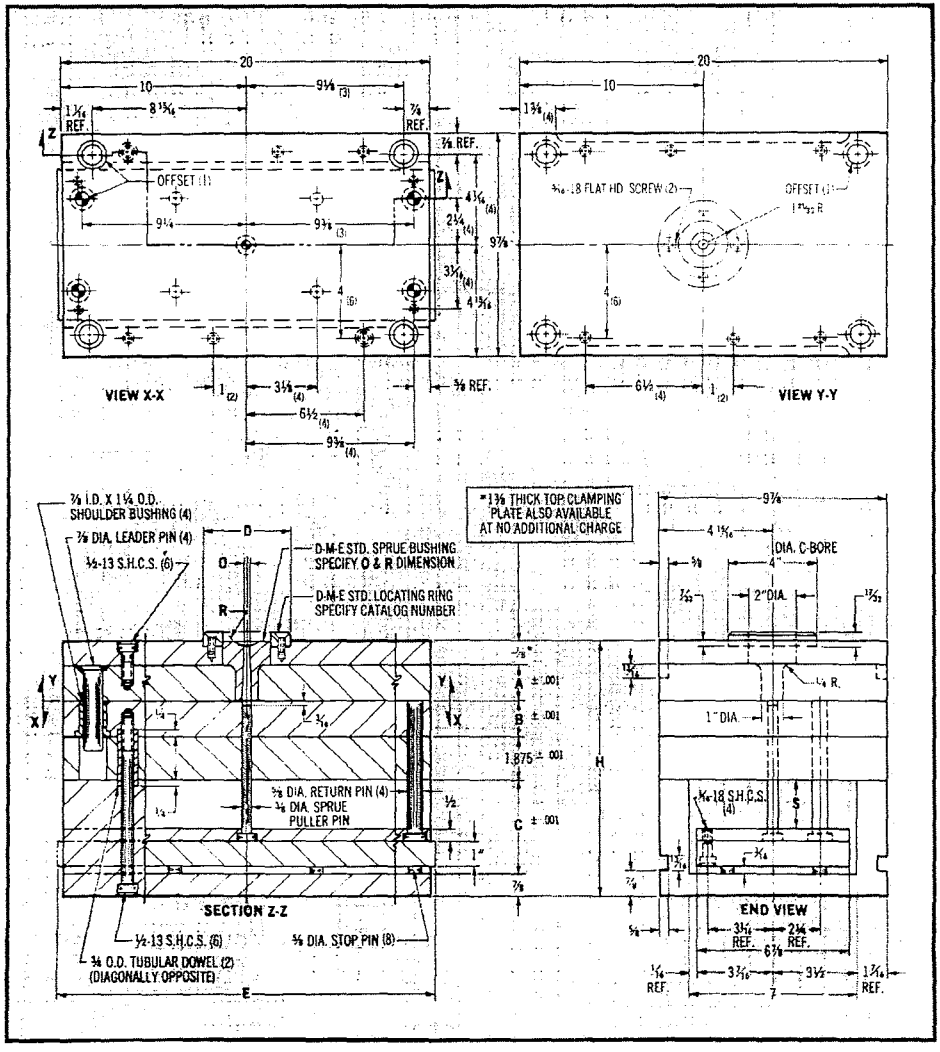

APPENDICES

APPENDIX A. DRAWINGS AND SPECIFICATION FOR TOOL MOLD

9⅞ x 20″
D-M-E Standard
A-Series
Mold Bases

GENERAL DIMENSIONS

D = DIAMETER OF LOCATING RING
Cat. No. 6501 (D = 3.990) Standard
Cat. No. 6504 (D = 3.990) Clamp Type
(For other rings, see pages K16-18)

E = LENGTH OF EJECTOR BAR
20″, 23½ or 29½

O = SMALL DIA. OF SPRUE BUSHING ORIFICE
5/32, 7/32, 9/32 or 11/32

R = SPHERICAL RADIUS OF SPRUE BUSHING
½ or ¾

EJECTOR STROKE DATA					
C	2½	3″	3½	4″	4½
S	13/16	1 5/16	1 13/16	2 5/16	2 13/16

C = Height of Riser
S = Maximum Stroke of Ejector Bar

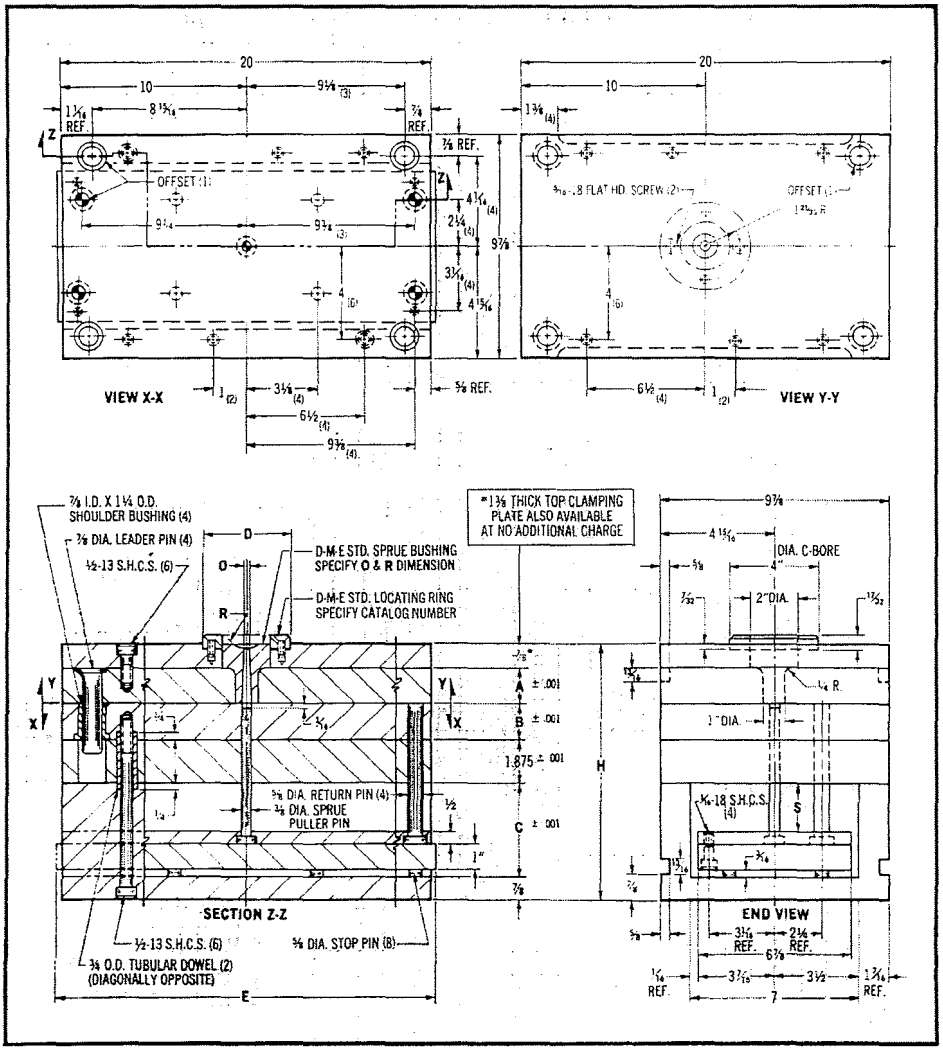

APPENDIX B. TEST RESULTS FOR HIPS

HIPS with L/D=13

13.0 °/sec

	Inner				Outer			
	1	2	3	4	5	6	7	8
(1)	3.03	3.05	2.96	3.08	2.63	2.64	2.33	2.51
(2)	3.04	3.02	2.93	3.03	2.61	2.66	2.35	2.53
(3)	3.01	3.03	2.92	3.07	2.61	2.66	2.35	2.53
(4)	3.04	3.01	2.89	3.07	2.63	2.65	2.34	2.53
(5)	3.05	2.99	2.90	3.09	2.60	2.62	2.31	2.51
(6)	3.06	2.99	2.90	3.00	2.60	2.64	2.33	2.54
Average	3.04	3.02	2.92	3.06	2.60	2.65	2.34	2.53
	1.10	1.09	1.05	1.11	0.94	0.96	0.84	0.91
	1.09				0.91			

8.0 °/sec

	1	2	3	4	5	6	7	8
(1)	3.02	3.01	2.86	3.04	2.65	2.70	2.38	2.58
(2)	2.96	2.97	2.84	3.04	2.64	2.71	2.36	2.57
(3)	3.01	2.91	2.76	2.99	2.62	2.67	2.39	2.56
(4)	3.03	2.97	2.82	3.06	2.64	2.72	2.40	2.58
(5)	3.00	3.00	2.87	3.02	2.63	2.69	2.37	2.56
(6)	2.94	2.93	2.78	2.98	2.59	2.66	2.33	2.54
Average	2.99	2.97	2.82	3.02	2.63	2.69	2.37	2.58
	1.09	1.08	1.02	1.10	0.95	0.98	0.86	0.93
	1.07				0.93			

3.0 °/sec

	1	2	3	4	5	6	7	8
(1)	2.98	2.96	2.88	2.96	2.73	2.85	2.48	2.67
(2)	2.93	2.92	2.83	2.92	2.69	2.81	2.46	2.63
(3)	2.93	2.92	2.83	2.91	2.70	2.81	2.46	2.64
(4)	2.92	2.79	2.81	2.90	2.68	2.79	2.44	2.62
(5)	2.95	2.93	2.85	2.94	2.70	2.80	2.44	2.64
(6)	2.96	2.88	2.88	2.95	2.76	2.87	2.50	2.70
Average	2.95	2.83	2.86	2.93	2.71	2.82	2.46	2.65
	1.07	1.03	0.90	1.07	0.99	1.03	0.90	0.96
	1.03				0.97			

1.5 °/sec

	1	2	3	4	5	6	7	8
(1)	2.99	2.96	2.84	3.04	2.94	3.12	2.97	2.70
(2)	3.01	2.98	2.85	3.05	2.92	3.12	2.97	2.71
(3)	2.99	2.98	2.86	3.05	2.93	3.12	2.97	2.76
(4)	2.99	2.99	2.86	3.05	2.93	3.13	2.97	2.76
(5)	2.99	2.98	2.86	3.05	2.94	3.13	2.97	2.70
(6)	3.00	2.99	2.87	3.04	2.93	3.12	2.96	2.76
Average	2.99	2.98	2.86	3.05	2.94	3.12	2.97	2.76
	1.01	1.01	0.97	1.03	0.99	1.06	1.00	0.93
	1.00				1.00			

HIPS with L/D=26

13.0 "/sec

	Inner				Outer			
	1	2	3	4	5	6	7	8
(1)	3.31	3.31	3.07	3.29	2.50	2.63	2.34	2.59
(2)	3.30	3.30	3.08	3.29	2.52	2.66	2.38	2.61
(3)	3.32	3.31	3.06	3.31	2.53	2.66	2.37	2.62
(4)	3.30	3.32	3.06	3.30	2.54	2.65	2.36	2.61
(5)	3.30	3.32	3.06	3.29	2.51	2.65	2.36	2.59
(6)	3.31	3.33	3.06	3.22	2.52	2.65	2.37	2.62
Average	3.31	3.32	3.07	3.28	2.52	2.65	2.36	2.61
	1.14	1.15	1.06	1.14	0.87	0.92	0.82	0.90
		1.12				0.88		

8.0 "/sec

	1	2	3	4	5	6	7	8
(1)	3.23	3.29	3.04	3.23	2.51	2.65	2.35	2.60
(2)	3.25	3.29	3.05	3.25	2.52	2.67	2.37	2.61
(3)	3.21	3.24	3.00	3.20	2.52	2.62	2.33	2.57
(4)	3.25	3.28	3.04	3.26	2.48	2.67	2.37	2.61
(5)	3.26	3.30	3.04	3.26	2.53	2.67	2.37	2.62
(6)	3.28	3.29	3.04	3.25	2.54	2.67	2.38	2.63
Average	3.25	3.26	3.04	3.24	2.52	2.66	2.36	2.61
	1.13	1.14	1.06	1.13	0.88	0.93	0.82	0.91
		1.12				0.88		

3.0 "/sec

	1	2	3	4	5	6	7	8
(1)	3.23	3.21	2.92	3.19	2.52	2.69	2.36	2.61
(2)	3.19	3.25	2.95	3.22	2.54	2.71	2.37	2.64
(3)	3.19	3.19	2.90	3.18	2.51	2.67	2.35	2.61
(4)	3.22	3.23	2.93	3.21	2.54	2.70	2.37	2.63
(5)	3.21	3.22	2.93	3.20	2.52	2.69	2.36	2.62
(6)	3.22	3.23	2.93	3.22	2.53	2.70	2.37	2.63
Average	3.21	3.22	2.93	3.20	2.53	2.69	2.36	2.62
	1.13	1.13	1.03	1.13	0.89	0.95	0.83	0.92
		1.10				0.90		

1.5 "/sec

	1	2	3	4	5	6	7	8
(1)	3.15	3.19	2.83	3.12	2.58	2.74	2.34	2.68
(2)	3.24	3.29	2.92	3.22	2.63	2.77	2.37	2.74
(3)	3.13	3.21	2.87	3.12	2.56	2.75	2.35	2.66
(4)	3.13	3.22	2.86	3.12	2.56	2.76	2.36	2.66
(5)	3.16	3.23	2.88	3.14	2.57	2.77	2.37	2.67
(6)	3.11	3.18	2.83	3.10	2.56	2.75	2.35	2.66
Average	3.15	3.22	2.87	3.14	2.57	2.76	2.36	2.68
	1.11	1.13	1.01	1.10	0.90	0.97	0.83	0.94
		1.09				0.91		

HIPS with L/D=39

13.0 "/sec

	Inner				Outer			
	1	2	3	4	5	6	7	8
(1)	3.18	3.33	3.10	3.27	2.28	2.52	2.23	2.43
(2)	3.15	3.31	3.07	3.23	2.26	2.49	2.21	2.39
(3)	3.20	3.36	3.12	3.28	2.29	2.52	2.22	2.42
(4)	3.19	3.35	3.10	3.28	2.30	2.51	2.22	2.41
(5)	3.16	3.33	3.08	3.24	2.28	2.49	2.20	2.39
(6)	3.17	3.30	3.07	3.25	2.29	2.50	2.20	2.40
Average	3.18	3.33	3.09	3.26	2.28	2.51	2.21	2.41
ND Value	1.14	1.20	1.11	1.17	0.82	0.90	0.80	0.86
			1.15				0.85	

8.0 "/sec

	1	2	3	4	5	6	7	8
(1)	3.12	3.31	3.06	3.22	2.30	2.52	2.23	2.42
(2)	3.08	3.30	3.00	3.22	2.29	2.52	2.22	2.42
(3)	3.11	3.29	3.03	3.23	2.29	2.52	2.23	2.41
(4)	3.13	3.31	3.03	3.20	2.30	2.52	2.23	2.42
(5)	3.12	3.28	3.02	3.20	2.29	2.52	2.22	2.42
(6)	3.13	3.29	3.04	3.20	2.29	2.53	2.23	2.42
Average	3.12	3.30	3.03	3.21	2.29	2.52	2.23	2.42
ND Value	1.13	1.19	1.10	1.16	0.83	0.91	0.81	0.87
			1.14				0.86	

3.0 "/sec

	1	2	3	4	5	6	7	8
(1)	3.08	3.29	2.97	3.20	2.27	2.49	2.18	2.39
(2)	3.06	3.29	2.96	3.19	2.26	2.49	2.17	2.39
(3)	3.07	3.31	2.98	3.19	2.27	2.50	2.19	2.36
(4)	3.07	3.31	2.97	3.19	2.26	2.49	2.18	2.40
(5)	3.08	3.32	2.99	3.17	2.26	2.50	2.16	2.39
(6)	3.04	3.28	2.95	3.20	2.25	2.47	2.18	2.40
Average	3.07	3.30	2.97	3.19	2.26	2.49	2.18	2.39
ND Value	1.12	1.21	1.09	1.17	0.83	0.91	0.80	0.87
			1.15				0.85	

1.5 "/sec

	1	2	3	4	5	6	7	8
(1)	3.06	3.33	2.93	3.22	2.27	2.51	2.10	2.38
(2)	3.04	3.28	2.88	3.18	2.25	2.50	2.06	2.36
(3)	3.02	3.26	2.83	3.16	2.26	2.51	2.08	2.36
(4)	3.02	3.26	2.84	3.17	2.26	2.51	2.12	2.32
(5)	3.03	3.27	2.84	3.17	2.27	2.52	2.12	2.38
(6)	3.04	3.27	2.84	3.16	2.29	2.53	2.13	2.40
Average	3.04	3.28	2.86	3.16	2.27	2.51	2.10	2.37
ND Value	1.12	1.21	1.06	1.18	0.84	0.93	0.78	0.88
			1.14				0.86	

APPENDIX C. TEST RESULTS FOR ABS

ABS with L/D = 13

13.0 °/sec

	Inner				Outer			
	1	2	3	4	5	6	7	8
(1)	2.89	3.08	3.00	2.81	1.71	1.84	1.59	1.68
(2)	2.90	3.04	2.96	2.84	1.73	1.84	1.60	1.70
(3)	2.90	3.00	2.95	2.84	1.73	1.83	1.61	1.70
(4)	2.92	3.27	3.11	2.78	1.65	1.77	1.53	1.61
(5)	2.86	3.05	2.97	2.83	1.71	1.83	1.60	1.69
(6)	2.90	3.04	2.94	2.87	1.72	1.86	1.59	1.70
Average	2.90	3.08	2.99	2.83	1.71	1.83	1.59	1.68
ND Value	1.25	1.33	1.29	1.22	0.74	0.79	0.68	0.72
		1.27				0.73		

8.0 °/sec

	1.00	2.00	3.00	4.00	5.00	6.00	7.00	8.00
(1)	2.82	2.91	2.84	2.74	1.76	1.92	1.66	1.77
(2)	2.88	2.97	2.87	2.78	1.78	1.90	1.68	1.81
(3)	2.82	2.91	2.80	2.74	1.77	1.92	1.69	1.80
(4)	2.73	2.86	2.94	2.81	1.70	1.84	1.73	1.81
(5)	2.84	2.96	2.84	2.78	1.79	1.95	1.70	1.83
(6)	2.82	2.91	2.83	2.75	1.77	1.91	1.66	1.80
Average	2.82	2.92	2.85	2.77	1.76	1.90	1.69	1.80
ND Value	1.22	1.26	1.23	1.19	0.76	0.83	0.73	0.78
		1.23				0.77		

2.0 °/sec

	1.00	2.00	3.00	4.00	5.00	6.00	7.00	8.00
(1)	2.69	2.67	2.58	2.63	1.83	1.97	1.74	1.87
(2)	2.69	2.67	2.58	2.63	1.83	1.97	1.74	1.87
(3)	2.70	2.69	2.60	2.64	1.83	1.98	1.74	1.87
(4)	2.71	2.72	2.63	2.64	1.81	1.97	1.73	1.84
(5)	2.71	2.71	2.63	2.63	1.81	1.97	1.73	1.85
(6)	2.70	2.70	2.60	2.64	1.81	1.96	1.73	1.85
Average	2.70	2.69	2.60	2.64	1.82	1.97	1.74	1.86
ND Value	1.20	1.20	1.16	1.17	0.81	0.87	0.77	0.83
		1.18				0.82		

1.0 °/sec

	1.00	2.00	3.00	4.00	5.00	6.00	7.00	8.00
(1)	2.62	2.60	2.50	2.55	1.72	1.90	1.64	1.77
(2)	2.65	2.63	2.52	2.58	1.72	1.90	1.64	1.77
(3)	2.68	2.63	2.54	2.60	1.71	1.94	1.64	1.79
(4)	2.66	2.65	2.53	2.59	1.69	1.87	1.61	1.75
(5)	2.63	2.60	2.50	2.56	1.72	1.90	1.64	1.78
(6)	2.79	2.64	2.49	2.69	1.64	1.86	1.62	1.73
Average	2.67	2.67	2.51	2.60	1.70	1.91	1.63	1.76
ND Value	1.20	1.23	1.15	1.19	0.78	0.87	0.75	0.80
		1.20				0.80		

ABS with L/D = 26

13.0 "/soc

	Inner				Outer			
	1	2	3	4	5	6	7	8
(1)	2.64	3.19	2.88	2.72	1.33	1.72	1.52	1.60
(2)	2.78	3.05	2.66	2.72	1.48	1.75	1.45	1.51
(3)	2.62	3.18	2.78	2.70	1.36	1.77	1.50	1.61
(4)	2.74	3.02	2.80	2.72	1.50	1.79	1.48	1.53
(5)	2.70	3.08	2.62	2.81	1.43	1.71	1.54	1.66
(6)	2.78	3.01	2.79	2.71	1.50	1.78	1.47	1.52
Average	2.71	3.09	2.79	2.73	1.43	1.75	1.49	1.57
ND Value	1.23	1.41	1.27	1.24	0.65	0.80	0.68	0.72
			1.29				0.71	

8.0 "/sec

	1	2	3	4	5	6	7	8
(1)	2.66	3.00	2.76	2.61	1.50	1.89	1.58	1.54
(2)	2.81	2.96	2.72	2.77	1.55	1.74	1.48	1.53
(3)	2.62	3.06	2.81	2.68	1.47	1.88	1.60	1.51
(4)	2.78	2.96	2.75	2.71	1.54	1.76	1.48	1.57
(5)	2.74	2.94	2.70	2.71	1.55	1.76	1.50	1.57
(6)	2.69	2.99	2.74	2.64	1.50	1.91	1.57	1.53
Average	2.72	2.99	2.75	2.67	1.52	1.82	1.54	1.55
ND Value	1.24	1.36	1.25	1.22	0.69	0.83	0.70	0.71
			1.27				0.73	

2.0 "/sec

	1	2	3	4	5	6	7	8
(1)	2.65	2.78	2.52	2.63	1.51	1.71	1.44	1.54
(2)	2.58	2.75	2.59	2.70	1.48	1.70	1.43	1.52
(3)	2.65	2.77	2.51	2.64	1.51	1.71	1.44	1.54
(4)	2.71	2.85	2.52	2.62	1.52	1.74	1.40	1.53
(5)	2.64	2.76	2.50	2.63	1.51	1.70	1.44	1.54
(6)	2.66	2.80	2.56	2.67	1.51	1.75	1.47	1.54
Average	2.65	2.79	2.53	2.65	1.51	1.72	1.44	1.54
ND Value	1.25	1.33	1.20	1.26	0.72	0.82	0.68	0.73
			1.26				0.74	

1.0 "/sec

	1	2	3	4	5	6	7	8
(1)	2.60	2.73	2.50	2.60	1.41	1.66	1.33	1.45
(2)	2.53	2.75	2.45	2.58	1.40	1.64	1.33	1.45
(3)	2.57	2.76	2.45	2.53	1.40	1.64	1.34	1.43
(4)	2.62	2.71	2.45	2.59	1.42	1.61	1.31	1.45
(5)	2.58	2.75	2.45	2.56	1.39	1.63	1.32	1.43
(6)	2.70	2.69	2.53	2.56	1.39	1.60	1.29	1.45
Average	2.61	2.73	2.47	2.55	1.40	1.63	1.32	1.45
ND Value	1.23	1.35	1.22	1.26	0.69	0.81	0.65	0.72
			1.28				0.72	

ABS with L/D = 39

13.0 "/sec

	Inner				Outer			
	1	2	3	4	5	6	7	8
(1)	2.42	2.99	2.74	2.50	1.32	1.85	1.35	1.36
(2)	2.44	2.93	2.71	2.54	1.35	1.84	1.34	1.36
(3)	2.39	2.94	2.74	2.46	1.32	1.87	1.36	1.38
(4)	2.41	2.95	2.72	2.50	1.31	1.84	1.40	1.40
(5)	2.45	2.90	2.72	2.55	1.33	1.84	1.32	1.44
(6)	2.43	2.95	2.74	2.49	1.30	1.86	1.35	1.40
Average	2.42	2.94	2.73	2.51	1.32	1.85	1.35	1.39
ND Value	1.17	1.43	1.32	1.21	0.64	0.90	0.66	0.67
			1.28				*0.72*	

8.0 "/sec

	1.00	2.00	3.00	4.00	5.00	6.00	7.00	8.00
(1)	2.45	2.97	2.71	2.54	1.31	1.83	1.41	1.38
(2)	2.44	2.96	2.71	2.54	1.30	1.83	1.40	1.38
(3)	2.42	2.97	2.71	2.51	1.31	1.84	1.44	1.39
(4)	2.40	3.12	2.88	2.45	1.22	1.99	1.30	1.21
(5)	2.41	2.98	2.73	2.52	1.31	2.00	1.41	1.37
(6)	2.19	3.26	2.95	2.25	1.14	1.81	1.56	1.22
Average	2.39	3.05	2.78	2.47	1.27	1.88	1.42	1.33
ND Value	1.15	1.47	1.34	1.19	0.61	0.91	0.69	0.64
			1.29				*0.71*	

2.0 "/sec

	1.00	2.00	3.00	4.00	5.00	6.00	7.00	8.00
(1)	2.44	2.91	2.58	2.58	1.22	1.49	1.27	1.32
(2)	2.49	2.80	2.50	2.59	1.25	1.46	1.24	1.34
(3)	2.48	2.78	2.48	2.58	1.25	1.46	1.23	1.34
(4)	2.51	2.81	2.51	2.61	1.26	1.48	1.26	1.35
(5)	2.49	2.80	2.50	2.59	1.25	1.47	1.25	1.34
(6)	2.48	2.80	2.50	2.58	1.26	1.48	1.25	1.34
Average	2.48	2.82	2.51	2.59	1.25	1.47	1.25	1.34
ND Value	1.26	1.43	1.28	1.32	0.64	0.75	0.64	0.68
			1.32				*0.68*	

1.0 "/sec

	1.00	2.00	3.00	4.00	5.00	6.00	7.00	8.00
(1)	2.24	2.97	2.59	2.51	1.12	1.48	1.21	1.20
(2)	2.39	2.80	2.45	2.50	1.15	1.38	1.13	1.25
(3)	2.38	2.83	2.46	2.51	1.15	1.40	1.13	1.23
(4)	2.39	2.80	2.45	2.50	1.14	1.37	1.13	1.23
(5)	2.38	2.81	2.53	2.46	1.13	1.38	1.16	1.21
(6)	2.39	2.79	2.44	2.50	1.14	1.37	1.13	1.23
Average	2.35	2.83	2.49	2.50	1.14	1.40	1.15	1.23
ND Value	1.25	1.50	1.32	1.32	0.60	0.74	0.61	0.65
			1.35				*0.65*	

APPENDIX D. TEST RESULTS FOR HDPE

HDPE with L/D = 13

13.0 °/sec

	Inner				Outer			
	1	2	3	4	5	6	7	8
(1)	2.75	2.76	2.69	2.68	2.33	2.44	2.27	2.36
(2)	2.76	2.74	2.68	2.70	2.37	2.44	2.27	2.36
(3)	2.77	2.74	2.69	2.69	2.34	2.44	2.27	2.36
(4)	2.75	2.74	2.67	2.70	2.34	2.45	2.28	2.38
(5)	2.76	2.75	2.69	2.69	2.37	2.45	2.26	2.36
(6)	2.77	2.73	2.70	2.70	2.36	2.45	2.28	2.37
Average	2.76	2.74	2.69	2.69	2.36	2.45	2.27	2.37
ND Value	1.09	1.08	1.06	1.06	0.93	0.96	0.89	0.93
	1.07				0.93			

7.0 °/sec

	1	2	3	4	5	6	7	8
(1)	2.73	2.74	2.67	2.70	2.32	2.42	2.26	2.33
(2)	2.73	2.72	2.67	2.66	2.26	2.45	2.20	2.38
(3)	2.74	2.74	2.68	2.68	2.37	2.48	2.31	2.37
(4)	2.75	2.74	2.69	2.69	2.39	2.47	2.29	2.38
(5)	2.75	2.74	2.69	2.70	2.38	2.47	2.30	2.39
(6)	2.73	2.74	2.68	2.69	2.37	2.47	2.30	2.38
Average	2.74	2.74	2.68	2.69	2.37	2.46	2.29	2.37
ND Value	1.08	1.08	1.05	1.06	0.93	0.97	0.90	0.93
	1.07				0.93			

3.0 °/sec

	1	2	3	4	5	6	7	8
(1)	2.61	2.62	2.54	2.56	2.40	2.51	2.33	2.40
(2)	2.64	2.64	2.56	2.58	2.42	2.54	2.34	2.43
(3)	2.66	2.64	2.58	2.59	2.42	2.55	2.34	2.42
(4)	2.66	2.67	2.58	2.60	2.44	2.54	2.36	2.44
(5)	2.66	2.67	2.59	2.59	2.45	2.54	2.35	2.44
(6)	2.66	2.66	2.57	2.58	2.44	2.54	2.35	2.43
Average	2.65	2.65	2.57	2.58	2.43	2.54	2.34	2.43
ND Value	1.05	1.05	1.02	1.02	0.96	1.01	0.93	0.96
	1.04				0.96			

0.5 °/sec

	1	2	3	4	5	6	7	8
(1)	2.26	2.23	2.08	2.07	2.64	2.85	2.46	2.64
(2)	2.21	2.25	2.06	2.02	2.69	2.89	2.50	2.65
(3)	2.17	2.24	2.06	2.14	2.67	2.87	2.45	2.60
(4)	2.18	2.22	2.03	2.07	2.63	2.90	2.47	2.63
(5)	2.13	2.21	2.03	2.16	2.63	2.83	2.45	2.64
(6)	2.22	2.22	2.08	2.11	2.62	2.84	2.44	2.64
Average	2.21	2.21	2.06	2.10	2.65	2.85	2.46	2.63
ND Value	0.92	0.92	0.86	0.87	1.10	1.20	1.03	1.10
	0.89				1.11			

HDPE with L/D = 26

13.0 "/sec

	Inner				Outer			
	1	2	3	4	5	6	7	8
(1)	2.73	2.76	2.57	2.71	2.26	2.39	2.14	2.28
(2)	2.70	2.73	2.56	2.71	2.28	2.40	2.15	2.30
(3)	2.72	2.73	2.56	2.69	2.26	2.40	2.16	2.30
(4)	2.74	2.77	2.59	2.73	2.28	2.41	2.18	2.31
(5)	2.75	2.77	2.57	2.75	2.29	2.40	2.18	2.33
(6)	2.75	2.77	2.59	2.73	2.28	2.43	2.19	2.32
Average	2.73	2.76	2.57	2.72	2.28	2.41	2.17	2.31
ND Value	1.10	1.11	1.03	1.09	0.91	0.97	0.87	0.93
		1.08				0.92		

7.0 "/sec

	1	2	3	4	5	6	7	8
(1)	2.71	2.73	2.55	2.69	2.28	2.40	2.18	2.30
(2)	2.72	2.74	2.56	2.70	2.28	2.40	2.20	2.30
(3)	2.71	2.74	2.56	2.72	2.28	2.41	2.19	2.31
(4)	2.72	2.75	2.57	2.72	2.30	2.42	2.18	2.32
(5)	2.71	2.74	2.57	2.72	2.29	2.41	2.19	2.33
(6)	2.72	2.74	2.59	2.72	2.29	2.41	2.18	2.30
Average	2.72	2.74	2.57	2.71	2.29	2.41	2.19	2.31
ND Value	1.09	1.10	1.03	1.09	0.92	0.97	0.88	0.93
		1.08				0.92		

3.0 "/sec

	1	2	3	4	5	6	7	8
(1)	2.64	2.66	2.47	2.61	2.33	2.44	2.19	2.35
(2)	2.63	2.67	2.48	2.61	2.33	2.45	2.19	2.36
(3)	2.65	2.67	2.48	2.61	2.33	2.46	2.20	2.36
(4)	2.65	2.68	2.48	2.62	2.33	2.46	2.20	2.36
(5)	2.64	2.66	2.47	2.62	2.33	2.45	2.19	2.36
(6)	2.64	2.67	2.47	2.61	2.33	2.45	2.19	2.36
Average	2.64	2.67	2.48	2.61	2.33	2.45	2.19	2.36
ND Value	1.07	1.08	1.00	1.06	0.94	0.99	0.89	0.96
		1.05				0.94		

0.5 "/sec

	1	2	3	4	5	6	7	8
(1)	1.93	2.12	1.67	2.01	2.66	2.90	2.45	2.72
(2)	1.95	2.04	1.75	2.01	2.68	2.90	2.44	2.71
(3)	2.03	2.08	1.79	2.00	2.67	2.92	2.46	2.71
(4)	1.95	2.15	1.71	2.01	2.66	2.91	2.41	2.71
(5)	1.93	2.12	1.72	2.03	2.68	2.92	2.44	2.73
(6)	2.00	2.11	1.75	1.91	2.66	2.87	2.39	2.72
Average	1.98	2.10	1.73	2.00	2.67	2.90	2.43	2.72
ND Value	0.86	0.91	0.75	0.86	1.15	1.25	1.05	1.17
		0.84				1.16		

HDPE with L/D = 39

13.0 "/sec

	Inner				Outer			
	1	2	3	4	5	6	7	8
(1)	2.46	2.55	2.42	2.67	2.01	2.08	2.02	2.22
(2)	2.46	2.55	2.44	2.69	2.01	2.11	2.02	2.22
(3)	2.47	2.56	2.48	2.70	2.00	2.12	2.02	2.24
(4)	2.49	2.53	2.47	2.68	2.01	2.11	2.03	2.21
(5)	2.48	2.55	2.47	2.68	2.01	2.12	2.02	2.23
(6)	2.48	2.55	2.45	2.68	2.02	2.12	2.02	2.21
Average	2.47	2.55	2.46	2.68	2.01	2.11	2.02	2.22
Total Avg.	1.07	1.10	1.06	1.16	0.87	0.91	0.87	0.96
		1.10				0.90		

7.0 "/sec

	1	2	3	4	5	6	7	8
(1)	2.49	2.55	2.46	2.67	2.02	2.11	2.03	2.23
(2)	2.48	2.56	2.46	2.67	2.02	2.12	2.04	2.22
(3)	2.47	2.55	2.47	2.67	2.02	2.11	2.02	2.23
(4)	2.45	2.55	2.45	2.65	2.02	2.10	2.03	2.24
(5)	2.48	2.53	2.48	2.67	2.03	2.15	2.05	2.25
(6)	2.46	2.55	2.44	2.65	2.03	2.13	2.03	2.24
Average	2.47	2.55	2.46	2.66	2.02	2.12	2.03	2.24
Total Avg.	1.07	1.10	1.06	1.15	0.87	0.91	0.88	0.96
		1.09				0.91		

3.0 "/sec

	1	2	3	4	5	6	7	8
(1)	2.41	2.48	2.39	2.64	2.06	2.17	2.09	2.27
(2)	2.44	2.49	2.44	2.66	2.08	2.19	2.10	2.29
(3)	2.43	2.49	2.41	2.64	2.07	2.17	2.09	2.28
(4)	2.42	2.50	2.41	2.67	2.08	2.18	2.10	2.28
(5)	2.42	2.50	2.41	2.67	2.07	2.18	2.10	2.28
(6)	2.43	2.49	2.42	2.66	2.07	2.18	2.09	2.28
Average	2.43	2.49	2.41	2.66	2.07	2.18	2.10	2.28
Total Avg.	1.04	1.07	1.04	1.14	0.89	0.94	0.90	0.98
		1.07				0.93		

0.5 "/sec

	1	2	3	4	5	6	7	8
(1)	1.72	1.99	1.73	2.19	2.30	2.50	2.40	2.66
(2)	1.62	1.91	1.75	2.10	2.30	2.48	2.32	2.66
(3)	1.65	1.83	1.69	2.05	2.32	2.53	2.42	2.70
(4)	1.64	1.85	1.77	2.10	2.33	2.53	2.37	2.71
(5)	1.63	1.86	1.75	2.03	2.34	2.54	2.37	2.70
(6)	1.62	1.84	1.68	2.02	2.37	2.55	2.43	2.73
Average	1.65	1.88	1.73	2.08	2.33	2.52	2.39	2.70
Total Avg.	0.76	0.87	0.80	0.96	1.08	1.17	1.11	1.25
		0.85				1.15		

MOLD FILLING/COOLING ANALYSIS PARAMETERS

DOW: MAGNUM* 1040 ABS

Thermal conductivity	0.15	W/m °C
Specific heat$_{Moldflow}$	2000	J/kg °C
Specific heat$_{C\text{-}Mold}$	2000	J/kg °C
Melt density	1000	kg/m^3
No flow temperature	140	°C
Ejection temperature	121	°C
Transition Temperature	105	°C

Temperature °C	Apparent Shear rate 1/s	Apparent Viscosity Pa-s
220	1000	355.7
240	100	1226.0
240	1000	266.7
240	10000	50.7
260	100	817.9
260	1000	201.7

Power Law Model Coefficients

A = 1.93 E+06
B = -7.076 E-01
C = -1.671 E-02

Cross/Arrhenius Model Constants

n =	0.25349	
t* =	8.0342 E+04	Pa
B =	7.3572 E-09	Pa-s
T_b =	1.4111 E+04	K

Cross/WLF Model Constants

n =	0.2535	
t* =	8.602 E+04	Pa
D_1 =	9.443 E+13	Pa-s
D_2 =	373.16	K
A_1 =	32.34	
A_2 =	51.6	K

RS 2/99

NOVA CHEMICALS' ENHANCED IMPACT POLYSTYRENE 782
MOLDFLOW DATA

Description	
Family Name	STYRENICS (PS, SAN, SBR, ..)
Trade Name	782
Manufacturer	NOVA Chemicals
Family Abbreviation	HIPS
Material Structure	Amorphous
Data Source	Other
Date Last Modified	OCT-21-2005
Date Tested	
Data Status	Confidential
Material ID	782
Grade Code	N782
Supplier Code	NOVA7II
Fibers/Fillers	Unfilled
Name	782 : NOVA Chemicals

Recommended Processing		
Mold Temperature	[°C]	49
Melt Temperature	[°C]	227
Mold Temp. (min.)	[°C]	27
Mold Temp. (max.)	[°C]	54
Melt Temp. (min.)	[°C]	216
Melt Temp. (max.)	[°C]	238
Melt Temp. (absolute max.)	[°C]	260
Ejection Temperature	[°C]	81
Maximum Shear Stress	[MPa]	0.3
Maximum Shear Rate	[1/s]	40,000

Density		
Melt	[g/cm³]	0.93891
Solid	[g/cm³]	1.0327

2-Domain Tait PVT Model		
b_3	[K]	367
b_4	[K/Pa]	2.95E-07
b_{1m}	[m³/kg]	0.0009854
b_{2m}	[m³/(kg·K)]	5.983E-07
b_{3m}	[Pa]	1.806E+08
b_{4m}	[1/K]	0.003764
b_{1s}	[m³/kg]	0.0009854
b_{2s}	[m³/(kg·K)]	2.479E-07
b_{3s}	[Pa]	2.68E+08
b_{4s}	[1/K]	0.004413
b_5	[m³/kg]	0
b_6	[1/K]	0
b_7	[1/Pa]	0

Mechanical Properties		
Elastic Modulus E_1 (0°)	[MPa]	2,197
Elastic Modulus E_2 (90°)	[MPa]	2,197
Poisson's Ratio ν_{12}	[ ]	0.401
Poisson's Ratio ν_{23}	[ ]	0.401
Shear Modulus G_{12}	[MPa]	784
Thermal Expansion α_1 (0°)	[1/°C]	8.4E-05
Thermal Expansion α_2 (90°)	[1/°C]	8.51E-05
Tensile Stress at Yield	[MPa]	25
Strain at Break	[%]	50

NOVA CHEMICALS' ENHANCED IMPACT POLYSTYRENE 782
MOLDFLOW DATA
(continued)

Specific Heat		
		Heating/
Temp.	C_p	Cooling Rate
[°C]	[J/(kg·°C)]	[°C/s]
230	2,221	-0.3333
220	2,207	0.3333
210	2,181	-0.3333
200	2,146	-0.3333
190	2,115	-0.3333
180	2,089	-0.3333
170	2,059	-0.3333
160	2,030	0.3333
150	1,993	-0.3333
140	1,960	-0.3333
130	1,930	-0.3333
120	1,899	-0.3333
110	1,870	-0.3333
100	1,833	-0.3333
90	1,737	-0.3333
80	1,576	-0.3333
70	1,487	-0.3333
60	1,432	-0.3333
50	1,389	-0.3333

Thermal Conductivity		
		Heating/
Temp.	k	Cooling Rate
[°C]	[W/(m·°C)]	[°C/s]
235	0.184	0
216	0.186	0
196	0.178	0
176	0.176	0
156	0.172	0
136	0.171	0
116	0.172	0
96	0.17	0
76	0.162	0
55	0.158	0
37	0.162	0
36	0.16	0

Default models are in *italics*

Cross-WLF Viscosity Model		
n	[ ]	0.3275
τ^*	[Pa]	21,721.4
D_1	[Pa·s]	1.691E+12
D_2	[K]	373
D_3	[K/Pa]	0
A_1	[ ]	28.77
A_2	[K]	51.6
Second Order Viscosity Model		
A	[ ]	19.902
B	[ ]	-0.81847
C	[ ]	0.0749
D	[ ]	-0.01637
E	[ ]	0.0019014
F	[ ]	9.977E-05
Shear Rate (Min.)	[1/s]	10
Shear Rate (Max.)	[1/s]	1E+06
Extension Viscosity Model (3D)		
A	[ ]	
B	[ ]	

Juncture Loss Method Coefficients		
C_1	[Pa^(1-c₂)]	
C_2	[ ]	

Transition Temperature		
T_{trans}	[°C]	88

Moldflow Viscosity Index	VI(200)165

Melt Mass-Flow Rate (MFR)		
Temperature	[°C]	200
Load	[kg]	5
Measured MFR	[g/10min.]	9

VITA

Rhyu Kevin Takarada, born June 25, 1980, is the son of entrepreneurial parents, Tony and Lilly Takarada. As a second generation, strong emphasis was placed onto Kevin to maintain cultural identity, thereby over the course of 12 years Kevin and his older sister Yoko, attended a local school in Japan during their American summer breaks. The other 9 months were spent in Miami but with the family business growing and becoming ever busier, Kevin began to work week-ends at the family restaurants at the age of 13.

After graduating from Christopher Columbus High School in 1998, Kevin attended Bucknell University in Lewisburg, PA, where he received a Bachelor of Science degree in Mechanical Engineering in 2002. As the first graduating class after 9/11, jobs were scarce yet Kevin was able to find work as a R/D intern at Johnson & Johnson in NJ. There he helped to develop new cardiac surgical devices and ultimately build an appreciation and interest in the field of R/D. After J&J, Kevin worked as a product engineer for Honda Transmission Mfg. in Ohio. As the project leader for the 2005 Honda Odyssey Transmission, Kevin was assigned the overwhelming task of assuring quality of the product prior to mass production. Utilizing his Japanese linguistic skills, Mr. Takarada was able to better amalgamate the two culturally clashing sides of American manufacturing, and Japanese R/D. Successful product launch came in the summer of 2004, at the same time Kevin decided to return back to the academic field.

At Lehigh University, Mr. Takarada initially pursued a Master of Engineering degree, but with persuasion from Dr. John Coulter, the degree sought was changed to a

Master of Science. Immediately after meeting Dr. Coulter, Kevin became a member of the Manufacturing Science Laboratory head by John Coulter himself. There he worked with Beaumont Technologies Inc., and began the study that ultimately amounted to this thesis.

Upon completion of his Master of Science degree, Mr. Takarada will work with a medium sized company called CML Technologies in Hackensack NJ, where he will design new lighting equipment for the automotive industry. His long term goals are to continue to learn through attendance at local universities, and continue to travel overseas to experience the various cultures that exist outside of the states. The ultimate goal in life is to discover an opportunity that suits personal interest, and develop a business that can capitalize on this opportunity.

END OF
TITLE